POLITECNICO DI TORINO

Master of Science course in Energy and Nuclear Engineering

Master of Science thesis

Thermochemical storage modelling and optimization within multi-energy systems

Supervisor

prof. Andrea Lanzini

Co-supervisors

prof. Matteo Gazzani (Utrecht University)

Dr. Francesco Demetrio Minuto

Candidate

Federica Malvindi

December 2018

Contents

Abstract

Within the framework of an increasing interest towards thermal energy storage, thermochemical storage systems (TCS) have been gaining the interest of many research activities, due to the high achievable energy density, compared other storage technologies, and to the absence, at least in principle, of thermal losses during the storage phase. In particular, salt hydrates are currently considered ones of most promising materials for TCS applications, leading to many experimental investigations on the material level. These systems are quite far from a commercialization process, and lack of information is verified on a system design level, which currently represents a field of investigation. This work aims to bridge the material and the system levels of analysis, by simulating salt-hydrates-based TCS systems within multi-energy systems (MES). To this purpose, an equilibrium-based thermodynamic analysis is firstly presented, aiming to the selection of three reference materials and corresponding hydration reactions. The TCS technology is then modelled within the optimization problem of MES, coherently with a MILP (mixed integer linear programming) problem formulation. Two MES configurations, aiming to the satisfaction of thermal and electric demands of a single household placed in Utrecht (The Netherlands), are simulated for all the reference salts. Most relevant results show TCS size, cost and yearly stored energy dependence on the key performance parameters introduced in the TCS model, i.e. the charging/discharging efficiency and the self-discharge parameter.

List of figures

List of tables

List of acronyms

AIPOs-Alluminophospates

LHTES-latent heat thermal energy storage

MES- Multi-energy systems

MILP-Mixed integer linear programming

MOF-Metal organic Framework

O&M-Operation and Maintenance

SAPOs-Silico-Alluminophospates

SOFC-Solid-oxide fuel cell

STES-Sensible thermal energy storage

TCS-Thermochemical storage

Scope and Motivation

The development of renewable energy technologies is nowadays strictly connected to the capability of realising efficient and economically competitive storage systems. The possibility of storing energy allows the optimal exploitation of intermittent energy sources, significantly reducing overall fossil-based energy consumption. Within this framework, thermochemical storage is becoming a hot topic in the field of thermal storage, due to higher theorical energy density achievable with respect to sensible and latent heat storage systems. This leads to the reduction of storing devices volumes, which is a crucial issue in domestic applications. Moreover, thermochemical storage is, in principle, isothermal with respect to the environment, which implies that thermal losses during the storage phase are (ideally) equal to zero. This is particularly suitable for seasonal storage applications.

In the past few years, many researcher activities where focused on reversible hydration reactions involving salt hydrates [1]-[3], characterized by high theoretical energy density values, desorption temperatures achievable with waste heat or renewable energy sources and discharge temperatures useful for low-temperature heat application (space heating and domestic hot water production)

Donkers et al. [1] reviewed more than five hundred reactions involving salt hydrates, to assess the most suitable ones for domestic applications, and deeply investigated three main promising materials and the related hydration reactions: potassium carbonate, magnesium chloride and sodium sulphide. At the state of art, only small prototypes exist [5][6][7] and the main part of the research activity is still at the material level, dealing with issues especially related to chemical instability.

This work aims to provide some guidelines for the further development of the technology by bridging the material level of analysis to the system level, modelling salt hydrates based thermochemical storage systems, with the materials selected by Donkers et al. [1], within multi-energy systems (MES) optimization problems. Two main case studies are simulated, given by different combinations of energy technologies, aiming to the satisfaction of a single household thermal and electric demands in Utrecht, in The Netherlands.

The work is organized in four chapters. *Chapter 1* introduces the concept of thermal and thermochemical storage. It is then composed by a review on the available materials and a thermodynamic analysis of the three selected materials. The last section analyses multi-energy systems concept and introduces mixed-integer linear programming (MILP) tools for setting and solving optimization problems.

In *Chapter 2*, the concepts of MES and MES optimization problems are introduced. The two case studies are then presented and theoretical and methodological approaches for the system modelling and the optimization problem settings and solving are presented. *Chapter 3* provides the most relevant results deriving from simulations, while in *Chapter 4* conclusions on the current results and future work are discussed.

Chapter 1

Introduction

1.1 Thermal storage

Thermal energy globally represents the largest energy end-use. In buildings and industrial processes almost half of the consumed energy is given by thermal energy, whose fraction produced by renewable energy technologies was equal to 10% in 2017 and is expected to grow 20% from 2018 to 2023 [8], as noticeable in **Figure 1.1.**

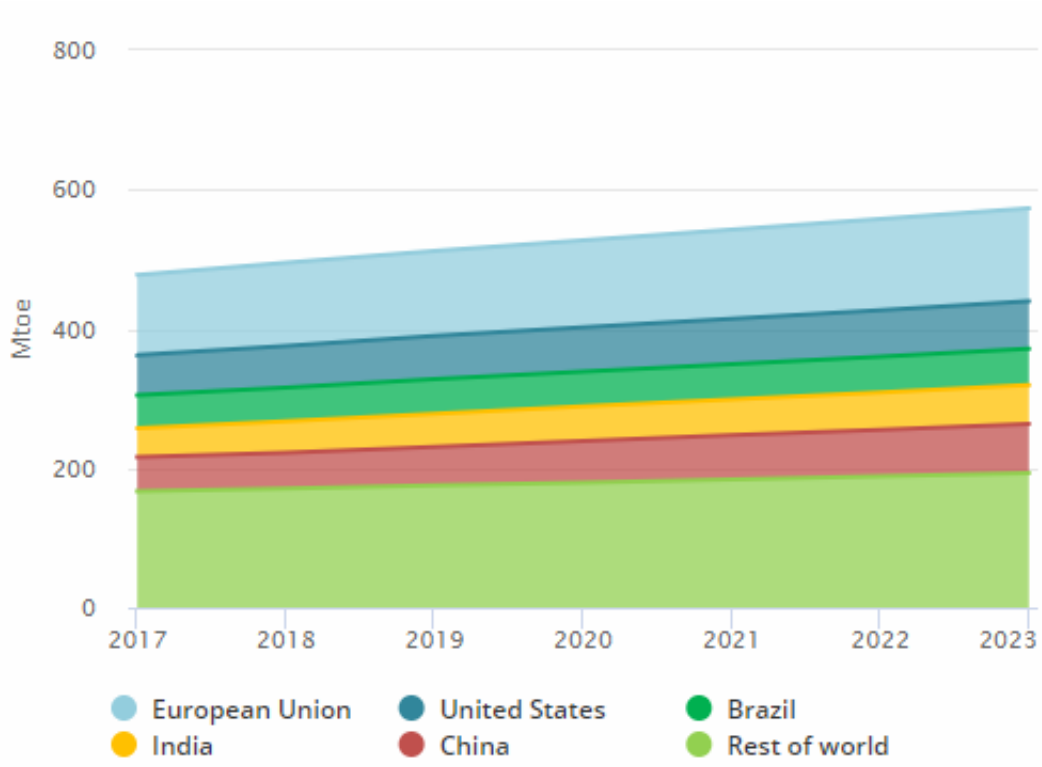

Figure 1.1. Worldwide renewable heat consumption [8]

Within this framework, it is evident that thermal energy storage (TES) plays a predominant role in nowadays energy scenario, presenting multiple interrelated advantages:

- It helps to balance energy demand and supply on a daily, weekly or seasonal basis. The latter case is especially needed when solar technologies are involved, whose share and

further development are strictly connected to the capability of realising efficient and economically competitive seasonal storage devices. In general, by balancing renewable energy sources (RES) fluctuations, thermal storage allows to increase renewable penetration within the energy mix.

- It increases the operating flexibility of a system, allowing peak shaving and smart demand side management techniques, and the generation capacity.
- It increases the overall efficiency of a generic energy system, in terms of reduction of energy consumption, CO2 emissions and costs.
- It enables the recovery of waste heat, e.g. in industrial processes.

Many different materials and technologies can be adopted for thermal energy storing purposes, for which a classification in three main categories is possible, according to the origin and type of the thermal energy involved:

1. Sensible thermal energy storage (STES): the stored energy is associated to the temperature variation of a liquid or solid storage medium.
2. Latent heat thermal energy storage (LHTES): the conserved energy is given by heat associated to a phase transition, which is mostly a solid-liquid transformation, due a reasonable occurring density variation.
3. Thermochemical storage (TCS): heat is stored in reversible chemical reaction and sorption processes.

Other classifications are possible and meaningful, considering for example the storage period:

- Short-term TES: storing time goes from hours to maximum one day. It is used for dealing with hourly and daily peak demand, reducing the size of the energy plant and/or taking advantages from the most convenient hourly energy prices. This type of storage can reach efficiencies also higher than 90%.
- Middle/long-term TES: it takes from weeks to months. When it exploits seasonal climate variations it is called seasonal storage. Depending on the technology involved, the efficiency may vary significantly but, in general, for these systems it can hardly exceed a value of 70%.

Another distinction can be made considering the “quality” of the heat conserved, i.e. its temperature. In this case, the possible typologies are:

- low temperature TES: heat is available (both in charging and discharging mode) at temperatures lower than 120°C. Cold energy storage systems are included in this category. Low temperature TES assumes big interest for waste heat recovery applications.
- High temperature TES: the temperature at which heat is available is higher than 120°C.

For any typology of TES, the most relevant and significant figures of merit to be considered are:

- **Storage capacity**: it represents the amount of energy that can be store within the system. It may be expressed per unit of mass or volume (GJ/m^3, kWh/m^3 or kWh/kg).
- **Efficiency**: it is the ratio between the energy provided to the user and the energy needed for fully charging the system. Thermal losses during the storage period and the charging/discharging operations are thus considered.
- **Power**: it is the amount of stored energy than can be charged or discharged within the system in the unit of time. This quantity is typically affected by heat transfer and/or involved species kinetic aspects.
- **Storage period**: it is the time for which energy is conserved within the storage system, with losses strictly dependent on the storage technology exploited.
- **Charging/Discharging time**: it represents the time needed for fully charging/discharging the storage device.
- **Cost**: it can be expressed per unit of energy (€/kWh) or per unit of power (€/kW). It depends on capital, operation and maintenance costs and it is affected by the lifetime of the system.

According to the specific TES typology, it is possible to take into consideration other figures of merits, ultimately correlated to the ones introduced. It should be underlined that also safety-related issues and environmental impacts are key parameters for the choice of a proper thermal energy storage system.

1.2 Thermochemical storage concept

Thermochemical storage consists in the storage of thermal energy in chemical reactions and sorption processes. The generic term "sorption" refers to both absorption and adsorption processes. Absorption is a bulk phenomenon occurring at molecular level between two species: the absorbent, that can be liquid or solid, and the absorbate, which is in liquid or gaseous state. The process involves covalent bonds between atoms and molecules, to which is associated a relatively high binding energy [6]. Adsorption is, instead, a surface phenomenon, occurring at the interface between two phases, where cohesive forces are established. Therefore, the material structure is unaltered, expansion doesn't occur, and a low activation energy is required [6] Depending on nature of the cohesive forces, adsorption can be further divided in:

- Physisorption: weak Van der Waals intermolecular forces and hydrogen bonding are established between adsorbent and adsorbate;
- Chemisorption: covalent bonds are involved in the process, which may also be irreversible;

In some cases, physisorption and chemisorption occur simultaneously, consequently a clear distinction is hardly realized [6].

Some authors include other categories within the sorption heat storage concept but boundaries between definitions are not so defined and significant differences may occur. In **Figure 1.2** a possible classification is presented.

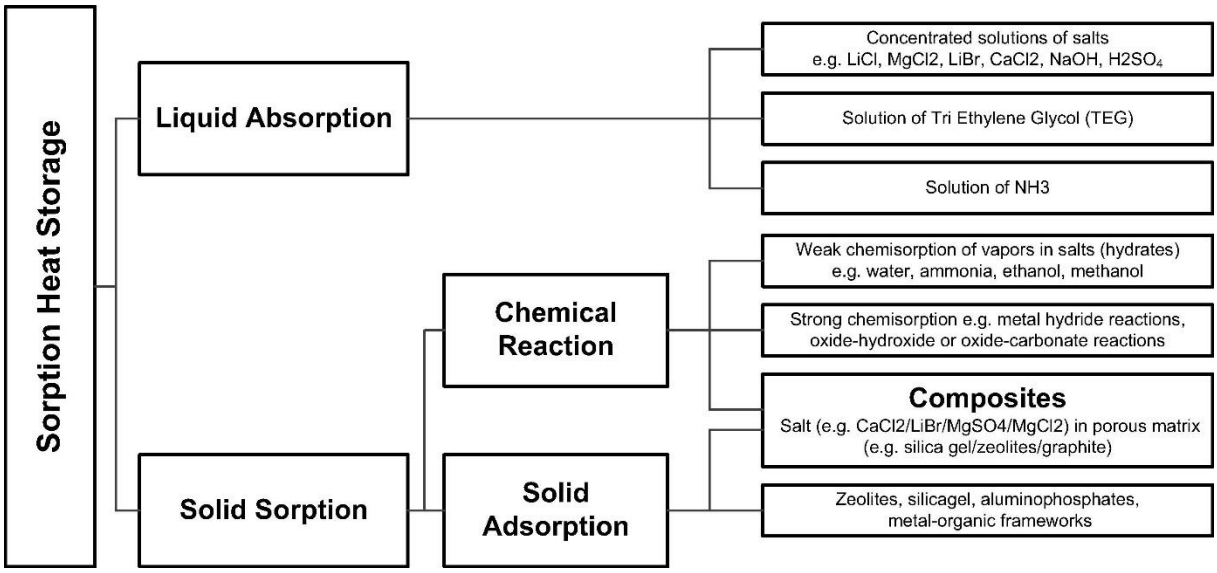

Figure 1.2. Sorption heat storage classification proposed in [6]

Reactions and materials involved in the classification are deeply analysed in *Section 2.3.*

For TES applications, only reversible sorption reactions are considered, that can be expressed in the general form:

$$AB + Q \leftrightarrow A + B \qquad (1.1)$$

AB is a generic compound, while Q represents the thermal energy needed to dissociate it in the species A and B. Considering the reverse direction, Q is the energy released due to products recombination. Its value is significantly affected by the nature of the involved intermolecular forces and is sufficiently high to guarantee attractive, compared to STES and LTES, energy density values. A comparison in terms of energy density and storage volume is shown in **Figure 1.3.**

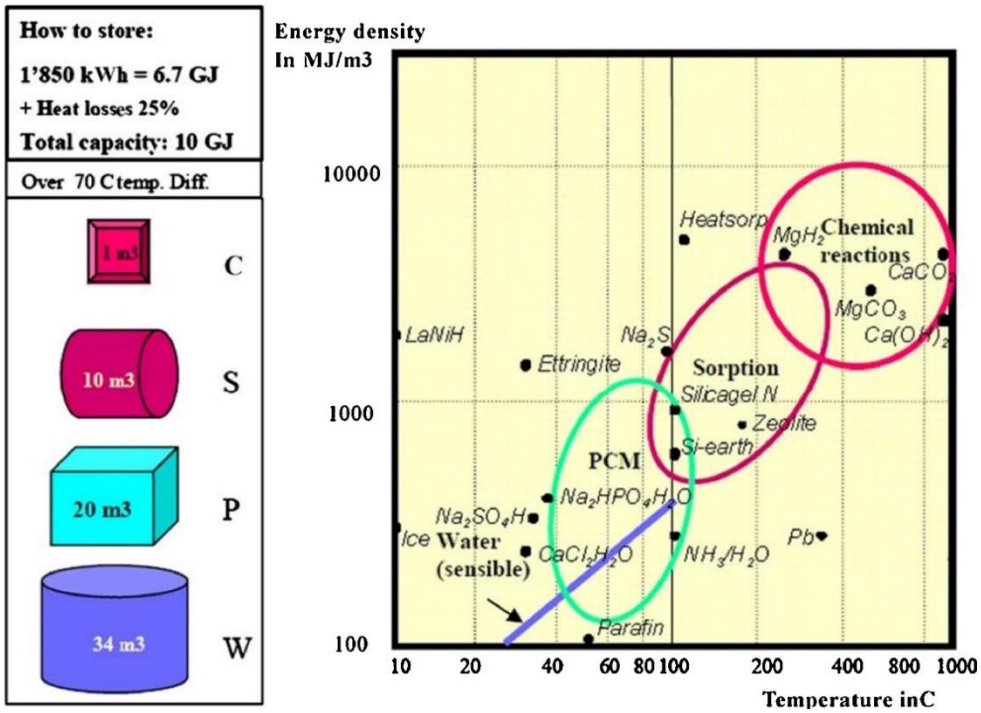

Fig. 1.3. Energy density and volume comparison between TES technologies [9].

For each storage cycle, three phases are realised:

1. Discharging phase: the exothermal reaction occurs, with heat release and products formations.
2. Charging phase: an external heat source allows the formation of the initial reactants, through the reverse reaction (endothermic) occurring.
3. Heat storage phase: reactants are conserved separately at ambient temperature, so that the storage is isothermal with the external environment and thermal losses are, in principle, equal to zero. When thermal energy release is needed the cycle starts again.

The working principle of thermochemical storage is drastically different with respect to sensible and latent heat storage. The latter are, indeed, direct methods for storing energy, whose working principle is illustrated in **Figure 1.4**

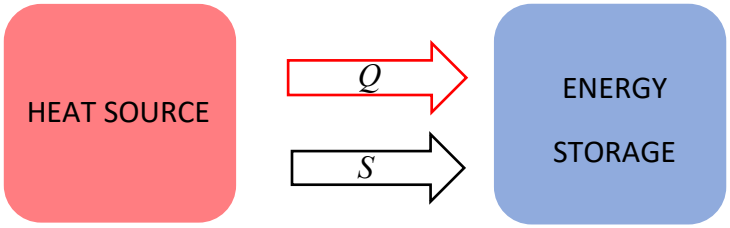

Fig. 2.4. Direct method for TES (charging mode).

Q is the thermal energy flow [J] from the heat source, while S represents the entropy flow [J/K]. From basic thermodynamic notions, considering a transition within the storage material from a generic thermodynamic state 1 to a state 2, it is possible to introduce the following equations:

$$\frac{\delta Q}{T} = \delta S \tag{1.2}$$

$$Q_{sensible} = \int_{state\ 1}^{state\ 2} \delta Q = \int_{state\ 1}^{state\ 2} TdS = \bar{T}\,(S_2 - S_1) \tag{1.3}$$

$$Q_{latent} = Q_{sensible} + T_{phase\ change}\Delta S_{phase\ change} \tag{1.4}$$

All terms are self-explaining. It is thus possible to notice that, in a direct method, to a thermal flow always corresponds an entropy flow, which is a thermodynamic limit. Indeed, if the figure of merit to be maximized is the thermal energy within the storage system or, better, the energy density, the only two options, from Eq. 1.3 and Eq.1.4, are:

1. To increase the temperature, which is not always possible since it depends on the available heat source;
2. To increase the entropy variation within the material, which is a clear limit given by the material itself (the entropy density within a material is limited).

Beside this thermodynamic limit, another technological limit should be considered, which is represented by the unavoidable thermal losses to the environment.

Thermochemical storage systems are, instead, indirect methods for storing energy. The working principle is shown in **Figure 1.5**.

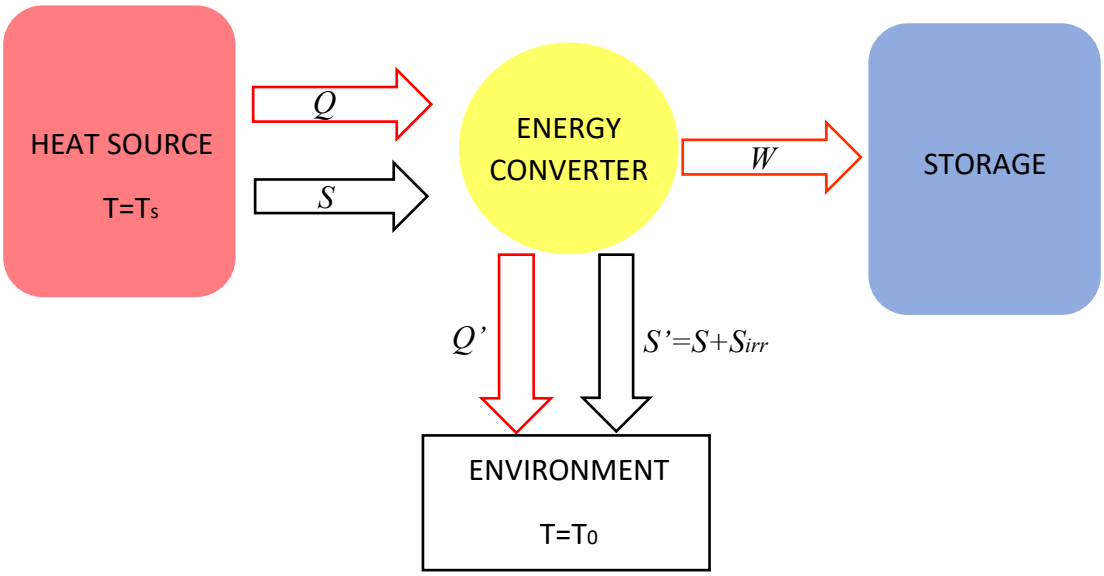

Fig. 1.5. Indirect method for TES (charging mode).

The energy converter in Figure 2.3. represents the energy conversion process from thermal to chemical energy, and vice versa, due to endothermic and exothermic reactions occurring, e.g. an absorption process. In charging mode, the energy converter delivers low temperature heat (Q') and entropy (S') flows to the environment (vice versa for discharging mode). This means that the system is not self-sufficient as regards charging and discharging phases and external devices for heat (and entropy) exchanges with the environment are needed (e.g. evaporators and condensers). Therefore, without external heat flows, the system cannot be discharged: during the storage phase, no thermal losses to the environment occur. This is incredibly attractive for long-term storage purposes. It is possible to evaluate the exergy W that can be stored applying an exergy balance on the energy converter component, from which Equation 1.5 is achieved:

$$W = Q\left(1-\frac{T_0}{T_s}\right) - Q'\left(1-\frac{T_0}{T_0}\right) - T_0 S_{irr} = Q\left(1-\frac{T_0}{T_s}\right) - T_0 S_{irr} \quad (1.5)$$

It therefore can be deduced that the achievable exergy depends on the heat source temperature, as for latent and sensible TES, and on the entropy S_{irr} associated to the irreversibility during the energy conversion process. The thermodynamic limit presented for LTES and STES is

completely overcome, since heat flows from/to the storage material are fully decoupled from the entropy flows.

1.3 Thermochemical storage materials overview

Great research effort has been devoting to the individuation of suitable thermochemical storage materials and optimal sorption-sorbate couples. Beside the figures of merit introduced in *Section 1.1*, particular attention is given to the chemical stability requirement, which is, at the state of art, an open issue. The most relevant selection criteria can be summarized as follows [6]:

- Large reaction enthalpy
- High uptake of sorbate
- Low desorption temperature
- Good mass transfer of the sorbate within the sorbent
- Good heat transport within the sorbent
- Thermal and chemical stability
- No corrosion issues
- Environmental safety
- Low-cost

When dealing with domestic applications, specific bounds are required [1][2]. For seasonal storage purposes, a yearly amount of about 10 GJ (2,778 MWh) needs to be stored (for well insulated dwellings [1]), leading to the first necessary criterion: an energy density value, on system level, at least equal to 1 GJ/m^3 (around 278 kWh), in order to limit the necessary storage volume (with this value 10 m^3 are already needed).This means that, on material level, the necessary energy density should be significantly higher; a value, for example, of 1.5 GJ/m^3 ($\cong$417 kWh/m^3) corresponds to an overall system efficiency of $1/1.5 \cong 0{,}67$, which appears to be relatively high and suggests, as suitable, a still larger material energy density. Other important criteria regard sorption and desorption temperature. For the first one, an ideal value should range around 65° C, suitable for domestic hot water production and consistent with low temperature space heating; for the latter one, an upper threshold of 120-100 °C would be required, reachable with solar technologies.

Once the suitable features are defined, a review of materials is presented, organized according to the classification proposed in [6] and in [10], which slightly differ but are both based on the individuation of four classes:

1. Solid adsorption
2. Liquid absorption
3. Chemical reaction
4. Composite materials

1.3.1. Solid adsorption

Solid adsorption, as stated in *Section 1.2*, involves weak intermolecular forces, so that the achievable energy density is relatively low (compared to absorption systems). In the following, materials used in solid adsorption processes for TCS are presented.

Zeolites

Zeolites are aluminosilicates of alkali or alkali earth elements, characterized by a porous tetrahedral hydrophilic structure

Their general formula is:

$$M_{x/n}\left[(AlO_2)_x(SiO_2)_y\right]zH_2O \qquad (1.6)$$

where n is the valence of the alkali/alkali earth cation M, z represents the number of water molecules per unit cell, x and y are integers, whose ratio is higher than one. Typical alkali and alkali earth elements are sodium, potassium, calcium or magnesium.

Zeolites exist in nature but, for commercial applications, they are commonly synthetized, which opens the attractive possibility of engineering them. Great research effort has indeed been spending in the study of zeolites on the micro-scale level, pointing out the macroscopic effects of micro-pores distribution and chemical composition, which may be significantly varied through the introduction of differently charged and sized ions. Both numerical and experimental investigations of water adsorption phenomenon on zeolites have been carried out [11]-[13], in order to assess material performances, especially in terms of hydrophilicity and reaction kinetic (e.g. diffusion coefficient).

Zeolite 13X, whose features are introduced in **Table 1.1**, is considered one of the most promising type for thermochemical storage, due to the large water uptake and reaction kinetic. Many numerical and experimental investigations have been accomplished for different operating conditions (e.g. desorption temperature, hydration pressure), material composition (that affects bed porosity, heat transfer properties), for which the energy density achievable may vary significantly. The typical procedure for the assessment of the energy associated to an absorption process involving zeolite (and, in general, any adsorbent), aims to the evaluation of the isosteric heat of adsorption, i.e. the energy released per mole of adsorbed water, for which many models are available. Typical values of isosteric heat of adsorptions ranges around 60 kJ/mol, while typical energy densities ranges between 0.4-0.6 GJ/m^3 [6].

surface area [m^2/g]	800-1000
micropore volume [cm^3/g]	0.26
average pore diameter [nm]	0.7
specific heat [kJ/kg K]	0.8-0.9
thermal conductivity [W/m K]	0.58

Table 1.1. zeolite 13 X properties [14]

Alluminophospates (AIPOs) and silico-alluminophospates (SAPOs)

Alluminophospates and silico-alluminophospates have recently being investigated as promising materials for TCS applications, due to interesting associated energy density values and favourable operation conditions (e.g. desorption temperature, adsorption water vapor pressure). Two of the most studied materials belonging to this category are SAPO-39 and AIPO-18, which shows energy densities of, respectively, 0.203 kWh/kg (0.731 MJ/kg) and 0.243 kWh/kg (8.75 MJ/kg) [6]. Desorption temperature is around 40°C, while sorption temperature is about 95°C [6]. Another promising material is APO-Tric, whose energy density is estimated to be 0.86 GJ/m^3 [6]. It shows energy density and sorption/desorption temperatures similar to that of previously mentioned AIPO-18 and SAPO-39, but it incorporates water within a smaller range of vapor pressure, which is its major advantage.

Metal organic frameworks (MOF)

Metal organic frameworks are compounds composed by metal ions linked by organic species, also studied for gas storage applications. They show relatively large water uptake and chemical stability. Only few operating conditions have been investigated, as a result of which one of the most promising material appears to be MIL-101. At a water vapor pressure of 55 mbar, with a desorption temperature around 140°C and a sorption temperature of 40°C, an energy density of approximately 1.6 GJ/m^3 can be achieved [6]. At the state of art, the main drawback are high production cost and the necessity of a humidifier in order to guarantee a vapor pressure of 55 mbar. Further operating conditions should be investigated.

1.3.2. Liquid absorption

Liquid absorption systems represent a very reliable and mature technology in the field of refrigeration, based on the exploitation of binary mixtures, such as f LiBr /H_2O and H_2O/NH_3, widely used, and the couples $LiCl/H_2O$, $CaCl_2/H_2O$. An absorption cycle is realized through a system composed by generator, condenser, evaporator and absorber. The working principle for TCS application is exactly the same, but, in this case, the useful effect is represented by the thermal power delivered by the absorber unit. Research activities have been developing about this topic, and only few operating conditions and system configuration have been investigated, among which multi-stage systems [15]. At the state of art, the main common drawback appears to be represented by the low reachable sorption temperatures [6].

1.3.3. Chemical reaction

Salt hydrates

Salt hydrates represent promising materials for TCS purposes, especially due to their high theoretical energy densities. They are deeply analysed in *Section 1.4.*

Oxides, hydroxides and carbonates

Oxide-hydroxide and oxide-carbonate reactions are characterized by high binding energy, much higher than the one associated to hydration reactions of salts. This leads to significantly high

hydration and dehydration temperatures, which make these materials more suitable for medium-high temperature applications. Example of common oxide/hydroxide reactions are:

$$CaO_{(s)} + H_2O_{(g)} \rightarrow Ca(OH)_{2(s)} \quad (1.7)$$

$$MgO_{(s)} + H_2O_{(g)} \rightarrow Mg(OH)_{2(s)} \quad (1.8)$$

For the first one, equilibrium temperatures (at standard conditions) range around 500 °C [], for the latter one around 200°C. Oxide-carbonate reactions are characterized by high equilibrium temperatures and low vapour pressure. Examples of materials are $CaO/\ CaCO_3$ and $Pb/PbCO_3$.

Ammoniates

A big variety of metal halides is involved in ammoniation/deammoniation reactions, with associated energy densities ranging from 563 kJ/kg to 2341 kJ/kg [6]. The latter value, referred to ammoniation reaction of $MgCl_2$, looks quite impressive (it is around 5,43 GJ/m^3). Equilibrium temperature ranges between 49°C and 334°C [6]. Examples of materials belonging to this category are NH_4Cl, $MgCl_2$, $CaCl_2$, $SrBr_2$ and many others, which have traditionally been investigated for refrigeration applications and only recently for low-temperature storage applications. A lab-scale reactor was built [16], based on $CaCl_2$ammoniation but, in general, research is still at early stages.

1.3.4. Composites

Composite materials are gaining the attention of many research activities, because, if properly designed, they allow to overcome typical problems of single-component materials, such as material degradation, instability (salt hydrates) and heat transfer and kinetic-related issues. They are composed, at least, by two materials: a support matrix, which is a porous structure, and the active material, which is contained in the pores of the matrix and is involved in the sorption process. Typical studied composites are salt hydrates within matrix of zeolite or silica gel. The host matrix porosity represents a trade-off parameter: it should be large enough to contain the highest possible amount of reactive material, but it should also properly enable sorbate transport within the material. It must be considered that also the matrix participates to the sorption phenomenon, so that a compromise should be reached as regard the pore size, since the presence of large pores increases the amount of active material retained but limits the participation of the matrix to the sorption process.

On of the most performing composite material reported in literature [17] is composed by a matrix of activated carbon, silica solution (to enhance mechanical strength) expanded graphite (to enhance heat transfer) and Lithium Chloride as active material. The salt weight percent within the material was varied between 35 and 45 and, at a vapor pressure of 25.4 mbar, energy densities between 0.72 GJ/m^3 and 1.43 GJ/m^3 were achieved ($T_{desorption}$=30°C, $T_{sorption}$=90°C) [6]. Other materials, using especially $MgCl_2$,$CaCl_2$,Mg_SO_4, KCl and LiCl as active materials, have been developed, showing values of energy density around 0.6 GJ/m^3 [6].

1.4 Thermodynamic analysis of Salts hydration reactions

Hydration reactions of salts have been deeply studying for thermochemical storage applications [1] [18], due to high theoretical energy density values associated. Donkers et al have recently reviewed more than 560 reactions [19], from which three promising salts were selected and further deeply investigated: potassium carbonate K_2CO_3, magnesium chloride $MgCl_2$ and sodium sulphide Na_2S. The selected salts represent the materials adopted in this work for the TCS modelling on system level within MES. It is thus essential, for the further development of the thesis, to fully characterize them, starting with the introduction of some basic thermodynamic concepts.

A generic dehydration/hydration reaction of a salt may be expressed as in Eq. 1.9:

$$salt \cdot nH_2O_{(s)} \leftrightarrow salt \cdot mH_2O_{(s)} + (n-m)H_2O_{(g)} \quad (1.9)$$

The salt undergoes a dehydration process from a number of water moles n to m, with consequent release of water vapour. In principle, the reactive gas may also be ammonia or methanol, but, for residential applications, water is considered the most suitable one (simpler to deal with from a plant complexity and safety-related issues point of views).

The decomposition reaction is endothermic, with an associated enthalpy of reaction $\Delta H_{n\rightarrow m}$ [J/mol], defined in Eq. 1.10 [1]**:**

$$\Delta H_{n\to m} = -\left(\sum_{\text{reactants}} \Delta H_i - \sum_{\text{products}} \Delta H_i\right) = -\Delta H_{m\to n} > 0 \qquad (1.10)$$

The reverse hydration reaction is exothermic, characterized by an enthalpy of reaction $\Delta H_{m\to n} < 0$.

It is possible to find an analogy between an absorption process and a liquid-vapour phase transition, since both involve transitions between vapour and condensed phases. At the equilibrium between two phases of the same substance, the modified Vant'Hoff relationship can be applied [Donkers et al] and is introduced in Eq. 1.11:

$$-\ln\frac{p}{p_0} = \frac{\Delta H^0_{m\to n}}{RT} - \frac{\Delta S^0_{m\to n}}{R} \qquad (1.11)$$

where p is the pressure [Pa], T is the temperature [K], $\Delta H^0_{m\to n}$ is the standard molar enthalpy of reaction [J/mol], $\Delta S^0_{m\to n}$ the standard molar reaction entropy [J/(mol K)] and R the ideal gas constant [J/ (mol K)]. Standard conditions, denoted by the apex "0", are characterized by the values of standard pressure and temperature p_0=1 bar and T_0=298.15 K.

Eq. 1.11 represents equilibrium properties associated to a general hydration reaction and is very useful for the hydration/dehydration process understanding and cycle design. It can, indeed, be represented in the Clausius-Clapeyron diagram $\ln p \div (-1/T)$, as a straight line with slope strictly related to the enthalpy of reaction ($\Delta H^0_{m\to n}/RT$).

Values of standard enthalpy and entropy of reaction can be easily found in literature for many common sorbent-sorbate couples and can also be calculated from standard enthalpy of formations of reactants.

The schematic representation of hydration and dehydration reactions in the Clapeyron diagram is shown in **Figure 1.6**.

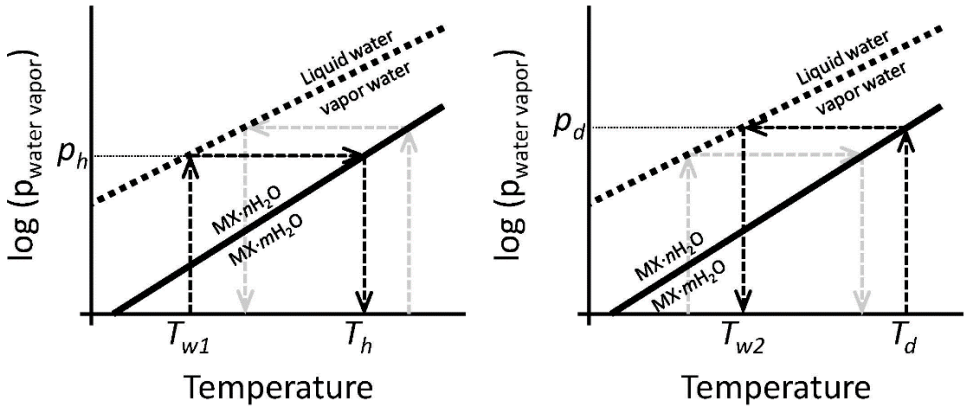

Figure 1.6. Representation of hydration and dehydration reactions in the Clapeyron diagram [1].

At the beginning of the hydration reaction, the system, which is composed by the hydrated form $MX \cdot mH_2O$, is put in contact with water vapor at temperature T_{w1}, corresponding to a pressure p_h, as can be noticed from water saturation curve. The applied condition, in terms of water vapour pressure, leads to the progressive hydration of the material into the form $MX \cdot nH_2O$, until the equilibrium temperature T_h is reached. The inverse process occurs for the dehydration phase: a temperature T_d, corresponding to a vapor pressure p_d, is applied to the material, in the initial form $MX \cdot nH_2O$, which dehydrates into $MX \cdot mH_2O$ as long as the vapor pressure reaches the equilibrium value p_d. The process can be better visualized and understood considering the whole storage cycle, shown in **Figure 1.7**.

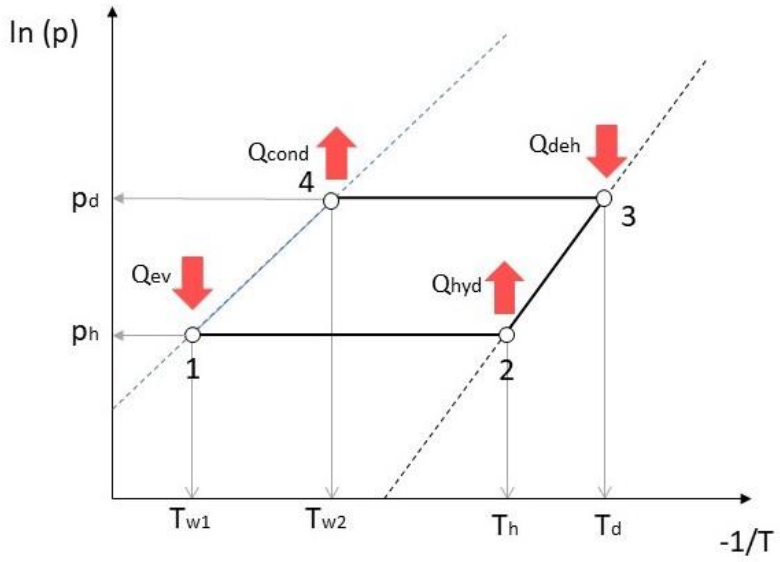

Figure 1.7. Representation of an adsorption cycle in the Clausius-Clapeyron diagram.

The presented graphical representation is based on an ideal single step cycle. The left dot line represents water liquid-vapor equilibrium curve, whose slope is associated to water enthalpy of vaporization. Water is evaporated through the heat flow Q_{ev} at temperature T_{w1} and pressure p_h (state 1), then reacts with the salt, with consequent release of heat Q_{hyd} (state 2). The material is, at this point, fully discharged: it is completely hydrated; considering the charging phase, an amount of sensible heat is required for reaching the dehydration temperature T_d, corresponding to the dehydration pressure p_d. In this condition, the endothermic dehydration reaction occurs due to the heat provided by a thermal flow Q_{deh}(state 3). Water is, consequently, desorbed and released as vapor, and the material is fully dry. Desorbed water is condensed, at temperature T_{w1} and pressure p_d (state 4). After material cooling down, which typically spontaneously occurs during the energy conservation phase, the cycle can restart bringing water in thermodynamic state 1.

When dealing with reversible chemical reactions, a very important concept to be considered is represented by the inversion temperature, defined as the temperature for which the Gibbs free energy variation is equal to zero:

$$\Delta G = \Delta H - T_{inv}\Delta S = 0 \rightarrow T_{inv} = \frac{\Delta H}{\Delta S} \qquad (1.12)$$

Considering reactions involving salts, the hydration reaction is spontaneous, i.e. characterized by a negative value of Gibbs free energy variation, while the occurring of dehydration reaction requires temperatures higher than the inversion temperature. The inversion temperature is, therefore, a key quantity to evaluate when studying a given material, because it suggests what kind of thermal source should be exploited for the material dehydration, thus representing one of the most significant filters for storage materials selection. Referring to **Fig. 1.7**, it thus results that the dehydration temperature T_d should be higher or equal to the inversion temperature.

Another essential parameter to evaluate is the hydration temperature T_h, i.e. the temperature reached by storage material after the hydration exothermic reaction. Its value should be compatible with the desired applications, i.e. space heating and domestic hot water production.

Attention must be paid also to water thermodynamic state 1, whose corresponding pressure and temperature result from an evaporation process, as previously stated. The availability of a low

temperature heat source for water evaporation is still an open issue, and, in practice, limits the range of values which can be assumed by T_{w1}.

Having provided a brief conceptual framework, it is now possible to evaluate one of the most significant property: the energy density. It can be evaluated from the molar enthalpy of reaction, as follows:

$$e = \frac{(n-m)\Delta H^0_{m\to n}}{\frac{M_n}{\rho_n}} \qquad (1.13)$$

being M_n [kg/mol] the molar mass and ρ_n[kg/m^3]the density of the highest hydrate. The energy density e is then evaluated in J/m^3.The other terms have already been introduced.

It is worth underlining that to assume standard conditions, for the evaluation of the energy density and the determination of equilibrium curves is an approximation, because of reaction enthalpy dependence on temperature; it can however be considered acceptable, since the temperature ranges involved in hydration/dehydration processes would lead to slightly variations.

If the thermochemical storage unit is a closed system, i.e. a system in which the working fluid is a part of the reactor and is stored in vessels, the energy density value is reduced, because the related volume occupation must be accounted.

For a generic salt, different hydration states are possible, which means that, in a full hydration/dehydration process, different sub-reactions occur. The overall energy density is thus given by the contribution of the enthalpy of reaction associated to all the transitions between hydrated states, and can be evaluated as follows [1]:

$$\Delta H^0_{1\to k} = \sum_{i=1}^{k-1} \left|\Delta H^0_{m_i\to n_i}\right| \cdot (n_i - m_i) \qquad (1.14)$$

where *k* represents the number of hydration states.

It is now possible to focus on the TCS materials taken as a reference in this work, as previously explained: potassium carbonate K_2CO_3, magnesium chloride $MgCl_2$ and sodium sulphide Na_2S. For all materials, values of enthalpy and entropy of reaction adopted in the following study are taken from literature and reported in **Table 1.2,** with the respective sources. It must be underlined that many values of enthalpy and entropy of reactions are available in literature, as well as many p-T experimental curves. The reference study, for the involved properties, in this work is represented by the research of Donkers et al [1][11], who validated experimentally equilibrium curves for the materials of interest. Significant variations may occur between different data sources, so that the provided quantities must be considered subject to error.

$MgCl_2$		
transition	*ΔS^0 [J/mol K]*	*ΔH^0 [KJ/mol]*
2-4 [1]	140	64.6
4-6 [1]	118	52
K_2CO_3		
0-1.5 [1]	155	63.6
Na_2S		
0.5-2 [1]	171	72
2-5 [1]	149	62.9
5-9 [1]	148	55.3

Table 1.2. Enthalpy and entropy of reactions values related to hydration transition of K_2C0_3 , $MgCl_2$, Na_2S.

Potassium carbonate hydrates reaching the form $K_2CO_3 \cdot 1.5H_2O$. The corresponding hydration reaction is:

$$K_2CO_{3(s)} + 1.5H_2O_{(g)} \rightarrow K_2CO_3 \cdot 1.5H_2O_{(s)} \qquad (1.15)$$

The maximum corresponding energy density corresponding is equal to 1.3 GJ/m^3, supposing an open configuration (1,24 GJ/m^3 in a closed system).

The equilibrium curve in the Clausius-Clapeyron diagram is achieved through Eq. 1.11, using standard enthalpy end entropy values reported in **Table 1.1**. Phase diagram of K_2CO_3 is shown in **Figure 1.8**.

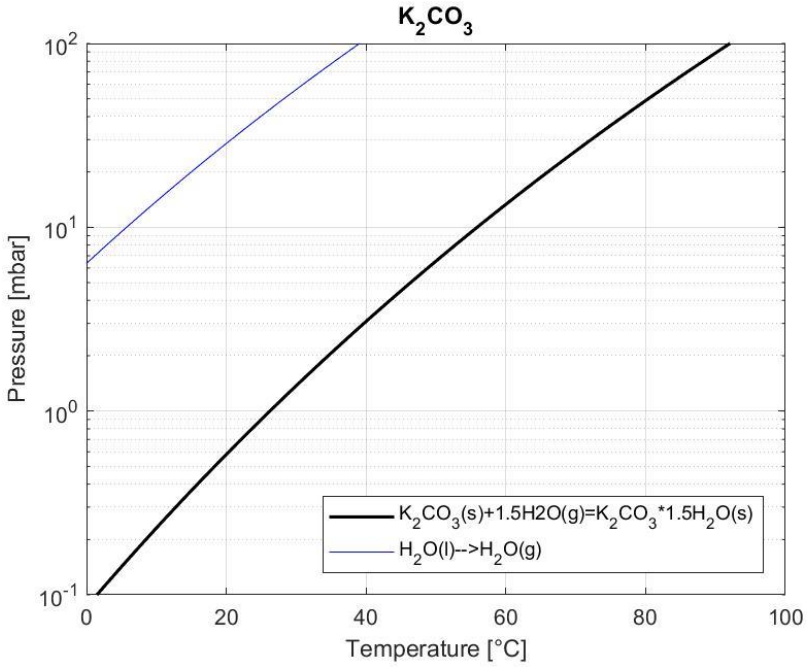

Figure 1.8. Phase diagram of K_2CO_3.

From the phase diagram some useful information can be deduced, such as hydration and dehydration temperatures. For example, during the charging phase, if the material is exposed to a water vapor pressure of 12 mbar, which is a typical design value, corresponding to a temperature of 10°C, a maximum hydration temperature of 59°C is experienced. During the dehydration phase, applying a temperature of 65°C, a vapour with a pressure of 20 mbar [19]. This type of consideration can be extended to an interval of pressures and temperatures, to the aim of identifying the most suitable condition, within the limits represented by the available external water evaporation and dehydration sources. Varying the evaporation pressure within a reasonable operating range, also another property varies, i.e. the enthalpy of reaction. This happens when different hydration reactions are possible for a given salt, occurring at different values of pressures and temperatures, as will be clear analysing magnesium chloride and sodium sulphide. From literature [19] it is known that, for conditions of low pressure and low

temperature, K_2CO_3 reacts with CO_2, producing potassium bicarbonate $KHCO_3$, which represents an undesired side reaction.

The second salt considered is magnesium chloride, whose phase diagram is represented in **Figure 1.9**.

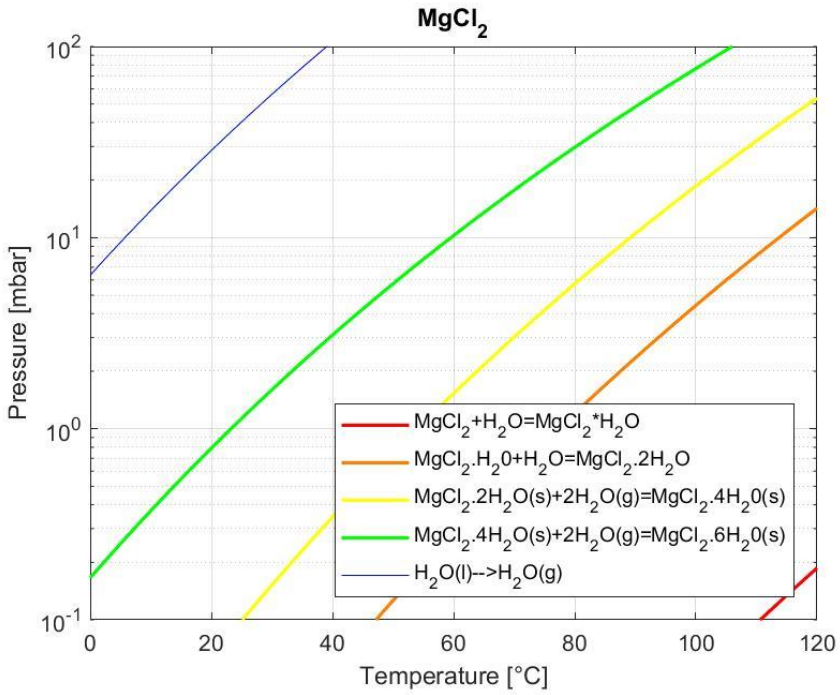

Figure 1.9. Phase diagram of $MgCl_2$.

In Donkers et al. [19], only 2-4 and 4-6 transitions are experimentally verified and considered. In any case, in the area below the dihydrate- tetrahydrate equilibrium, HCl formation occurs, with consequent material degradation. The reference reactions are thus:

$$MgCl_2 \cdot 2H_2O_{(s)} + 2H_2O_{(g)} \rightarrow MgCl_2 \cdot 4H_2O_{(s)} \quad (1.16)$$

$$MgCl_2 \cdot 4H_2O_{(s)} + 2H_2O_{(g)} \rightarrow MgCl_2 \cdot 6H_2O_{(s)} \quad (1.17)$$

In the upper-left area of the diagram (above the green line) the deliquescence phenomenon occurs, i.e. the material dissolves in the absorbed water. An effective representation of the

amount of energy which can be store consists in evaluating the enthalpy of reaction as a function of the hydration temperature. This investigation is accomplished at different values of evaporation pressure and is shown in **Figure 1.9**.

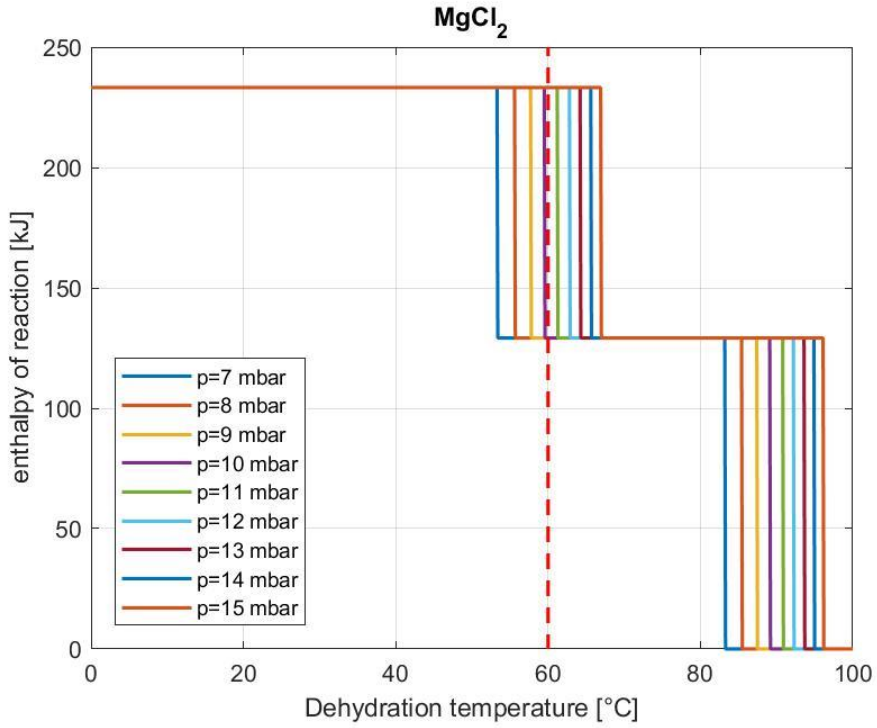

Figure 1.10. Variation of the enthalpy of reaction with respect to the hydration temperature.

The represented plot is achieved through the calculation of equilibrium temperatures, from Eq. 1.11, at different values of pressure. The different levels of enthalpy of reaction are associated to the presence of different hydration states and discontinuities are observed at equilibrium temperatures, where the occurring of a hydration (or dehydration) step corresponds to an increase (or decrease) of ΔH.

It is evident that, to higher hydration states, correspond higher values of enthalpy of reaction and, consequently, higher energy density values, but the hydration temperature is lower compared to the one achievable at lower hydration states. This means, in other words, that for higher hydration states a bigger quantity of energy can be stored, but available at lower temperature. For example, one suitable value, in order the hydration temperature to be compatible with domestic water production and space heating, ranges around 60°C, which is highlighted in **Figure 1.9**. In order to guarantee this threshold value, it is possible to exploit the

material hydration leading to $MgCl_2 \cdot 6H_2O$ formation, which has the highest enthalpy of reaction associated, but only for a specific range of water vapour pressure ($p > 10$ mbar). Therefore, as a general consideration, to increase the pressure of the water vapour, available from an evaporation process induced by a low-temperature source, leads to the increase of the hydration temperature associated to a given hydration reaction.

Opposite conclusions can be reached considering the dehydration temperature, as may be easily deduced from the phase diagram in **Figure 1.8**: higher dehydration temperatures correspond to lower hydration states and water vapor pressures. This clearly suggests that a trade-off is required.

Considering that, in most of the studies, the design evaporation pressure stands around 12 mbar, within this work the reference hydration reaction for magnesium chloride is assumed to be the whole transition from $MgCl_2 \cdot 2H_2O$ to $MgCl_2 \cdot 6H_2O$:

$$MgCl_2 \cdot 2H_2O_{(s)} + 4H_2O_{(g)} \rightarrow MgCl_2 \cdot 6H_2O_{(s)} \qquad (1.18)$$

The corresponding energy density is equal to 1.93 GJ/m^3 (, while dehydration and hydration temperatures are, respectively, 104°C and 61°C, evaluated at the typical evaporation and condensation temperature of, respectively, 10°C (p=12 mbar) and 18°C (p=20 mbar) [19].

The last material considered is sodium sulphide, whose considered hydration reactions are reported in the following:

$$0.5Na_2S_{(s)} + 1.5H_2O_{(g)} \rightarrow Na_2S \cdot 2H_2O_{(s)} \qquad (1.19)$$

$$2Na_2S_{(s)} + 3H_2O_{(g)} \rightarrow Na_2S \cdot 5H_2O_{(s)} \qquad (1.20)$$

$$5Na_2S_{(s)} + 4H_2O_{(g)} \rightarrow Na_2S \cdot 9H_2O_{(s)} \qquad (1.21)$$

Sodium sulphide phase diagram is shown in **Figure 1.10**.

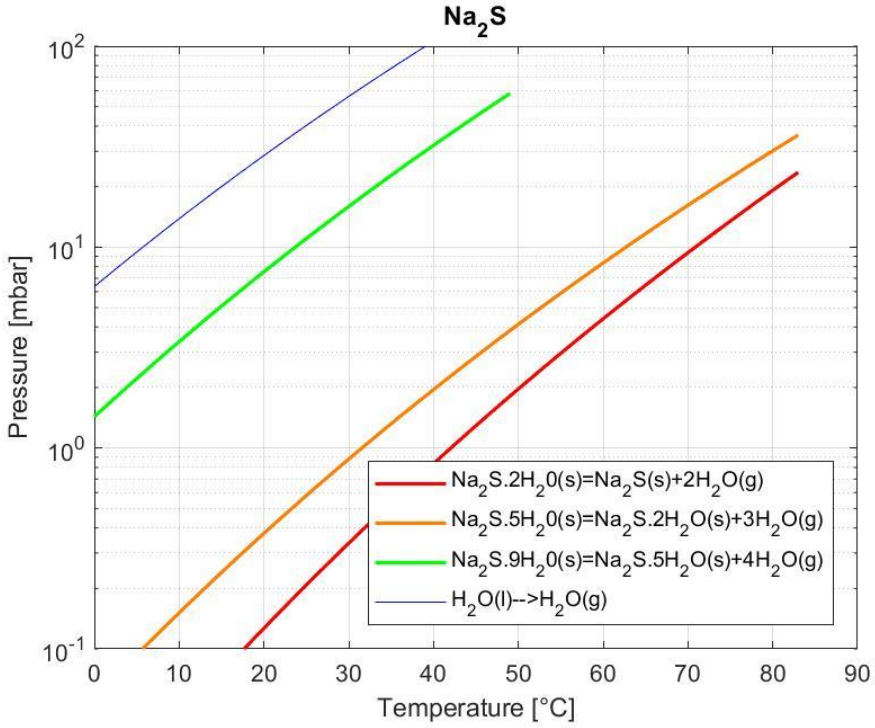

Figure 1.11. Phase diagram of Na_2S.

It must be pointed out that the, since Na_2S is very hygroscopic, the last water molecules within the material are very difficult to remove. Consequently, the anhydrous form is rarely observed, thus commonly the 0.5-5 transition in considered as the complete hydration reaction. In **Fig. 1.8**, for conditions (qualitatively) above the interruption of curves, the formation of a solution of sodium sulphide in water is observed. One of the main drawbacks is the occurring of a side reaction, for all the values of temperatures and pressure, which consists in the CO_2 adsorption [19]:

$$Na_2S_{(s)} + H_2O_{(g)} + CO_{2(g)} \rightarrow Na_2CO_{3(s)} + H_2S_{(g)} \quad (1.22)$$

Sodium carbonate formation occurs instantly in ambient conditions, which leads to the material degradation and to the necessity of adopting a closed system configuration.

Even in this case it could be interesting to make thermodynamic equilibrium-based considerations. To this purpose, the variation of enthalpy of reaction with respect to the hydration temperature is reported in **Figure 1.11.**

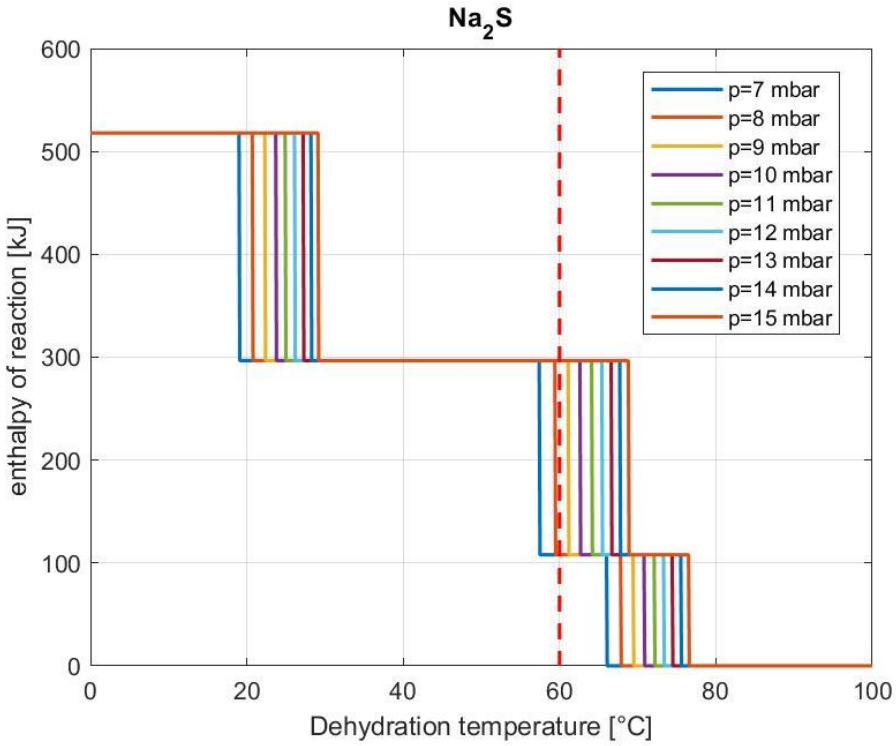

Figure 1.12. Variation of the enthalpy of reaction with respect to the hydration temperature.

The same qualitative considerations and comments done for the case of magnesium chloride are valid. In this case, to guarantee an acceptable hydration temperature, the maximum hydration state that can be reached is $Na_2S \cdot 5H_2O$, corresponding, in **Figure 1.11**, to the intermediate level of enthalpy of reaction. For this reason, within this work, the reference hydration reaction for sodium sulphide is represented by:

$$0.5Na_2S_{(s)} + 1.5H_2O_{(g)} \rightarrow Na_2S \cdot 2H_2O_{(s)} \qquad (1.23)$$

The associated energy density is equal to 2,79 GJ/m^3, the hydration temperature, is 66°C while the dehydration temperature is 82°C, for water vapor temperature and pressure conditions previously introduced [19].

At this point, as a result of the thermodynamic analysis developed, the choice of reference reactions for the thermochemical modelling appears fully justified. The corresponding parameters of interest are summed up in **Table 1.2**.

	Energy density [GJ/m^3] (open system)	Energy density [GJ/m^3] (closed system)	Hydration temperature [°C]	Dehydration temperature [°C]
K_2CO_3	1.3	0.96	66	82
$MgCl_2$	1.93	1.24	61	104
Na_2S	2.79	1.58	59	65

Table 1.3. Values of energy density and hydration and dehydration temperature at vapor pressure of, respectively, p=12 mbar and p=20 mbar [19].

As a final, important remark, all considerations developed, and quantities achieved in this paragraph are based on a *thermodynamic equilibrium approach.* They are, thus, theoretical values, significantly affected by reaction kinetics and heat transfer properties within the storage material. To take into account these phenomena, experimental analysis and also some numerical simulations have been developing. Therefore, in practice, this approach should be and is, through many research efforts, coupled with in-depth experimental investigation, also due to one of the major issues related to salt-hydrates exploitation for thermochemical storage, which is chemical stability. Side reactions have been superficially mentioned during the hydration reactions introduction and evaluation in this section, but their occurring has a dramatic impact on a storage system performance, in terms of energy density achievable and maximum number of cycles before material degradation. Moreover, hysteresis phenomena and partial melting of the structure are commonly observed during experimental testing. At the state of art of the technology, also for materials selected as the most promising ones, these issues have yet not been overcome, which has been leading to an intense research effort on the material level.

Chapter II

Methodology

In this chapter the optimization tool, developed by Gabrielli et al. [20] and supplemented with the modelling of thermochemical storage systems, is presented. A brief introduction about the concept of multi-energy system is provided, then the two case studies, objects of the current study, are introduced. Eventually, the whole methodology for the optimization problem setting is provided.

2.1 Multi-energy systems optimization problems

Multi-energy systems (MES) are decentralized systems based on multiple energy carriers and technologies, interacting at different levels (e.g. district, city, region, country levels). They are becoming a new paradigm of power production, allowing to increase systems performances from a technical, economic and environmental point of view, thus representing a valid solution for the decarbonization of the energy sector. Due to their complexity, MES are tricky and challenging engineering optimization problems, that have been attracting, in the last years, many research activities [21]. Different optimization tools, whose majority make use of mixed-integer linear programming (MILP), have thus been developed for the design and operation of MES, including some commercial tools such as EnergyPlan and DERCAM. When dealing with MES optimization problems, the large number of variables and constraints leads to the necessity of simplifying the time horizon and resolution, which can be accomplished through different techniques. Many of the developed tools assume one-year horizon and resort to the selection of design days, i.e. a restricted number of days representative of the yearly behaviour in terms of weather conditions, energy prices and energy demand. When seasonal storage systems are included in the MES configuration, traditional approaches based on the selection of design days are not acceptable, due to the discontinuity between the design days. Two novel approaches are thus presented in Gabrielli and co-workers for overcoming this issue, essentially based on coupling design days, as deeply discussed in [20].

The optimization problem of a multi-energy system allows to individuate the optimal configuration of the system, for the minimization of an objective function (e.g. the total cost), in terms of technologies to be installed, corresponding size and operation. In the current work, the problem is implemented in MATLAB and solved through the use of the commercial software IBM CPLEX.

The schematic representation of the optimization framework is shown in **Figure 2.1**.

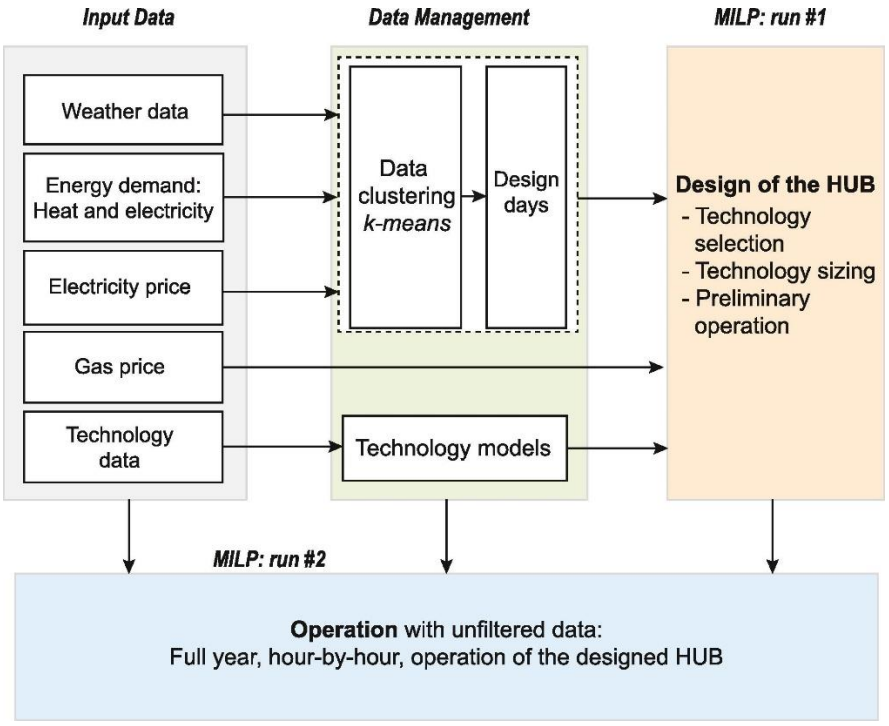

Figure 2.1. Optimization framework for MES design [20]

In **Fig. 2.1**, the clustering algorithm "k-means" represents an algorithm which allows to identify the design days as the most representative of the simulated year, and their sequence along the year []. To be specific, considered an initial range of days $1 \leq y \leq 365$, a sequence of day σ(y) is obtained so that $1 \leq \sigma(y) \leq D$, where D represents the number of design days adopted for the simulation.

The optimization problem is formulated as MILP, in the general form [20]:

$$\min_{x,y}(\mathbf{c}^{T}\mathbf{x} + \mathbf{d}^{T}\mathbf{y}) \qquad (2.1)$$

$$\mathbf{Ax} + \mathbf{By} = \mathbf{b} \qquad (2.2)$$

$$\mathbf{x} \geq 0 \in \mathbf{R}^{N_x}, \qquad \mathbf{y} \in \{0,1\}^{N_y} \qquad (2.3)$$

where **x** is the continuous decision variables vector, **y** the binary decision variable vector; **c** is the cost vector associated to continuous decision variables, **d** is the cost vector associated to binary decision variables; **A** and **B** are constraint matrices and **b** is the constraint known-term. N_x and N_y are dimensions of, respectively, **x** and **y**. The number of variables can be, in large multi-energy systems, significantly high, which directly translates into computational complexity, especially increased by the presence of binary decision variables.

2.2 Case studies

Thermochemical storage technology, based on K_2CO_3, $MgCl_2$ and Na_2S hydration reactions, is simulated in two different multi-energy systems. For both the cases, the user is represented by a single household placed in Utrecht, in the Netherlands. All the relevant data characterizing the user (yearly electric and heating demand, rooftop area exc.) will be provided in *Section 2.3*. In all the simulated scenarios, two boundary conditions regarding imported and exported energy are applied: no heat import is allowed, neither electricity export to the grid.

2.2.1 Case 1

The first simulated case includes a natural gas boiler, a solar thermal system and a thermochemical storage device, as illustrated in **Figure 2.2.**

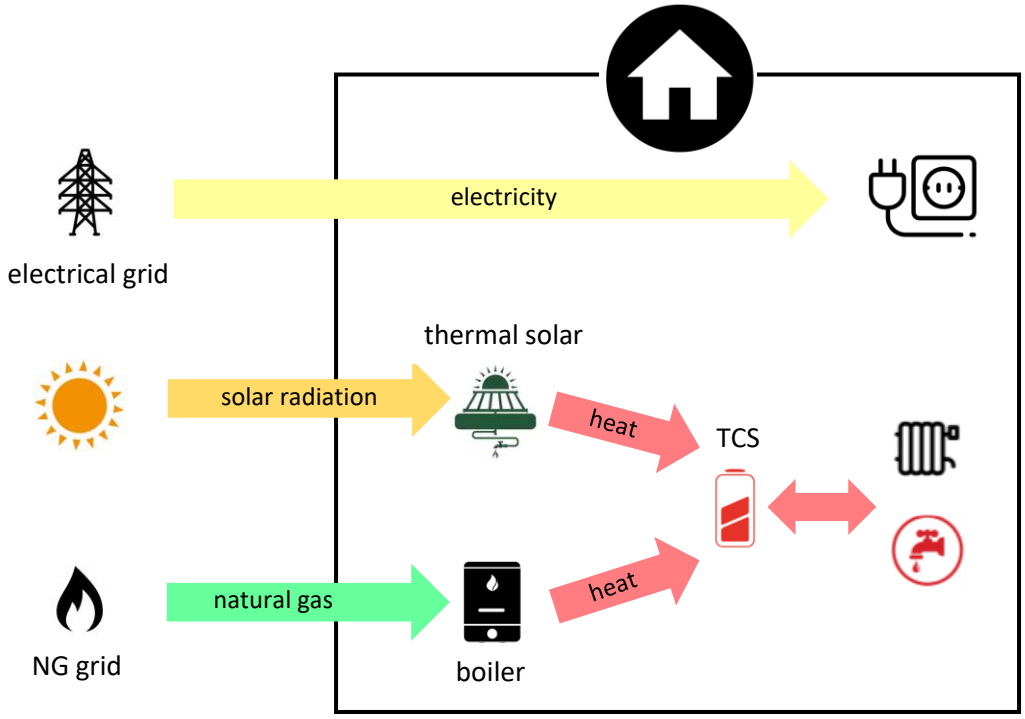

Figure 2.2. Schematic representation of Case 1: solar thermal system, natural gas boiler and TCS

This case has been studying and considering as the most promising scenario for the application of thermochemical storage, thanks to the relatively high available dehydration temperature (T>100°).

The natural gas boiler imports natural gas from the grid and produces thermal energy which, in principle, can be used for both satisfying the instantaneous thermal demand and dehydrating the storage material. Solar thermal collectors, placed on the house rooftop, convert solar radiation into thermal energy. The thermochemical storage system receives heat as input for the dehydration of material during the charging phase, while it releases thermal energy to the user during the discharging phase.

As regard the electric demand satisfaction, none of the technologies is involved, therefore all the needed electricity is imported from the grid.

2.2.2 Case 2

The second simulated MES is a micro-cogeneration system composed by a solid oxide fuel cell (SOFC) and the thermochemical storage. The fuel cell is fed by natural gas and produces electricity due to an overall exothermal process, which allows heat recovery. Typical SOFC operating temperature ranges between 600°C and 1000 °C, so that high-temperature reaction residuals are available for thermal recovery. Reaction products are typically heated in an after burner, in order to provide a larger amount of heat delivered to users and partly used to pre-heat fuel and air flows feeding the SOFC. The overall heat recovery process leads to a thermal efficiency, in domestic applications, around 30% (this value slightly varies according to operating parameters and system design). The schematic representation of the investigated case study is represented in **Figure 2.3**.

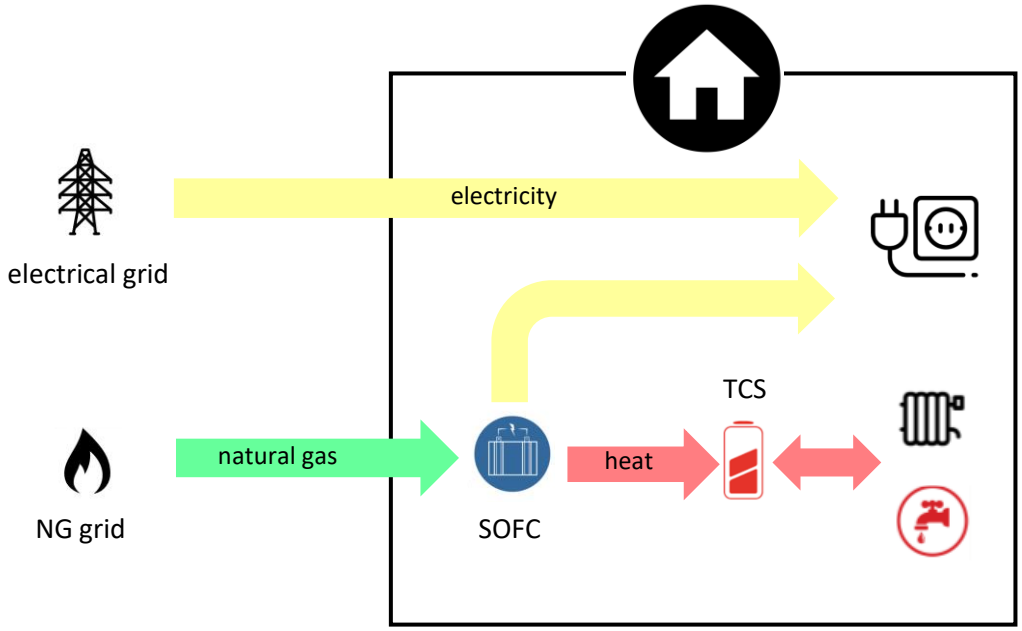

Figure 2.3. Schematic representation of Case 2: SOFC and TCS

2.3 Input data

The MILP implementation of the optimization problem requires as inputs [20]:

1. Utrecht weather conditions in year 2017, consisting in air temperature and solar irradiance for each hour of the year, since the simulation has an hourly resolution. Temperature and irradiance profiles are shown in **Figure 2.4** and **Figure 2.5**.

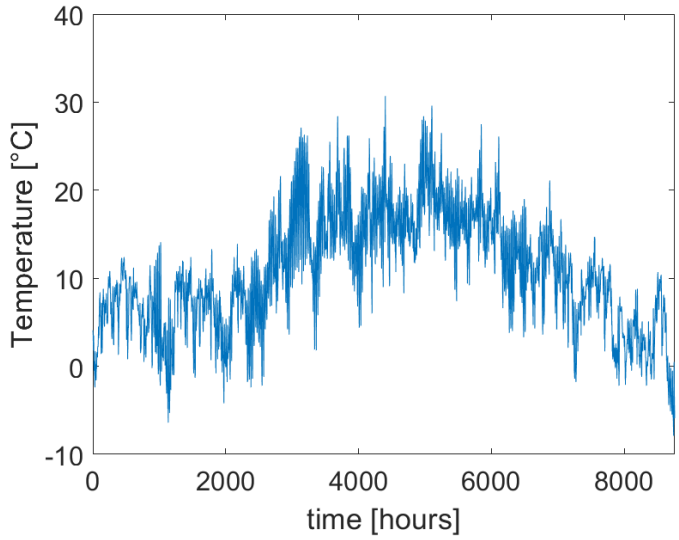

Figure 2.4. Temperature profile in Utrecht in 2017

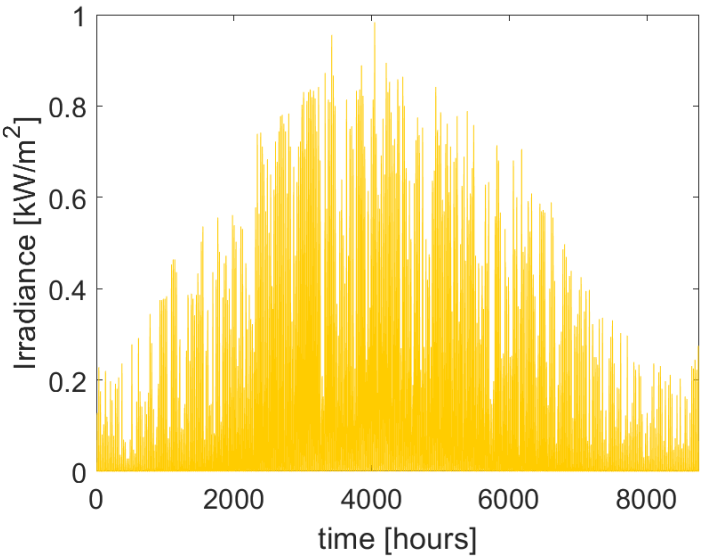

Figure 2.5. Irradiance profile in Utrecht in 2017.

2. Electricity and natural gas costs. For all the simulated cases, only user electricity self-consumption is foreseen. Natural gas import price is constant throughout the year, equal to 0.0641 €/kWh, while electricity price has a very volatile profile, due to a complex market regulation and a broad portfolio of electricity production technologies.

Electricity and natural gas import profiles are shown in **Figure 2.6** and **Figure 2.7** respectively

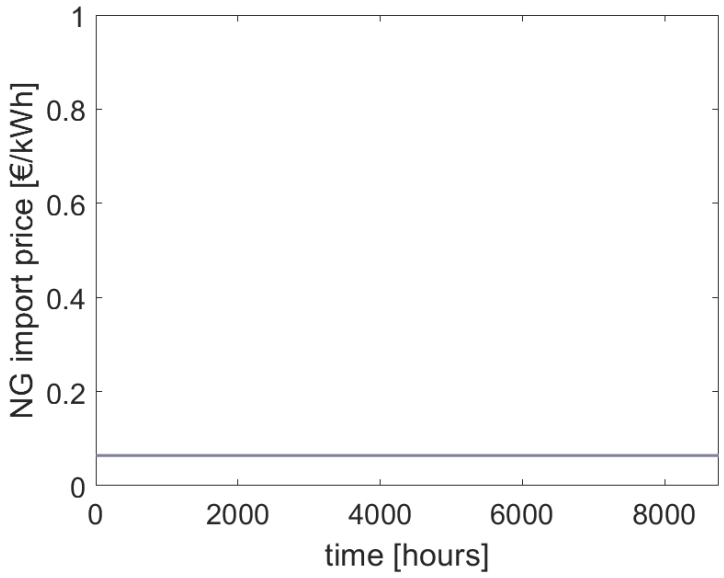

Figure 2.6. Natural gas import price in 2017 (Utrecht).

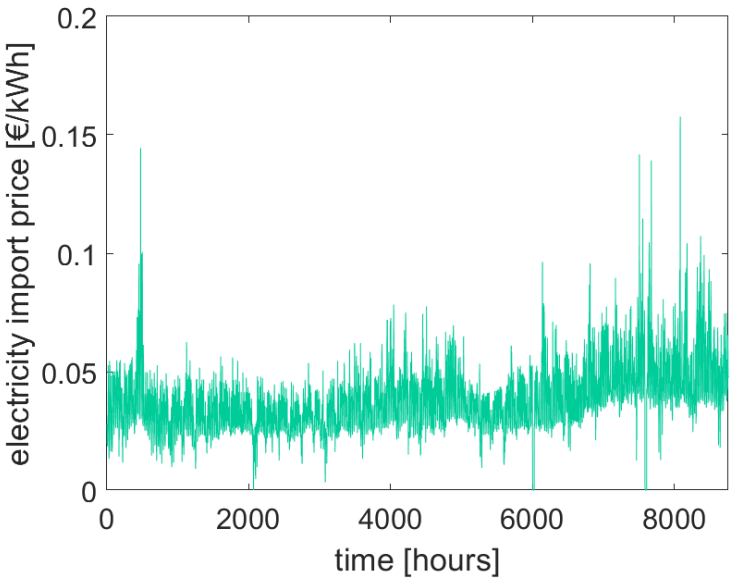

Figure 2.7. Electricity import price in 2017 (Utrecht).

3. Electricity and heat demand profiles for the considered year (2017) with an hourly resolution, shown in **Figures 2.8** and **Figure 2.9.** As previously stated, thermal energy demand is associated to space heating and domestic hot water production needing.

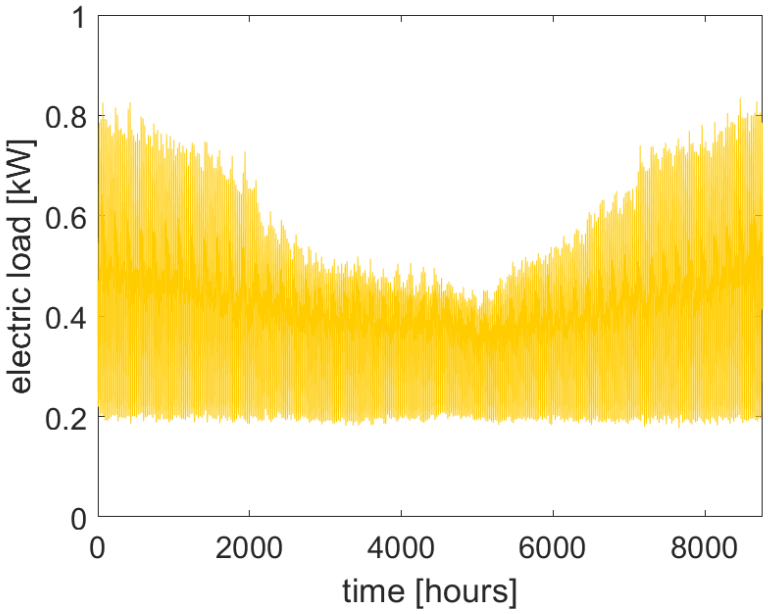

Figure 2.8. Electricity demand in 2017 (Utrecht).

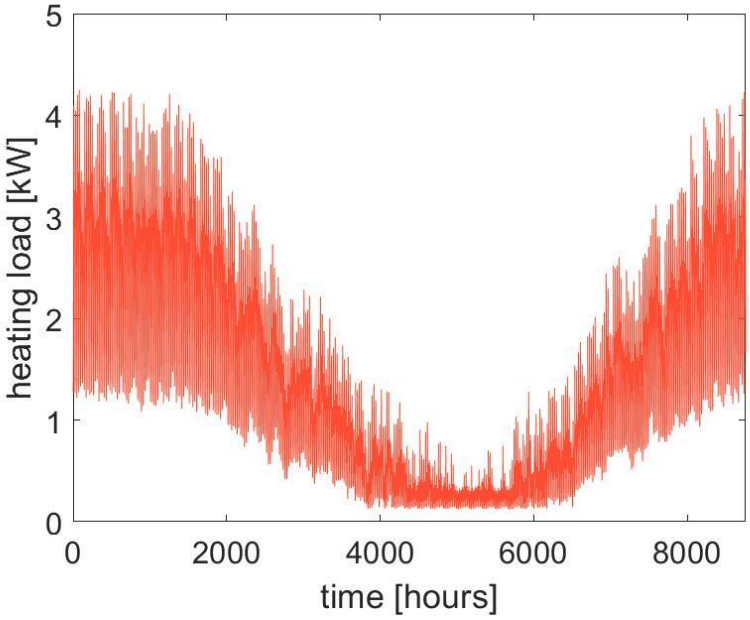

Figure 2.9. Heating demand in 2017 (Utrecht).

4. The set of available storage and conversion technologies within the MES and the related cost and performances coefficients. All the considered parameters, whose meaning will be clarified in *Section 2.5*, are presented in Appendix A.

2.4 Decision Variables

Decision variables may be continuous or binary and can be defined as design (e.g. size) or operation variables. They represent the solutions of the MES optimization problem, i.e. all the unknown variables whose optimal value is chosen in order to minimize the objective function (which will be introduced in *Section 2.6*). Decision variables are [20]:

- The size of the technologies selected as a result of the optimization problem. It is the rated input power for non-solar conversion technologies [kW], the installed area for solar conversion technologies, the energy capacity for storage technologies [kWh]. If a technology is not selected, the returned size is equal to zero.
- Binary variables, representing the on/off status of technologies. They assume value equal to one when the technology is installed, zero otherwise.
- Input and output power for each technology and each hour of the simulated year.
- The energy stored in the storage technology, for each hour of the year.
- Hourly imported electrical and gas power.

2.5 Constraints

The constraints of the optimization problem can be divided into two groups: performance of the conversion and storage technologies and energy balances. The first category includes relations expressing technologies performances, in terms of produced thermal and electrical power. Affine and piece-wise affine correlations are used and derived from first-principle models or manufacturer data fitting [20]. Performances and balances constraints hold for all the simulation time steps.

2.5.1 Performances of the technologies

Natural gas boiler

The generated thermal power P_t [kW] is expressed as [20]:

$$P_t = \alpha F_t \qquad (2.4)$$

$$0 \leq F_t \leq S \qquad (2.5)$$

being F_t the input power [kW], α a conversion coefficient and S is the size (i.e. rated power [kW]). The dependence of boiler performances on the size are neglected [20].

Thermal solar panels

Output thermal power P_t [kW] is expressed as [20]:

$$P_t = \eta I_t S \qquad (2.6)$$

$$0 \leq S \leq A_{rooftop} \qquad (2.7)$$

being S is the installed area [m^2], I is the solar irradiance [kW/m^2], $A_{rooftop}$ the rooftop area [m^2], equal to 16,71 m^2; η is the conversion efficiency. It must be underlined that a further constraint equation is needed to limit the sum of the PV and solar thermal panels installed area to a value equal or lower than the rooftop area.

Solid oxide fuel cells

SOFC performances are modelled through the use of a piecewise affine approximation, based on first principle models. The resulting equation (Eq. 2.8), expression of the produced electric power P_t, is applied to all line segments *i* approximating the curve of performance [20]:

$$P_t \leq \alpha_i F_t + \beta_i S x_t \qquad (2.8)$$

$$\partial S x_t \leq F_t \leq S x_t \qquad (2.9)$$

where α and β are correlation coefficients of the i-th line segment, S is the size (the rated power), F_t is the inlet fuel power (natural gas lower heating value); x_t is binary variable representing the on ($x_t = 1$) and off (x_t=0) status of the technology; ∂S represents the minimum inlet power consumption, while the maximum one is the size [20]. Being fuel cells co-generative systems, an equation for the produced thermal power Q_t is introduced [20]:

$$Q_t = P_t(\rho - 1) \qquad (2.10)$$

being ρ, provided as input parameter, the average ratio of first-principle to electrical efficiency:

$$\rho = \frac{\eta_I}{\eta_{el}} = \frac{Q_t + P_t}{F_t} \cdot \frac{F_t}{P_t} = \frac{Q_t + P_t}{P_t} \qquad (2.11)$$

Further equations describing the dynamic behaviour of the technology are exhaustively presented in [21] and, specifically, consider start-up/shut-down power trajectories, ramp-up/ramp-down limitations and transients.

It eventually must be underlined that the oxidant assumed within the model is air, instead of pure oxygen.

Salt hydrates-based thermochemical storage systems

The materials selected for the implementation of thermochemical storage within the optimization framework are sodium sulphide Na_2S , magnesium chloride $MgCl_2$ and potassium carbonate K_2CO_3, for which different hydration reactions are possible, as known from the *Chapter I*. The ones taken into considerations for the simulations are the following:

$$0.5Na_2S(s) + 1.5H_2O(g) \rightarrow Na_2S \cdot 2H_2O(g) \quad (2.12)$$

$$K_2CO_3(s) + 1.5H_2O(g) = K_2CO_3 \cdot 1.5H_2O(s) \quad (2.13)$$

$$2MgCl_2(s) + 4H_2O(g) = MgCl_2 \cdot 6H_2O(s) \quad (2.14)$$

The values of costs, energy density and materials density used as input data for the simulation are summarized in **Table 2.1**.

	Material cost [€/kg]	Energy density [GJ/m^3]	Density [kg/m^3]	Cost [€/kWh]
Na_2S	0.348 [4]	2.81	1580	0.704
K_2CO_3	1 [1]	1.30	2428	6.829
$MgCl_2$	0.154 [4]	1.93	1568	0.451

Table 2.1. Thermochemical storage materials data

The energy density values are introduced in *Section 1.4,* while the costs per kWh are achieved as follow:

$$c_{energy} = \frac{c_{mat} \cdot \rho}{e} \qquad (2.15)$$

where c_{mat} is the material cost $\left[\frac{€}{kg}\right]$, ρ is the density of the highest hydrate $\left[\frac{kg}{m^3}\right]$ and e the volumetric energy density $\left[\frac{kWh}{m^3}\right]$.

The modelling within the optimization framework is based on the storage technology model developed in [20] and further modified. It starts from the introduction of an energy balance, given by the following linear equation:

$$E_t = E_{t-1}(1 - \Lambda\Delta t) + \eta P_t \Delta t \qquad (2.16)$$

where:

- E [kWh] represents the energy within the storage system;
- t is the subscript related to time discretization (hourly resolution);
- Δt is the simulation time step (1 hour);
- P_t [kW] is the charging/discharging power, assuming positive and negative values respectively;
- Λ [1/h] is a self-discharge parameter [20], accounting for thermal losses, since the storage is not perfectly isothermal, especially during charging and discharging phases. It also includes losses due to the imperfect sealing of the storage device, which may lead to humidity penetration and, consequently, to material discharging. This appears reasonable to occur especially in summer, when the vapour pressure content of the external air is higher.
- η represents the charging/discharging efficiency, defined as:

$$\eta_{charging} = \frac{E_{input}}{E_{stored}} \qquad (2.17) \qquad \eta_{discharging} = \frac{E_{released}}{E_{stored}} \qquad (2.18)$$

All terms are self-explaining. For these conceptually different parameters, the same value is assumed within the simulation, reported in Appendix A, with all the input parameters.

The following linear constraints, limiting stored energy and input/output power in proper ranges, are also applied [20]:

$$0 \leq E_t \leq S \qquad (2.19)$$

$$-\frac{S}{\tau} \leq P_t \leq \frac{S}{\tau} \qquad (2.20)$$

being S the size [kWh] and τ [h] is the time required to fully charge and discharge the storage.

An equation coupling energy values at the end and at the beginning of the year is eventually required:

$$E_0 = E_T \qquad (2.21)$$

where t=0 stands for the first hour of the year, T=8760.

A further equation, coupling energy values at the end of each day and at the beginning of the following one, is also implemented and expressed in Eq. 2.22, according to one of the two novel approaches for time horizon modelling presented in [20] (method M1).

$$E_{y,1} = E_{y-1,24}(1 - \Lambda\Delta t) + \eta P_{\sigma(y)}\Delta t \qquad (2.22)$$

Where the first subscript y indicates the day of the year ($1 \leq y \leq 365$), while the second one stands for the hour of the day; $\sigma(y)$ represents the sequence of design days, as introduced in *Section 2.1.*

Since the aim of the simulations is to fully understand the role of thermochemical storage within different types of MES, and, consequently, to provide useful guidelines for the further development of the technology, great importance is especially assumed by three parameters: the charging/discharging efficiency η, the self-discharge coefficient Λ and the storage system specific investment cost. A sensitivity analysis is thus carried out for each type of material and configuration, adopting the following ranges and steps of variation:

$$0.6 \leq \eta \leq 0.8 \quad , \qquad \Delta\eta = 0.01 \qquad (2.23)$$

$$0 \leq \Lambda \leq 0.015 \quad , \qquad \Delta\Lambda = 0.001 \qquad (2.24)$$

$$\mathrm{c_{mat}} \leq \mathrm{c_s} \leq 10 \cdot \mathrm{c_{mat}} \quad , \qquad step = 2 \cdot c_{mat} \qquad (2.25)$$

being c_{mat} the cost of material [€/kWh].

2.5.2 Energy balances

The three energy carriers considered are electricity, heat and natural gas. For each time-step and for each energy carrier $j \in N$, the following energy balance must be satisfied [20]:

$$\sum_{i \in M} \left(U_{j,i,t} + P_{j,i,t} - V_{j,i,t} - F_{j,i,t}\right) - L_{j,t} = 0 \qquad (2.26)$$

where M is the set of available technologies, whose index is i; U is the imported energy, P id the energy produced, V the exported energy, F the energy absorbed and L the user energy demand [20].

2.6 Objective function

The objective function of the optimization problem is the total annual cost of the simulated system, which results from the combination of investment cost, maintenance cost and operation cost. The investment cost J_c can be expressed as [20]:

$$J_c = \sum_{i \in M} (\lambda_i S_i + \mu_i)\omega_i \qquad (2.27)$$

where i is the index associated to the M technologies; λ is the variable cost coefficient [€/kW], μ is the fixed cost coefficient [€] [20]; ω is the annuity payment factor, which allows to calculate the equivalent yearly investment cost corresponding to a loan to be repaid in a number of years equal to the system lifetime. Its expression is given in Eq. 2.28.

$$\omega = \frac{r}{1 - \frac{1}{(1+r)^t}} \qquad (2.28)$$

being r the interest rate, assumed equal to 6%, and t the number of payments periods, equal to the system lifetime (it must be underlined that for each component within a MES different values of lifetime are considered).

The annual operation cost J_o can be calculated considering the yearly imported and exported energy flows. Its expression is [20]:

$$J_o = \sum_{j \in N} \sum_{i \in M} \sum_{t=1}^{T} (u_{j,t} U_{j,i,t} - v_{j,i,t} V_{j,i,t}) \Delta t \qquad (2.29)$$

where, as previously introduced, N and M represent, respectively, the set of carriers and the set of technologies, whose corresponding indexes are j and i; t is the instant of time, going from the first hour of the simulated year to the last one (T=8760); u and v are the import and export prices; U and V are the import and export powers; Δt is equal to one hour, since the resolution is hourly [20].

The annual maintenance cost J_m is calculated as a fraction ψ of the investment cost [20]:

$$J_m = \sum_{i \in M} \psi_i J_{c,i} \qquad (2.30)$$

The total yearly cost is given by the sum of the three different costs.

Chapter III

Results

In this chapter the most relevant results of the simulations are presented. As known from *Chapter 2*, the optimization problem is characterized by many decision variables involving all technologies and carriers. For the purpose of this work, i.e. assess TCS role within multi-energy systems, the most relevant design variables are considered to be: i) the installed size, ii) the corresponding volume, iii) yearly stored energy and iv) system costs.

Results are organized in two sections, representing the two reference case studies introduced in *Section 2.2*.

3.1 Case 1

The first case study is a MES composed by solar thermal panels, a natural gas boiler and a thermochemical storage system.

As introduced in *Section 2.5.1*, a sensitivity analysis is performed for the main parameters characterizing the TCS technology, for the three reference TCS materials.

3.1.1 Role of charging/discharging efficiency

The optimization problem is solved for values of charging/discharging efficiency η in a range between 0.6 and 0.8, with a considered step $\Delta\eta = 0.01$, with the hypothesis of self-discharge coefficient equal to zero ($\Lambda = 0$).

Potassium Carbonate ($\mathbf{K_2CO_3}$)

The optimal installed size (energy capacity) of the TCS system as a function of η is shown in **Figure 3.1**.

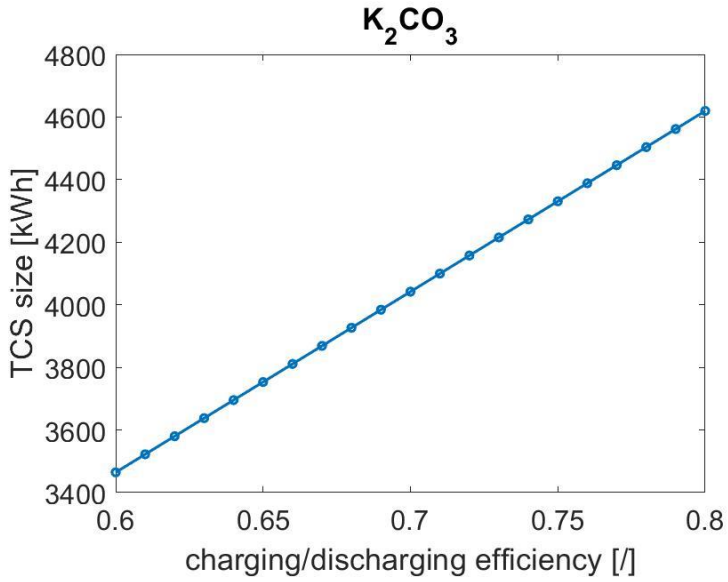

Figure 3.1. Optimal energy capacity as a function of charging/discharging efficiency (Case 1, material=K_2CO_3).

The first useful information that can be achieved is that, for all the considered efficiencies, the TCS technology is selected, i.e. it belongs to the optimal configuration, which is not trivial. A linear behaviour, from a minimum value of around 3,5 MWh to a maximum of 4,6 MWh, is observed, according to which, increasing the charging/discharging efficiency, it results convenient to increase the installed size. The system always chooses the maximum size that can be installed according to Eq. 2.20, which represents a size constraint. With reference to the TCS energy balance in Eq. 2.16 ($E_t = E_{t-1}(1 - \Lambda\Delta t) + \eta P_t \Delta t$), the linear behaviour can thus be explained considering that the input/output power P is fixed as the maximum possible, so that the storable energy varies linearly with respect to the efficiency.

It may be interesting to evaluate the optimal sizes associated to the other technologies involved, and asses the influence of the charging/discharging efficiency (or, better, of the consequent TCS size variation) on their values, as shown in **Figure 3.2**.

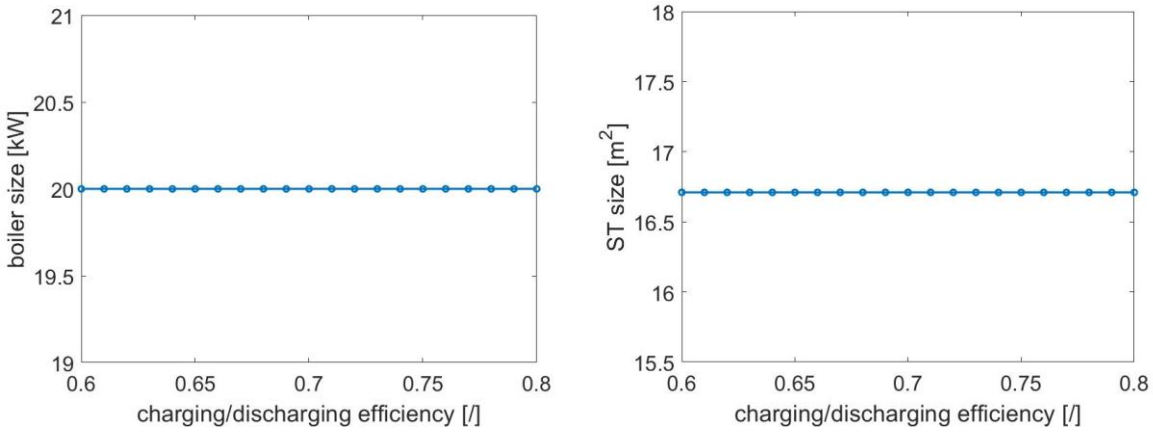

Figure 3.2. Boiler size [kW] (left) and solar thermal system size [m^2] (right) dependence on TCS system charging/discharging efficiency (Case 1, TCS material:K_2CO_3)

Boiler and solar thermal system optimal sizes are not affected by the storage efficiency. They assume, respectively, a constant value of 20 kW which appears quite high for a back-up boiler but coherent with domestic boiler values, and of 16, 7 m^2, that correspond to the maximum roof availability.

In order to provide a more immediate interpretation of the obtained results concerning TCS, a plot analogous to the one shown in **Figure 3.1** is illustrated in **Figure 3.3**. The y-axis is replaced with the volume of material corresponding to the optimal size, simply dividing the latter one by the energy density.

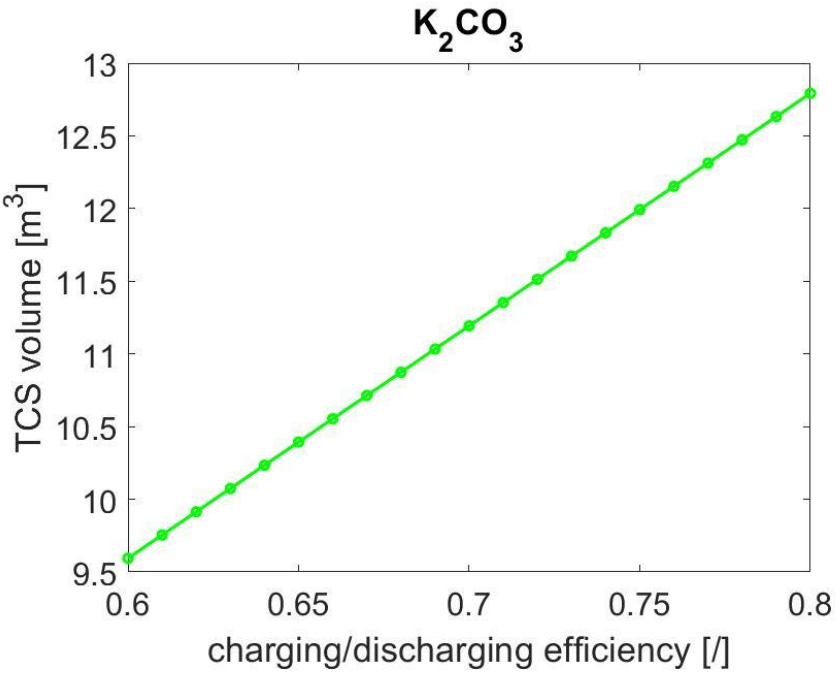

Figure 3.3. TCS volume as a function of charging/discharging efficiency (Case 1, TCS material: K_2CO_3)

A linear behaviour of the volume is observed, within a range between approximately 9.5 m^3 and 13 m^3. The volumes required appear to be quite large, due to the relatively low energy density of potassium carbonate with respect to the optimal values of energy to be stored resulting from the optimization process. A system like this seems hardly feasible, especially for domestic applications.

It is significant now to evaluate how the TCS technology is operated during the year, i.e. to consider the energy stored at each timestep of the simulation. The hourly energy profile is shown in **Figure 3.4**.

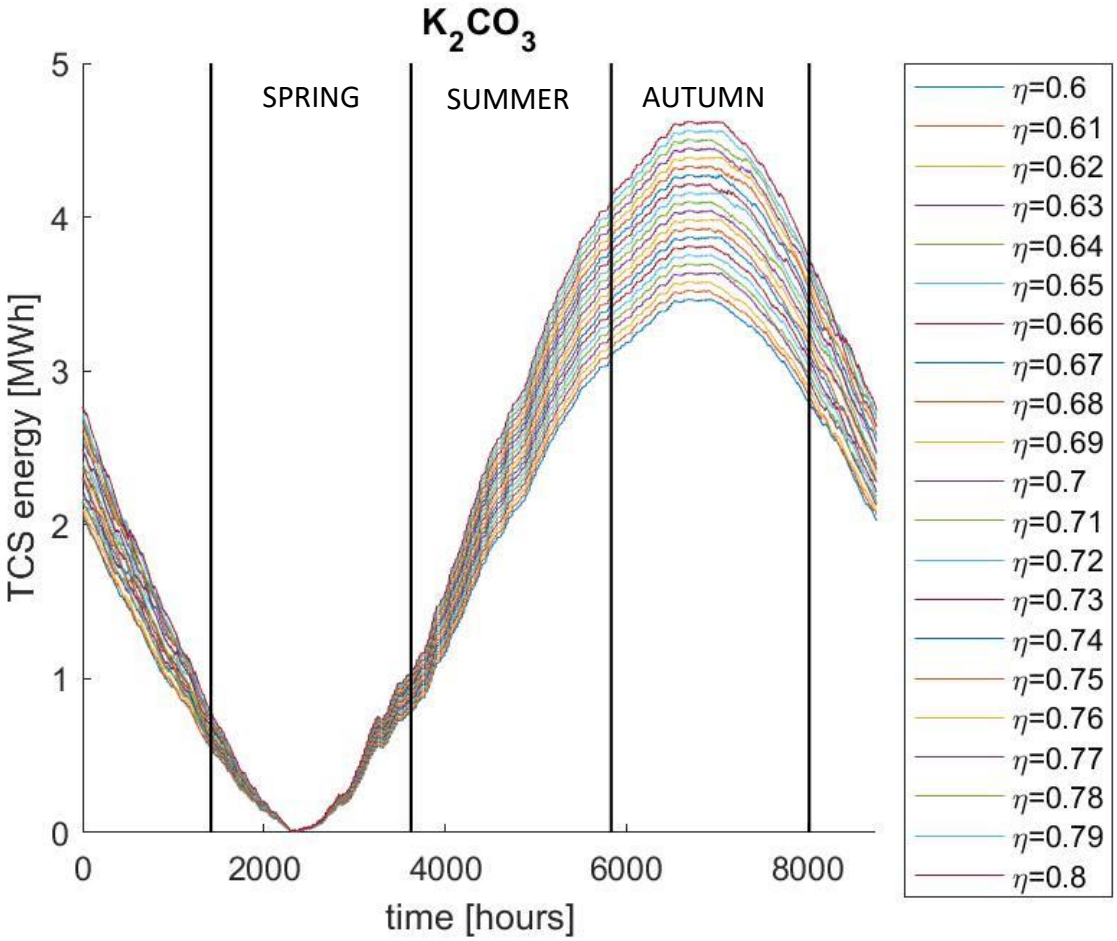

Figure 3.4. Hourly yearly profile of the energy stored within the TCS system (Case 1, TCS material: K_2CO_3, sensitivity parameter: η).

The represented curves all show a minimum of the energy density value equal to zero, which means fully discharged condition. This condition is verified for all curves during spring. The maximum is instead variable with respect to η, ranging in the interval 2-5 MWh.

The influence of η on the stored energy is completely coherent with the previous considerations: going towards higher values of efficiency, the stored energy increases, at every hour of the year. The peaks of the curves indicate the reaching of the maximum energy storable for different values of charging/discharging efficiency η. These values become more meaningful if compared with the total annual thermal energy requirement, equal to 12,4 MWh (value obtained thorough integration of thermal demand in **Figure 2.9**). For the maximum considered efficiency, for example, about one third of the annual heat demand can be stored within the MES.

The most evident and very significant result is represented by the perfectly seasonal operation of the TCS: during "summertime" (March-August) it is continuously fully charged, during wintertime fully discharged.

It is now interesting to consider the cost associated to the simulated MES configuration, or, better, to the configuration resulting as the optimal solution, thus allowing a comparison with other MES configurations. The total cost, evaluated for all the values of efficiencies simulated, is expressed in € per thermal kWh produced. Its behaviour is shown in **Figure 3.5**.

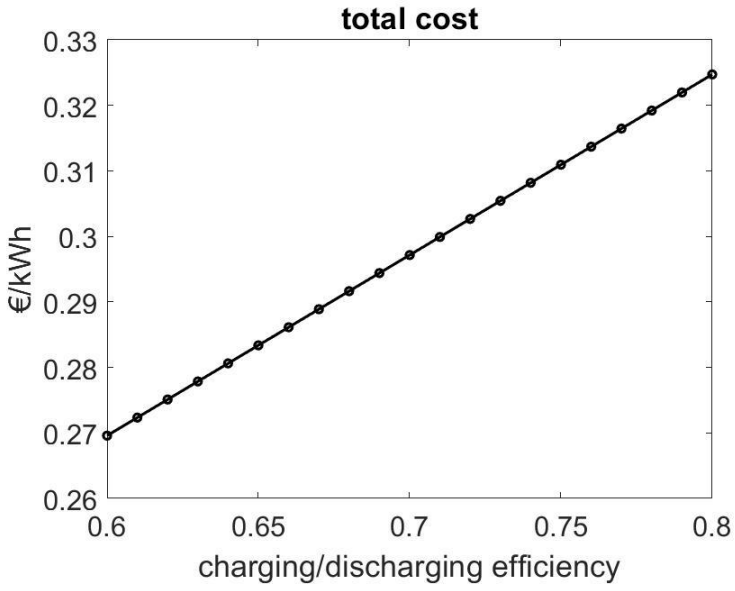

Figure 3.5. System specific cost as a function of charging/discharging efficiency (Case 1, K_2CO_3).

The dependency of cost on efficiency is linear, since it reflects the TCS linear size increase. Its value ranges around 0,30 €/kWh_{th} (it ranges between 0,27 and 0,33 €/kWh_{th}). To be specific,

the component of the total cost which is linear is the investment cost, while O&M costs are almost constant, as shown in **Figure 3.6**

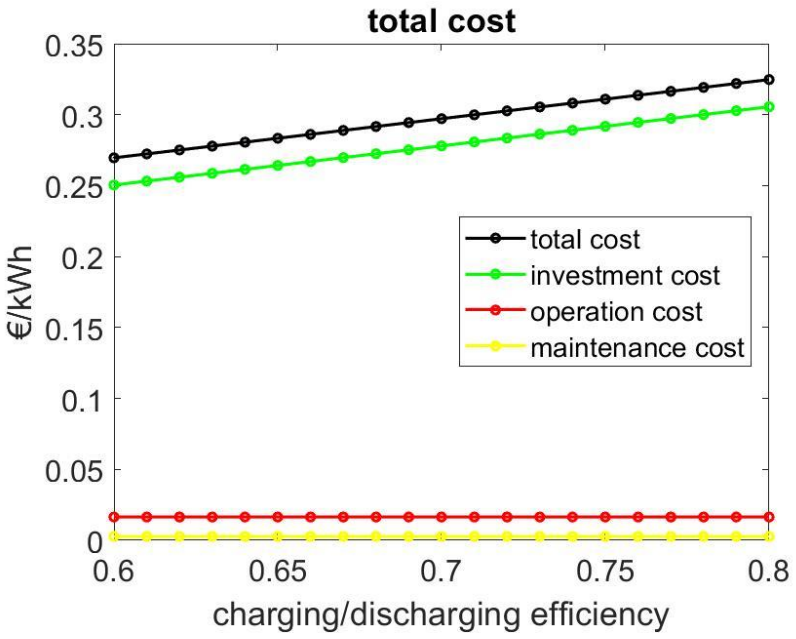

Figure 3.6. System specific costs €/kWh$_{th}$ as a function of charging/discharging efficiency (Case 1, K_2CO_3).

Investment cost is observed to vary within a range 0,25-0,3 €/kWh$_{th}$, while the order of magnitude of operation and maintenance costs is significantly different: a constant value between 0 €/kWh$_{th}$ and 0.05 €/kWh$_{th}$ is shown.

Sodium Sulphide (Na_2S) and Magnesium Chloride ($MgCl_2$)

Size dependence on charging/discharging efficiency results to be equal, both quantitively and qualitatively, to the one observed for potassium carbonate (**Figure 3.5**). The relative plots for the two materials are reported in Appendix B(**Eq. B.1**) . This is a very important aspect to be pointed out: the optimization process always results in the choice of the maximum size compatible with the constraint expressed by Eq. 2.20, independently on the material and the cost difference between the different salts.

Given that the optimal size is the same for the two materials, different correlated volumes are achieved, according to their energy density values. TCS volumes are shown in **Figure 3.7**.

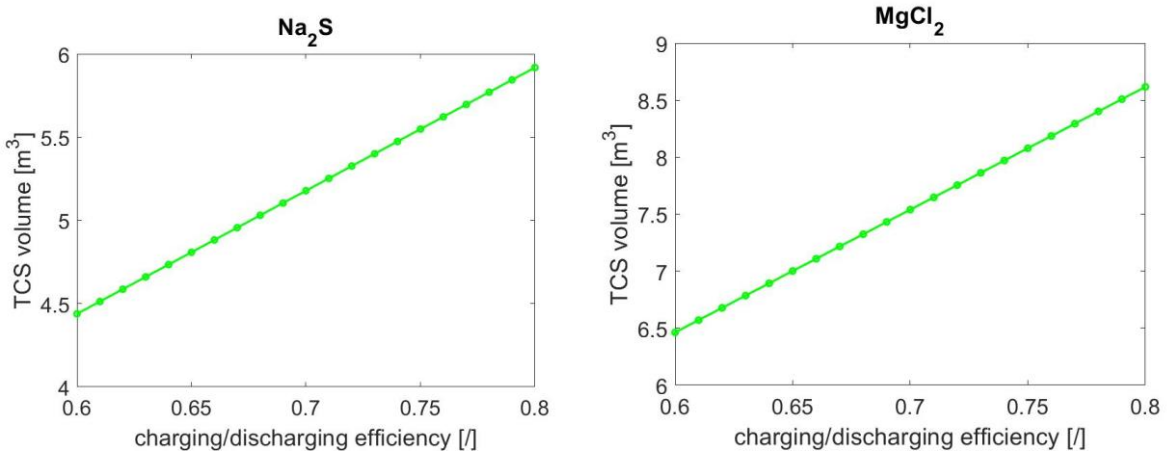

Figure 3.7.TCS material volume as a function of charging/discharging efficiency for Na_2S (left) and $MgCl_2$ (right) (Case 1).

TCS volumes range linearly between 4,4 m^3 and 6 $m^3$for sodium sulphate, between 6,5 and 9 m^3 for magnesium chloride. The involved TCS material volume values look more realistic than in case of K_2CO_3, especially as regard Na_2S, as expected because of its relatively high energy density.

Stored energy profiles are quantitatively and qualitatively analogous to potassium carbonate profile, experiencing a fully seasonal behaviour, with lower amount of energy stored corresponding to lower values of η. Since potassium profile has already been reported, Na_2S and $MgCl_2$ are reported in Appendix B (**Figure B.2** and **Figure B.3**).

Cost variations as a function of η are then investigated, as shown in **Figure 3.8.**

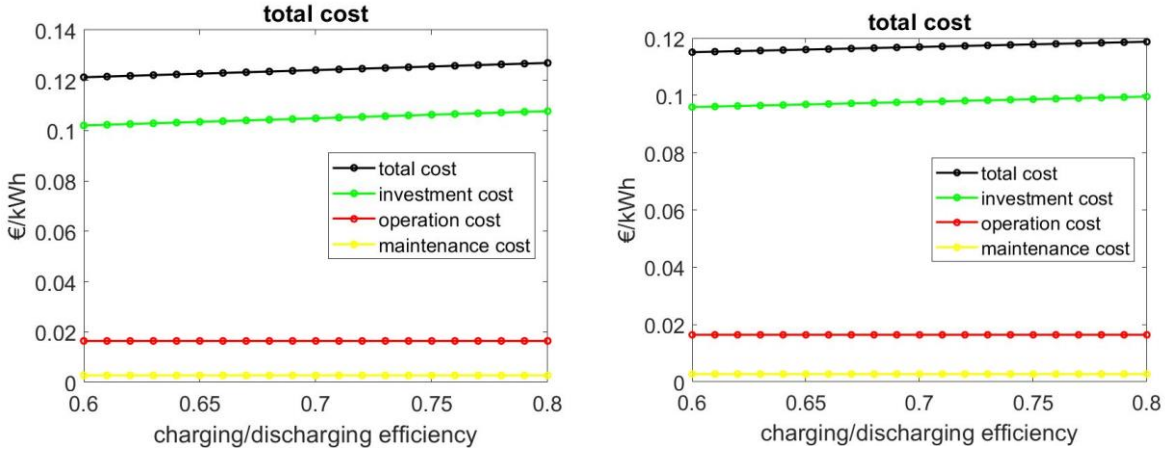

Figure 3.8. System costs as a function of charging/discharging efficiency for Na_2S (left) and $MgCl_2$ (right) (Case 1).

A slightly linear increase is observed for investment costs, ranging around 0.12 €/kWh for both salts with small differences. Operation and maintenance costs, as for potassium carbonate, are much lower than investment cost, and constant along the considered η interval.

It is thus evident that the total cost, associated to the considered MES configuration, is significantly higher (almost doubled) for potassium carbonate (**Figure 3.6**), which has a lower energy density with respect to the other salts, and, consequently, a higher mass/volume required. This affects the total cost due to the fact that investment cost is the predominant cost component.

3.1.2 Role of self-discharge coefficient

The influence of the self-discharge parameter Λ is evaluated within a range $0 \leq \Lambda \leq 0.015$, with a step ΔΔ=0.001, at a given value of η equal to 0.8.

Potassium Carbonate (K_2CO_3)

In **Figure 3.9** TCS optimal size variation is shown. It is worth noticing that, for all the following plots and represented quantities, the first (Λ=0) value is the same as the last one achieved in the previous sensitivity analysis (4,6 MWh), since both evaluated at Λ=0 and η=0.8.

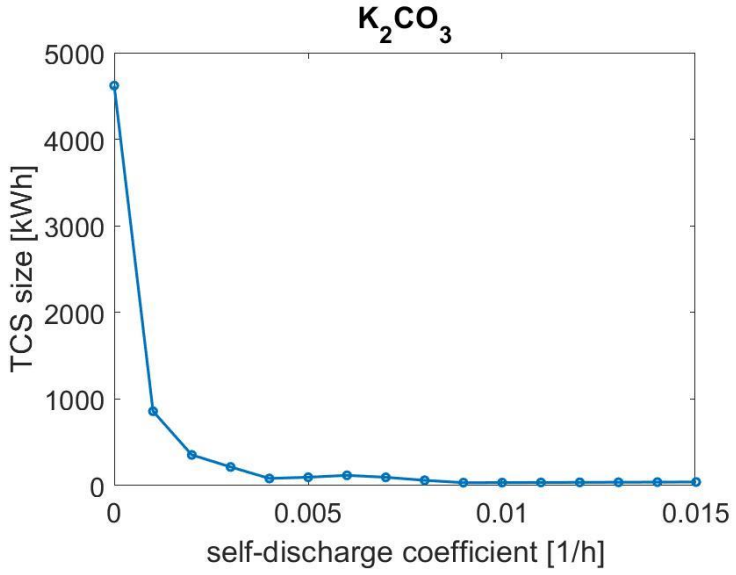

Figure 3.9. Optimal energy capacity [kWh] as a function of self-discharge coefficient (Case 1, material=K_2CO_3).

The curve experiences a steep decrease for values of Λ between 0 and 0.002. Out of this range, the optimal size becomes dramatically low, tending to zero for higher thermal losses values, for which it is not convenient to exploit the storage technology. In other words, this means that the TCS device cannot lose more than the 0.1-0.2 % of its energy per hour.

The TCS system volume variation is illustrated in **Figure 3.10.**

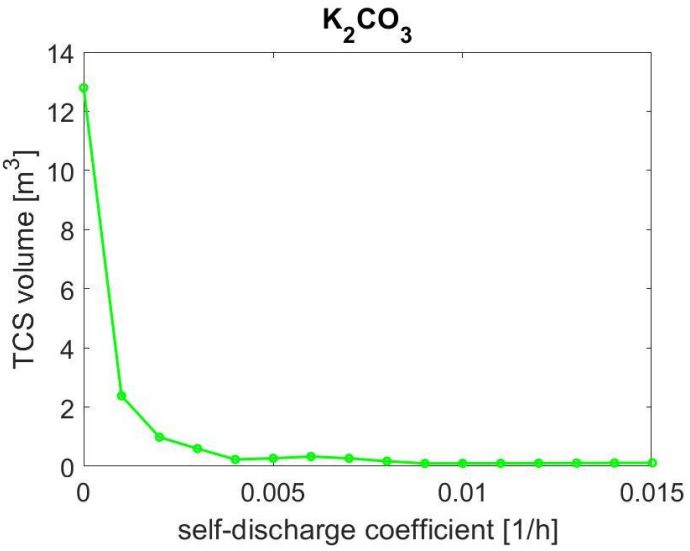

Figure 3.10. TCS volume as a function of self-discharge coefficient (Case 1, TCS material: K_2CO_3).

The first value, corresponding to a condition of absence of losses, is equal to around 13 m^3 ; then, a sudden decrease is verified until a value slightly higher than 0 m^3 is reached from $\Lambda \geq 0.004$.

It is worth evaluating the yearly energy profile, for the different considered values of Λ, as shown in **Figure 3.11**

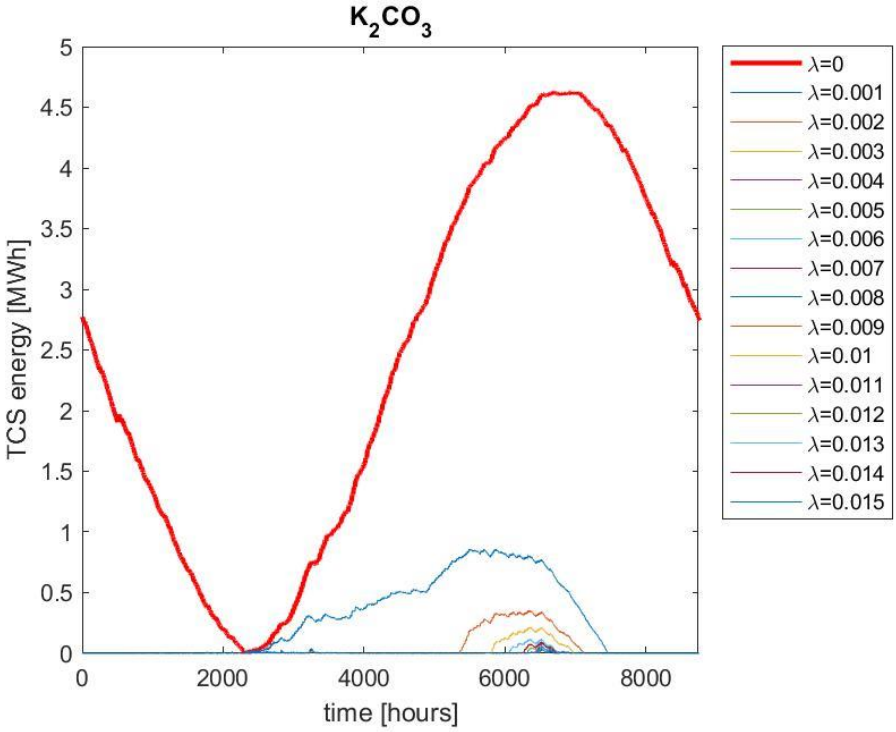

Figure 3.11. Hourly yearly profile of the energy stored within the TCS system (Case 1, TCS material: K_2CO_3, sensitivity parameter: Λ)

As expected from the size variation analysis, the stored energy dramatically decreases, all over the year, for $\Lambda \geq 0.001$. From this value on, the TCS technology cannot be operated seasonally anymore: it is charged and discharged during "summer" months (for the first value of Λ they approximately go from March/April to August, but this range is reduced for increasing Λ), as better shown in **Figure 3.12**.

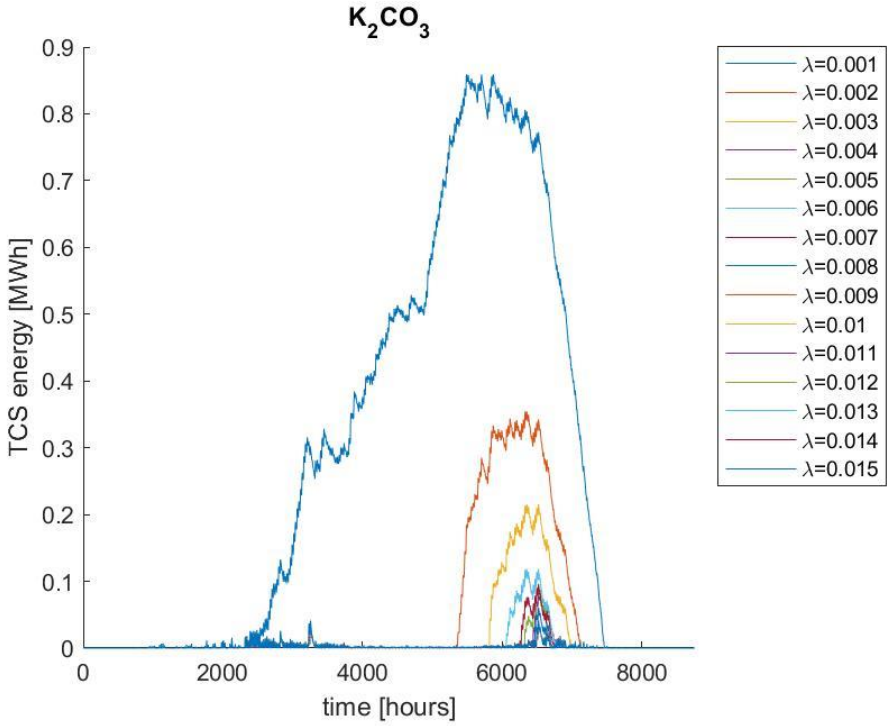

Figure 3.12. Hourly yearly profile of the energy stored within the TCS system for $\Lambda \geq 0.001$ (Case 1, TCS material: K_2CO_3,).

TCS stored energy values range approximately between 0 (the storage is fully discharged) and 0,85 MWh, which correspond to almost the 7% of the annual heating demand (12,4 MWh).

The effect on self-discharge parameter on the system total cost is illustrated in **Figure 3.13.**

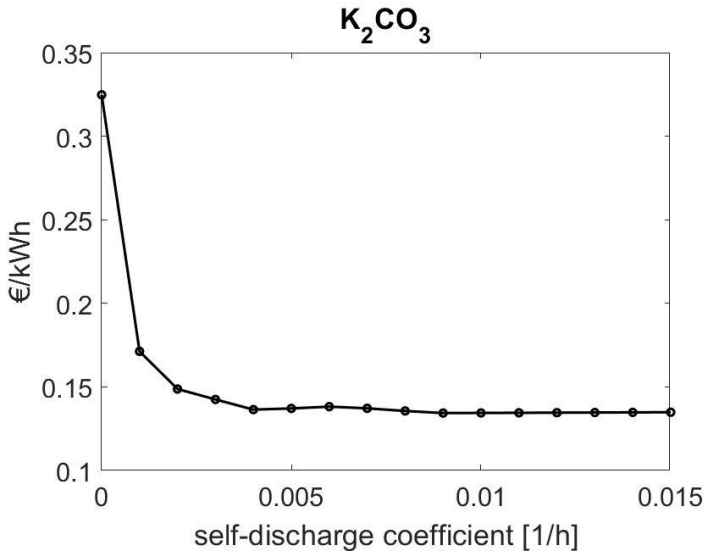

Figure 3.13. System specific costs €/kWh_{th} as a function of self-discharge coefficient (Case 1, K_2CO_3).

System costs range from a value of 0,34 €/kWh_{th}, corresponding to a condition of maximum efficiency and zero losses, to, abruptly, around 0,15 €/kWh_{th}. This behaviour can be justified considering that the size reduction leads to a decrease of the investment cost, which, as previously noticed, is the main component of the total cost. Qualitatively analogous information can be achieved for the other two materials, so, considering that the first (Λ=0) cost value is known from the previous analysis, this type of plot will not be represented for Na_2S and $MgCl_2$.

Sodium Sulphide (Na_2S) and Magnesium Chloride ($MgCl_2$)

The effect of self-discharge parameter variation on the optimal installed size for sodium sulphide and magnesium chloride is pretty similar to the one observed for potassium carbonate, so that they are reported in Appendix B (**Figure B.4**)

The corresponding values of volume are also quantitatively less meaningful than qualitatively, so that they are reported in Appendix B (**Figure B.5**)

Yearly energy profile of sodium sulphide is then represented in **Figure 3.14**.

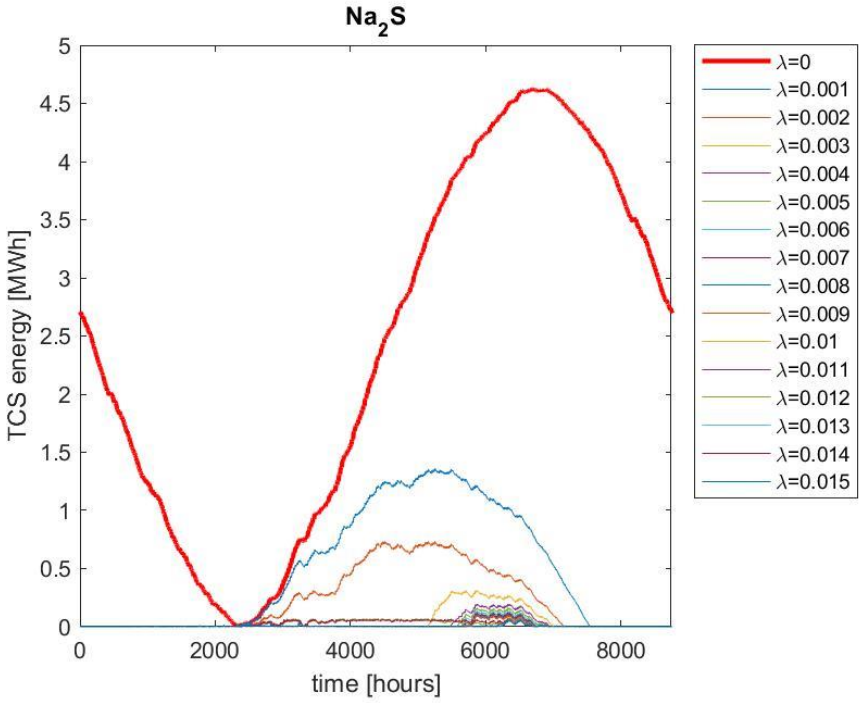

Figure 3.14. Hourly yearly profile of the energy stored within the TCS system (Case 1, TCS material: Na_2S, sensitivity parameter: Λ).

The sudden decrease of the energy for $\Lambda \geq 0.001$ is verified for all the hours of the year, as was noticed for the size. For Λ=0.001 almost a maximum energy of around 1,4 MWh is reached in summer, corresponding to a fraction of thermal demand achievable equal, approximately, to 11%. This value is slightly higher than in case of potassium carbonate.

Since energy profile of magnesium chloride is quantitatively and qualitatively analogous, it is reported in Appendix B (**Figure B.6**)

3.1.3 Role of cost of TCS system

Salt hydrates-based TCS systems are far from a commercialisation process. As previously mentioned, at the state of art, only small prototypes exist and the TCS system design is still an open primary issue. It is thus quite speculative the attempt to find specific values of TCS on a system level (considering evaporators, condenser, tanks exc.), which justifies the choice of investigate a range of feasible system costs, going from one to ten times the material cost:

$$c_{mat} \leq c_s \leq 10 \cdot c_{mat} \quad , \qquad step = 2 \cdot c_{mat} \qquad (Section\ 2.5.1)$$

In **Table 2.1** material costs have been reported, which are 0,348 €/kWh for sodium sulphide, 1 €/kg for potassium carbonate and 0.154 €/kg for magnesium chloride.

The analysis is accomplished for constant values of η and Λ, assumed equal to, respectively, 0.8 and 0.

Size variation

The size variation of a potassium carbonate-based TCS as a function of system cost is illustrated in **Figure 3.15**.

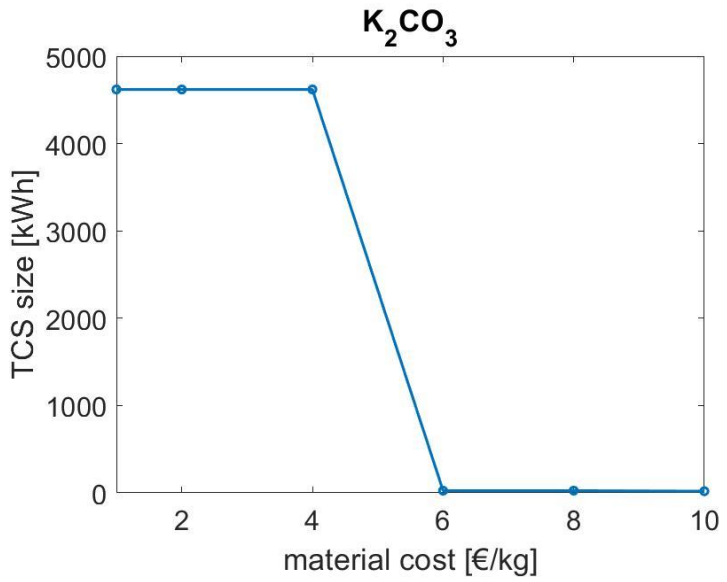

Figure 3.15. Optimal energy capacity [kWh] as a function of cost of TCS system [€/kg] (Case 1, material=K_2CO_3).

For system costs lower than $4 * c_{mat}$, i.e. 4 €/kg, the installed size is observed to be constant. For higher costs, the TCS technology is not included within the optimal solution of the considered MES.

A different result is achieved both for sodium sulphide and magnesium chloride, as illustrated in **Figure 3.16** and **Figure 3.17**.

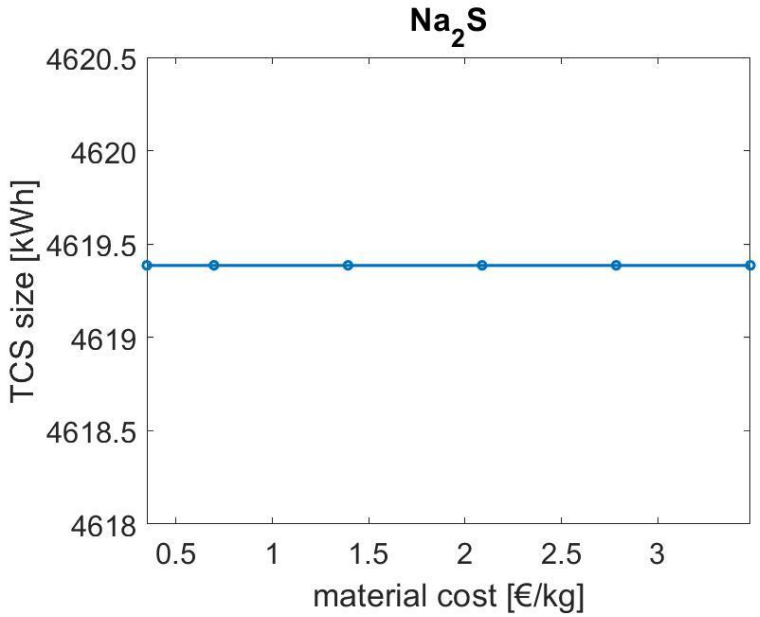

Figure 3.16. Optimal energy capacity [kWh] as a function of cost of TCS system [€/kg] (Case 1, material=Na_2S).

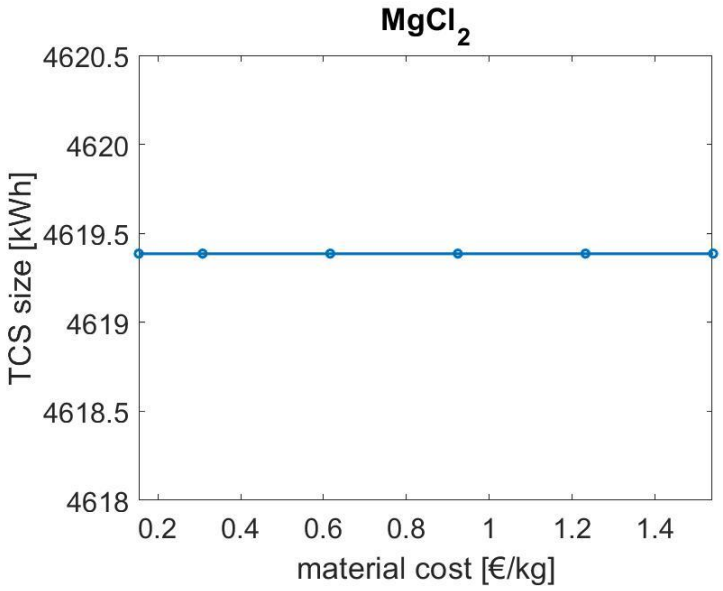

Figure 3.17. Optimal energy capacity [kWh] as a function of cost of TCS system [€/kg] (Case 1, material=$MgCl_2$).

The installed size is constant over the range of cost considered, i.e. the technology always belongs to the optimal solution. This is verified for Na_2S and $MgCl_2$ since their material cost is significantly lower if compared to K_2CO_3 cost.

Volume variation

The volumes corresponding to the achieved optimal sizes within the range of costs considered are shown, for the three materials, in **Figure 3.18**, **Figure 3.19** and **Figure 3.20.**

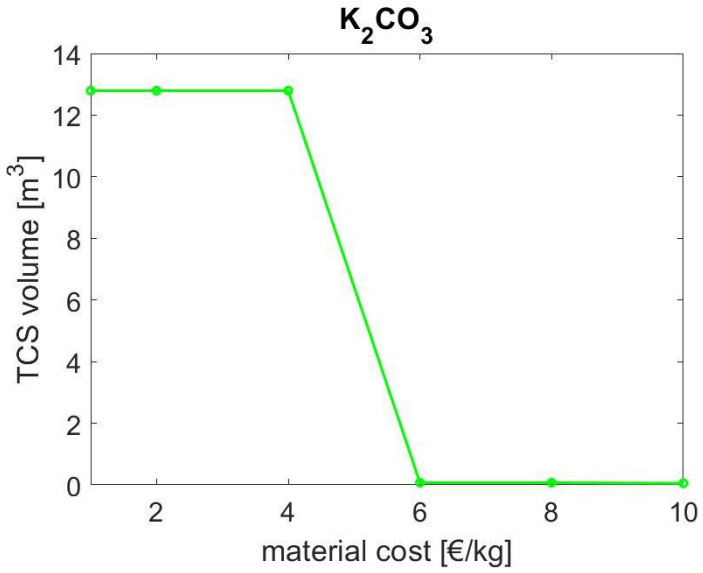

Figure 3.18. TCS volume as a function of cost of TCS system [€/kg] (Case 1, material=K_2CO_3).

A constant value of around 13 $m^3$is observed for costs lower that six times the material cost, then a sudden decrease to 0 is verified.

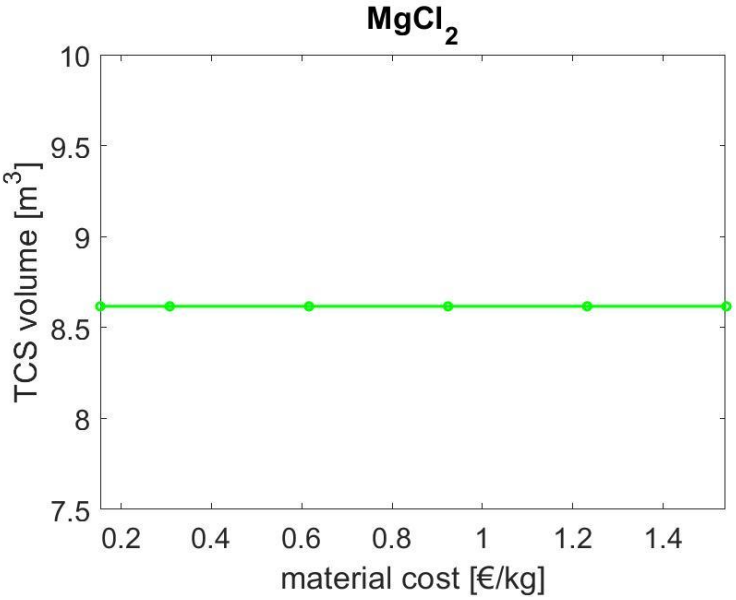

Figure 3.19. TCS volume as a function of cost of TCS system [€/kg] (Case 1, material=$MgCl_2$).

The volume is constant and almost equal to 8,6 m^3 for the considered cost range.

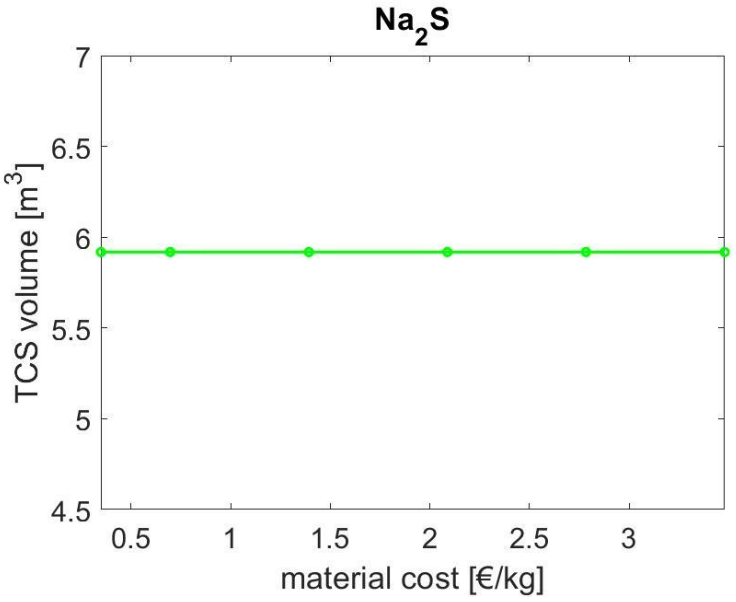

Figure 3.20. TCS volume as a function of cost of TCS system [€/kg] (Case 1, material=Na_2S).

The volume is constant and equal to almost 6 m^3 for the values of cost considered.

System specific cost variation

It is interesting to evaluate how the specific cost, previously defined, of the MES is affected by TCS system cost variation. Results are shown in **Figure 3.21**, **Figure 3.22** and **Figure 3.23**.

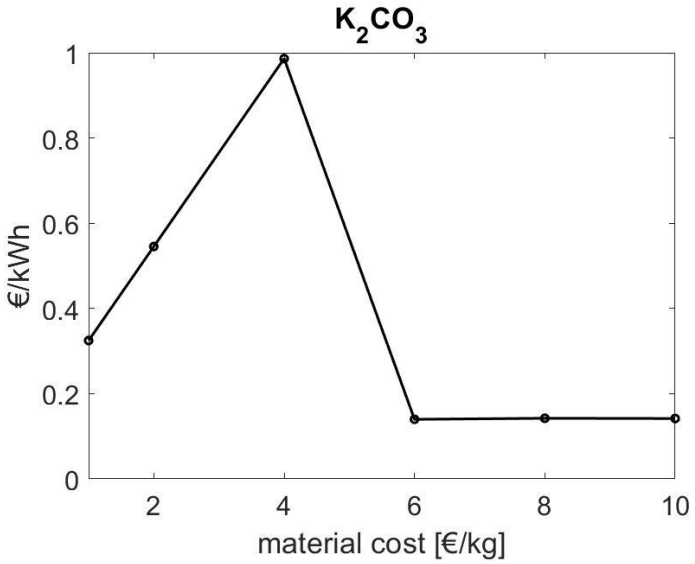

Figure 3.21. MES total cost [€/kWh] as a function of cost of TCS system [€/kg] (Case 1, material=K_2CO_3).

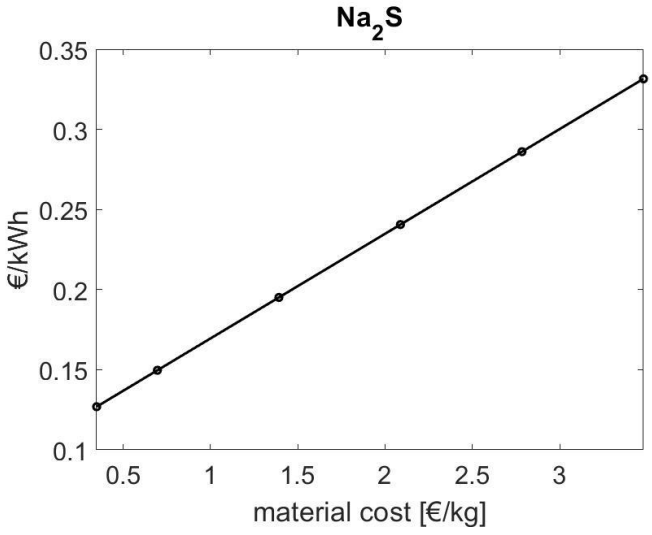

Figure 3.22. MES total cost [€/kWh] as a function of cost of TCS system [€/kg] (Case 1, material=Na_2S).

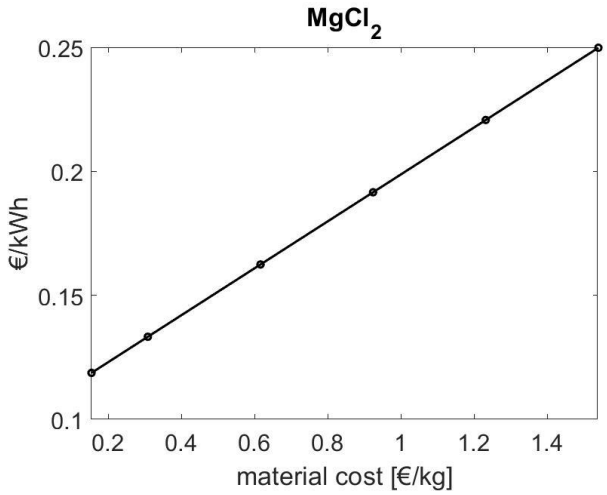

Figure 3.23. MES total cost [€/kWh] as a function of cost of TCS system [€/kg] (Case 1, material=$MgCl_2$).

Starting with potassium carbonate, the cost value increases for higher TCS costs, until the TCS technology is not anymore selected as part of the optimal MES configuration, so that the cost becomes zero. The linear increase of MES cost, which is verified for the three materials, is due to the fact that the size (and the volume) is constant and the TCS cost is increased.

3.1.4 Final comments on Case 1

To the aim of summing up the most relevant comments on the illustrated results, the following considerations are introduced:

i. The TCS technology is included within the optimization problem for all the values of charging/discharging efficiency considered.
ii. The TCS size increases linearly with η, which means that for higher efficiencies it is much more convenient to exploit the TCS technology. The maximum reached value, for any of the considered materials, is about one third of the total annual thermal energy requirement.
iii. Higher installed volumes correspond to materials with lower energy density, which is trivial (it is trivial only if the installed size is the same, which is the case);
iv. The TCS storage shows a seasonal operation, which is one of the major goals of the technology.
v. The system total cost is higher for most expensive material, since it is mostly affected by the investment cost.
vi. The self-discharge parameter increasing has a dramatic effect on system performances: for $\Lambda \geq 0.1$ % the installed size tends abruptly to zero. The effect is almost the same for all the considered salts.
vii. The effect of TCS cost variation considerably affect the system cost, determining a sensible increase of the latter one (higher than 0.10 €/kWh). For the most expensive salt (K_2CO_3), the technology is not installed for a TCS system cost higher than four times the material cost.

3.2 Case 2

The simulated MES is a co-generative system composed by a natural gas fuel cell and TCS system. The analysis, in terms or investigated quantities and considered sensitivity parameters, is completely analogous to the one developed in Case 1. This justifies the choice of gathering all results in Appendix B, and recalling them during explanation

3.2.1 Role of charging/discharging efficiency

The effect of charging/discharging efficiency of the TCS system on i) the installed size and corresponding volume, ii) yearly stored energy and iii) system costs are presented in the following for the three materials considered. For all values of efficiency considered, the installed SOFC capacity is equal to 5 kW.

Sodium sulphide (Na_2S)

The optimal size capacity variation, and the correlated (through the energy density) volume variation, is investigated for sodium sulphide and shown in **Figure 3.24**.

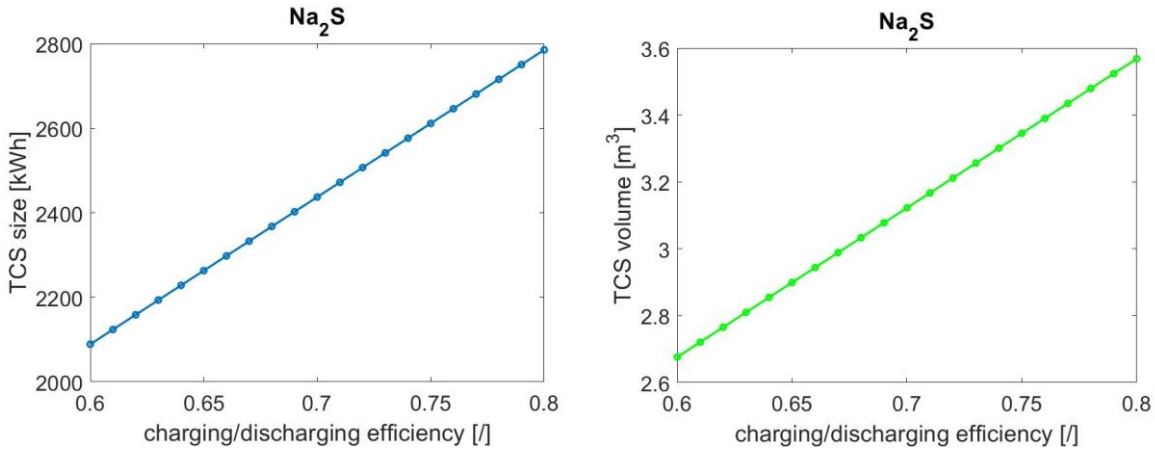

Figure 3.24 Optimal energy capacity [kWh] (left) and correlated TCS volume [m^3] (right) as a function of charging/discharging efficiency (Case 2, Na_2S).

The first important observation is that the TCS technology is included in the optimal solution for all the values of efficiency considered. This means that it represents a better solution than having the SOFC as only technology, which is not trivial. On the other hand, it is worth underlining that the simulation of a MES which also includes a natural gas boiler does not select the TCS technology, at least for current costs of involved technology.

As in Case 1, also in this case, the dependence of size on charging/discharging efficiency is linear, for which to higher values of η correspond higher value of sizes. This means that the TCS technology exploitation within the system increases, which looks reasonable. The maximum reached size is almost equal to 2.8 MWh, which represents about a quarter of the total annual thermal energy demand (12,4 MWh).

Values of TCS material volume corresponding to optimal sizes range between 2,7 and 3,5 m^3, which looks relatively low and consequently attractive.

Hourly yearly profiles are considered in **Figure 3.25.** A seasonal operation is possible also in this case, with continuously fully charging in summer and fully discharging in winter, which is an important result since it represents the goal of the technology. The TCS system is thus operated analogously to Case 1, but in this case lower maximum stored energy are achievable.

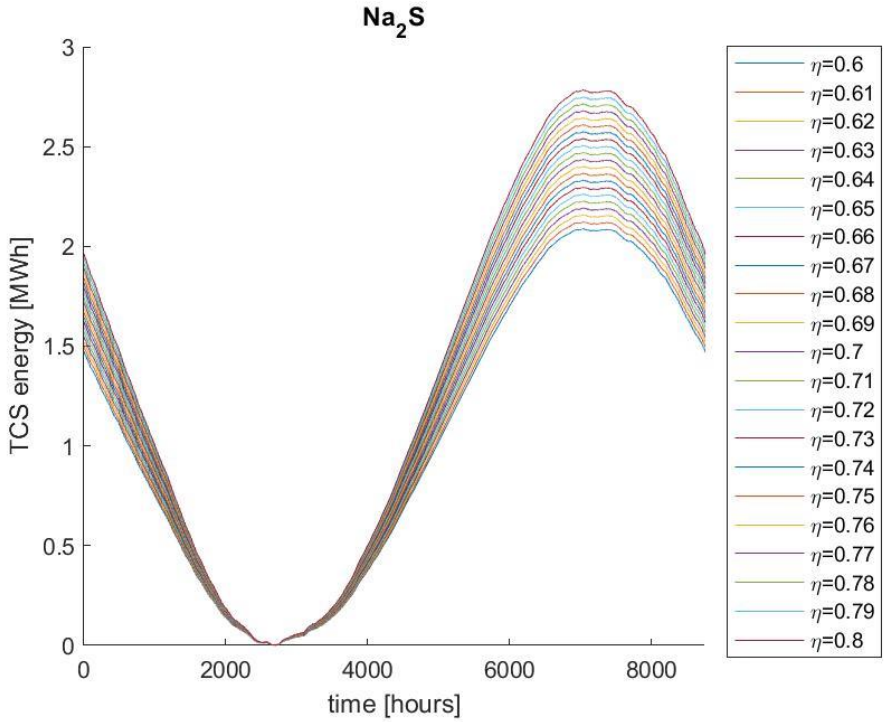

Figure 3.25. Hourly yearly profile of the energy stored within the TCS system (Case 2, TCS material: Na_2S)

In **Figure 3.26** the system cost as a function of charging/discharging coefficient is shown, from which it can be deduced that its value slightly increases (between 0.371 and 0.375). In this case, operation cost is significantly higher than in the previous case, reducing the investment cost

contribution to the total cost. This happens because the SOFC is always operated and, consequently, natural gas is always imported all over the year.

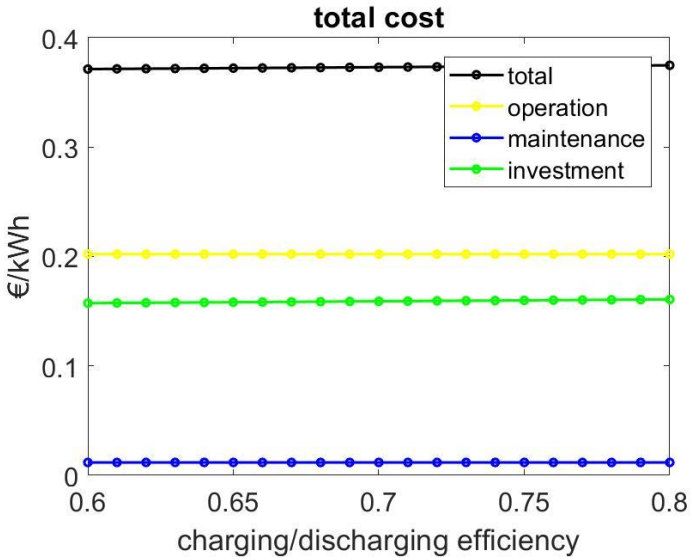

Figure 3.26. System costs as a function of charging/discharging efficiency (Case 2, TCS material: Na_2S).

As better represented in **Figure 3.27**, total cost is much higher, for the same material, in this MES configuration than in Case 1, in which it ranges around 0,12 €/kWh.

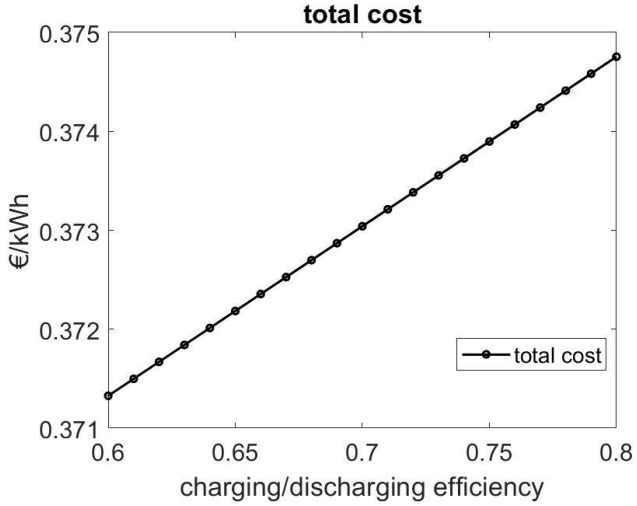

Figure 3.27. System costs as a function of charging/discharging efficiency (Case 2, TCS material: Na_2S).

Potassium Carbonate (K_2CO_3)

Potassium carbonate size variation with respect to charging/discharging efficiency is shown in **Figure 3.28**. The same range of variation observed for sodium sulphide is obtained, which again confirms that the optima size is independent on the material and varies linearly with η. The corresponding values of volume are higher than in case of sodium sulphide, due to K_2CO_3 lower density.

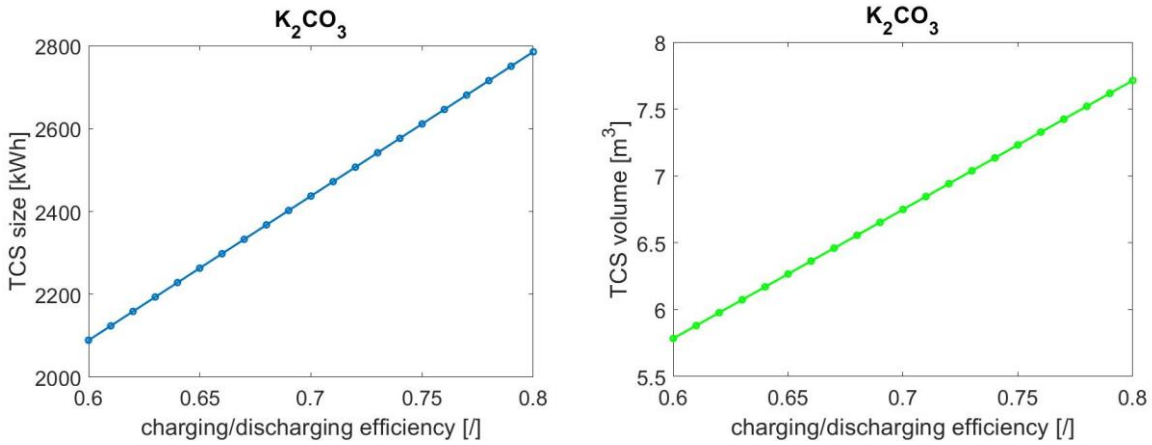

Figure 3.28. Optimal energy capacity [kWh] (left) and correlated TCS volume [m^3] (right) as a function of charging/discharging efficiency (Case 2, K_2CO_3).

As regards the stored energy profile, shown in **Figure 3.29**, the same qualitative and quantitative observations done for sodium sulphide are valid.

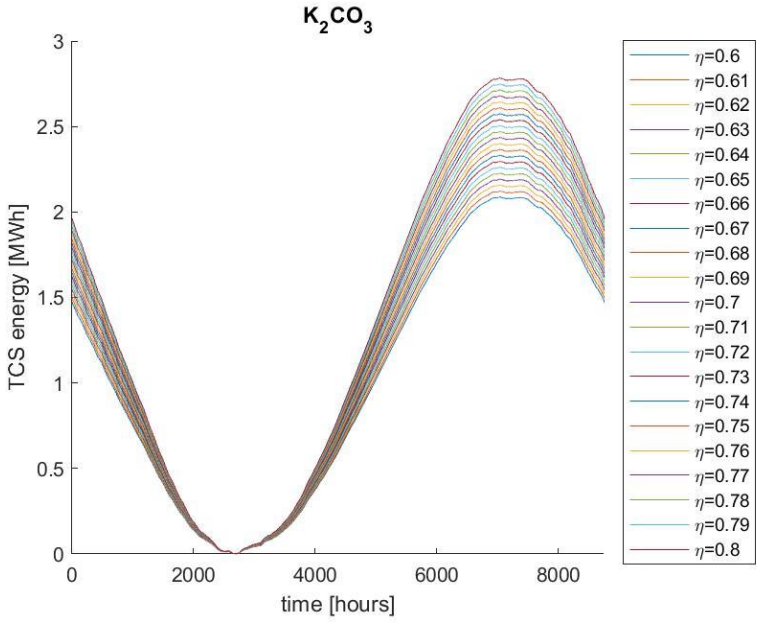

Figure 3.29. Hourly yearly profile of the energy stored within the TCS system (Case 2, TCS material: K_2CO_3)

System costs as a function of charging/discharging efficiency are shown in **Figure 3.30**. Since the material cost is higher than the one associated to sodium sulphide, investment cost is significantly higher and experiences a larger variation in the range of η considered, approximately from 0,46 €/kWh to 0,50 €/kWh. These values are significantly high compared to the previously simulated MES configuration, for which it was assessed around 0.3 €/kWh. Also in this case operational cost experienced a significant increase with respect to Case 1.

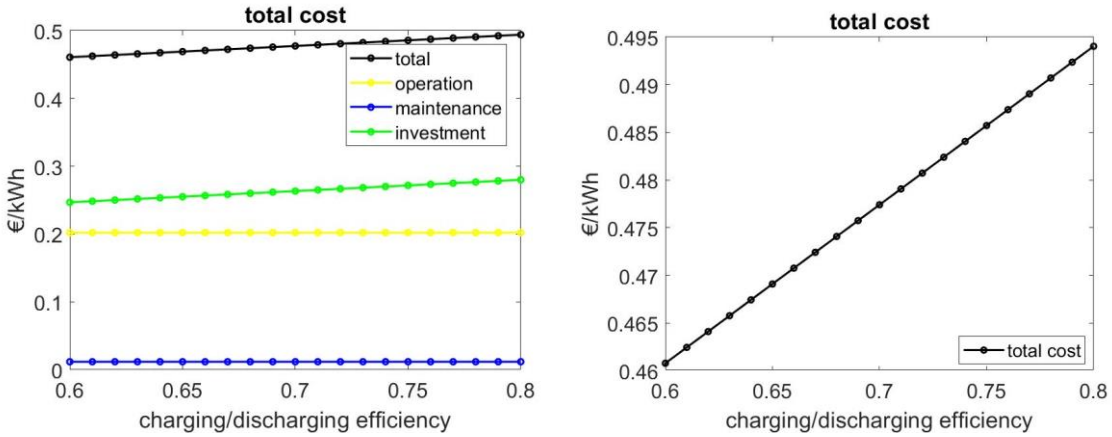

Figure 3.30. System cost components (left) and total cost (right) as a function of charging/discharging efficiency (Case 2, TCS material: K_2CO_3).

Magnesium Chloride ($MgCl_2$)

Magnesium chloride case, due to the qualitative analogy with the previous materials, is reported in Appendix B.

3.2.2 Role of self-discharge parameter

Sodium sulphide (Na_2S)

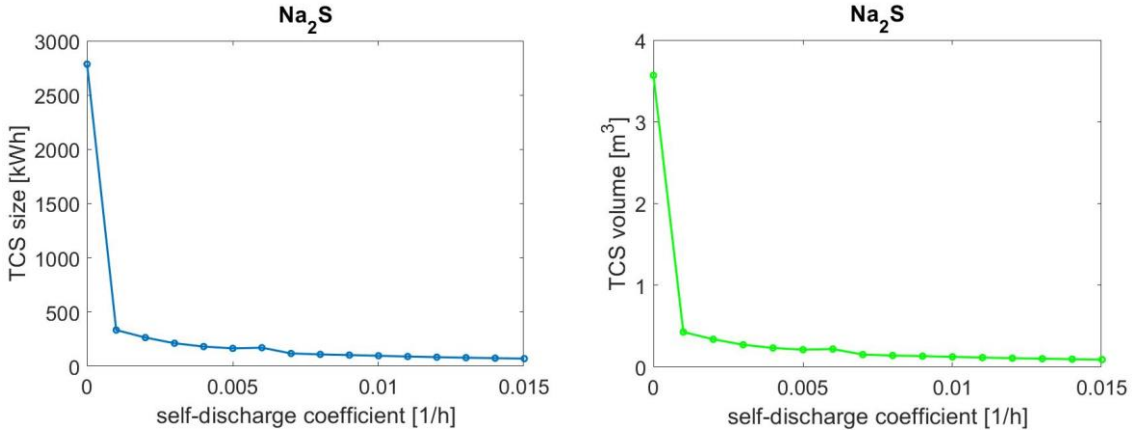

Figure 3.31. Optimal energy capacity [kWh] (left) and correlated TCS volume [m^3] (right) as a function of self-discharge coefficient (Case 2, Na_2S).

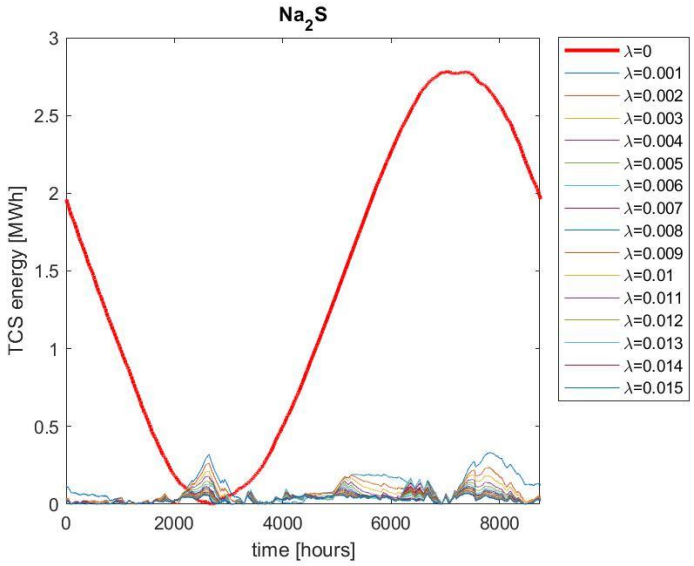

Figure 3.32. Hourly yearly profile of the energy stored within the TCS system (Case 2, TCS material: Na_2S)

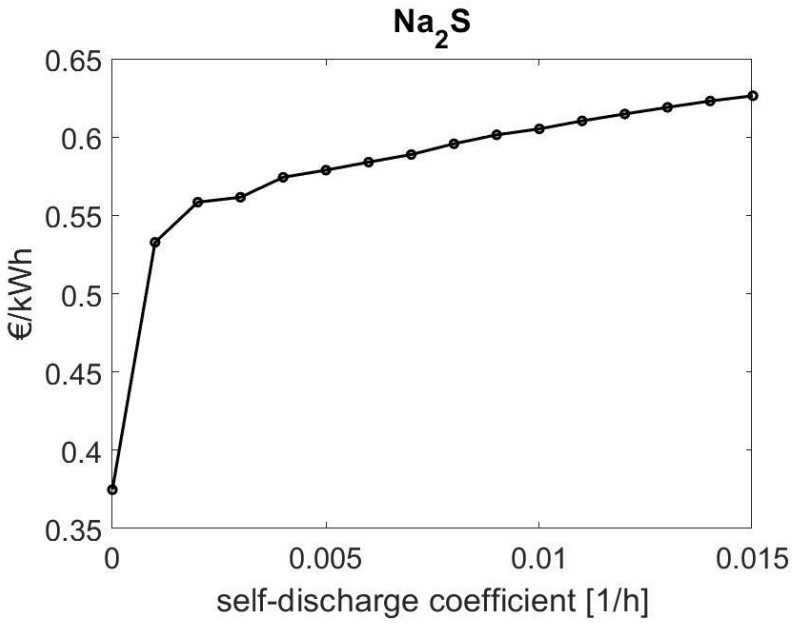

Figure 3.33. System specific costs [€/kWh$_{th}$] as a function of self-discharge coefficient (Case 2, Na_2S).

Size dependency on self-discharge parameter is the same achieved in Case 1 analysis, with a steep decrease immediately after the condition of absence of losses (Λ=0). This behaviour is still more dramatic in this case, because from $\Lambda \geq 0.001$ the TCS technology is practically not exploitable. Furthermore, starting from this value, the operation is completely not seasonal, being TCS system fully charged and discharged within small periods of time (order of months).

An interesting difference with respect to Case 1 is that the total system cost increases for increasing values of Λ. This happens because the reduction of TCS size forces to increase the SOFC size, in order to guarantee the user thermal demand satisfaction.

Potassium carbonate and magnesium chloride cases, due to analogy with the sodium sulphide results, are reported in Appendix B.

3.2.3 Role of cost of TCS system

Potassium Carbonate (K_2CO_3)

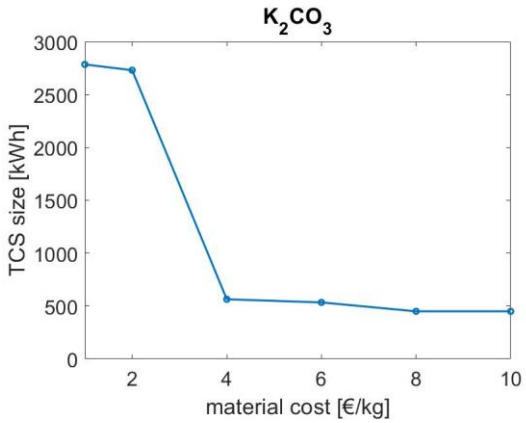

Figure 3.34. Optimal energy capacity [kWh] as a function of cost of TCS system [€/kg] (Case 2, material=K_2CO_3).

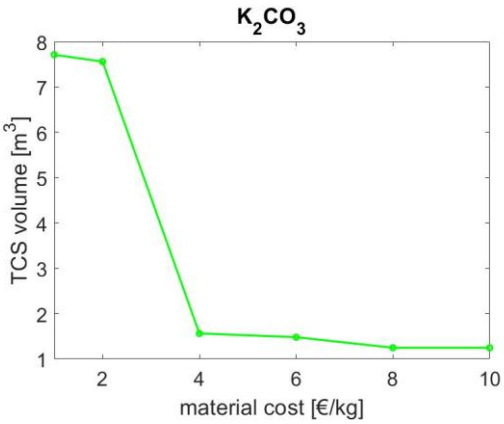

Figure 3.35. TCS material volume [m^3] as a function of cost of TCS system [€/kg] (Case 2, material=$MgCl_2$).

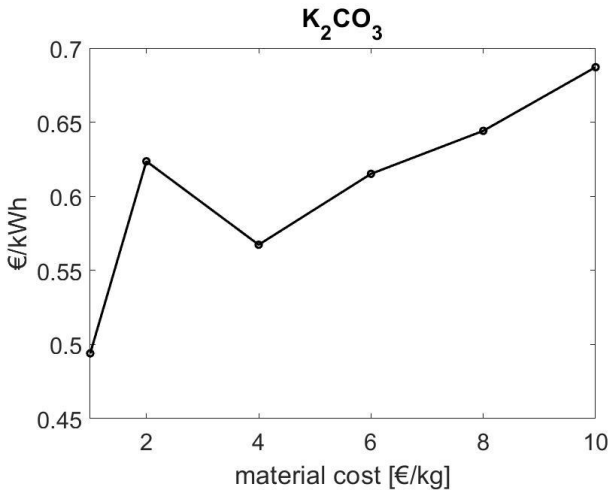

Figure 3.36. TCS material volume [m^3] as a function of cost of TCS system [€/kg] (Case 2, material=K_2CO_3).

Since potassium carbonate has the highest material cost associated, its behaviour is significantly different from the previous two cases (the other two other material results are showed in). The installed size slightly decreases for a cost value equal to twice the material cost. Then the slope of the curve becomes higher and a sudden decrease is verified for a value of $4 * c_{mat}$. From this value on, the size is almost constant, ranging around a value of 500 kWh. This behaviour is fully reflected in the material volume requirement.

The MES total specific cost shows a very interesting behaviour: for $0 \leq c \leq 2 * c_{mat}$ it increases, because the TCS size decrease is lower than the consequent SOFC size increase. Then, for $2 * c_{mat} \leq c \leq 4 * c_{mat}$, TCS reduction is so large that the total specific cost decreases. Eventually, for $c \geq 4 * c_{mat}$, it starts to increase again, with a lower slope than in the first interval, coherently with the TCS size decreasing (and consequent SOFC size increasing).

3.2.4 Final comments on Case 2

The most significative relevant result can be summed up in the following comments:

i. The TCS technology is included within the optimization problem for all the values of charging/discharging efficiency considered, which means that the MES configuration with storage is preferable (it is optimal) to the one without it (the SOFC alone).
ii. The TCS size increases linearly with η, which means that for higher efficiencies it is much more convenient to exploit the TCS technology. The maximum reached value, for any of the considered materials, is about a quarter of the total annual thermal energy requirement.
iii. Higher installed volumes correspond to materials with lower energy density, which is trivial (it is trivial only if the installed size is the same, which is the case);
iv. The TCS storage shows a seasonal operation, which is one of the major goals of the technology.
v. The system total cost is higher for most expensive material, since it is mostly affected by the investment cost.
vi. The self-discharge parameter increase has a dramatic effect on system performances: for $\Lambda \geq 0.2\%$ the installed size tends abruptly to zero. The effect is almost the same for all the considered salts.
vii. The effect of TCS cost variation considerably affect the system cost, whose increase is linear for sodium sulphide and magnesium chloride. Since potassium carbonate is significantly more expensive than the other two salts, a different behaviour for both size and system cost is observed. The size decreases for increasing cost values, which forces to oversize the fuel cell. The resulting cost, which accounts for both the technologies costs, reflects a combination of the two effects.

4. Conclusions and future work

The present work has been organized in two conceptual sections: material investigation and modelling within MES optimization problems. The first part, mainly consisting in a thermodynamic equilibrium-based analysis, justifies the choice for the reference materials or, better, the reference hydration reactions, since more transitions between hydrated states are possible for magnesium chloride and sodium sulphide. In particular, the main filter applied for the material selection has been considered to be the hydration temperature, which must be consistent with bot space heating and domestic hot water production applications. Material-related parameters, i.e. energy density and cost, provide the input to thermochemical storage technology within the MES. TCS modelling has been introduced within the optimization framework developed by Gabrielli et.al [20], essentially basing on an energy balance equation, in which two main performance parameters are introduced: the charging/discharging efficiency η, accounting for charging/discharging losses, and the self-discharge coefficient Λ, related to thermal losses and eventual losses due to humidity penetration. These parameters are strictly dependent on system design, which is still an open issue for salt hydrates and, in general, thermochemical storage. Considering this, the sensitivity analysis on these parameters represents the real contribution of this work, providing some useful guidelines on their optimal values.

The first important result is represented by the fact that the TCS technology is always installed for the considered range of charging/discharging efficiencies, i.e. it belongs to the optimal solution. It increases linearly for increasing η, which translates into a higher exploitation of the technology (being the thermal demand fixed). This induces slightly higher values of investment costs, which represents the major component of total system cost.

For a value of Λ equal to zero and for η varying from 0.6 to 0.8, the TCS system is **operated seasonally**, i.e. it is continuously fully charged in summer and continuously fully discharged in winter. This is an important result, being the main desired application for the technology.

The value of Λ has a dramatic impact on system performances: for values higher than 0,1 % in Case 1, higher than 0,2 % in Case 2, the installed size decreases abruptly, which means that it is not anymore feasible. This is an important result, because it provides useful thresholds for TCS system design. The self-discharge coefficient may be, indeed, experimentally determined for prototypes and compared to the threshold values.

For the further development of the work, as regard the modelling aspect, another model for the TCS system is suggested, for a possible comparison with the one developed. It could be interesting to simulate transitions between states: the energy may indeed be expressed as a sum of contributions of the energies of the hydrated states present at each timestep. This approach would be more related to the kinetic of the process.

Furthermore, chemical degradation phenomena should be considered within the model.

Appendix A

	α	β	δ	κ	ρ	λ	μ [€]	ψ
boiler	0.92	0	0	0	0	{194.1; 82.4; 65.2} [€/kW]	{0;6.88;10.4} $*10^{-3}$	0.02
NG_SOFC	{0.71 0.61 0.51 0.41}	{-0.05- 0.02 0.04 0.11}	0.14	1	1.46	{4260; 2580; 1320} [€/kW]	{0;3.20; 8}$*10^{-3}$	0.08
Solar thermal	0	0	0	0	0	500 [€/m^2]	0	0.03

Cost and performance coefficients of the simulated technologies [20]

Appendix B

Case1

Role of charging/discharging efficiency for Na_2 S and $MgCl_2$

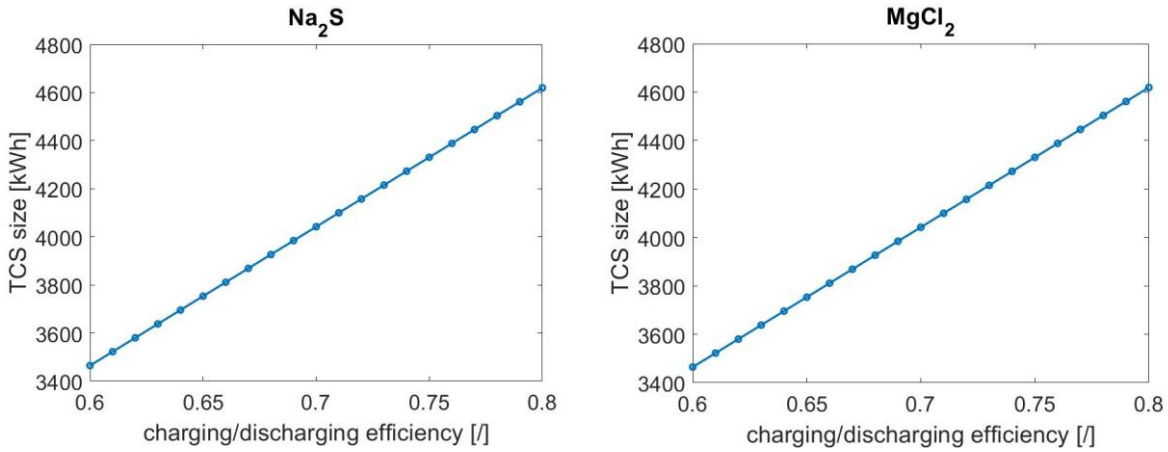

Figure B.1. Optimal energy capacity [kWh] as a function of charging/discharging efficiency for Na_2S and $MgCl_2$ (Case 1).

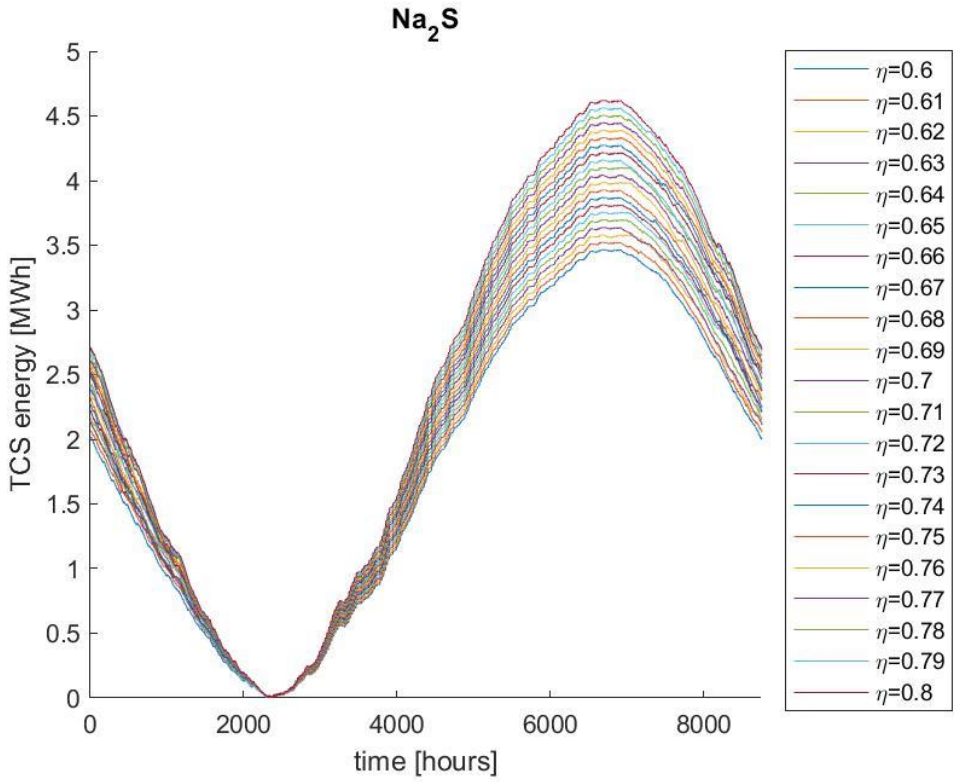

Figure B.2. Hourly yearly profile of the energy stored within the TCS system (Case 1, TCS material: Na_2S, sensitivity parameter: η)

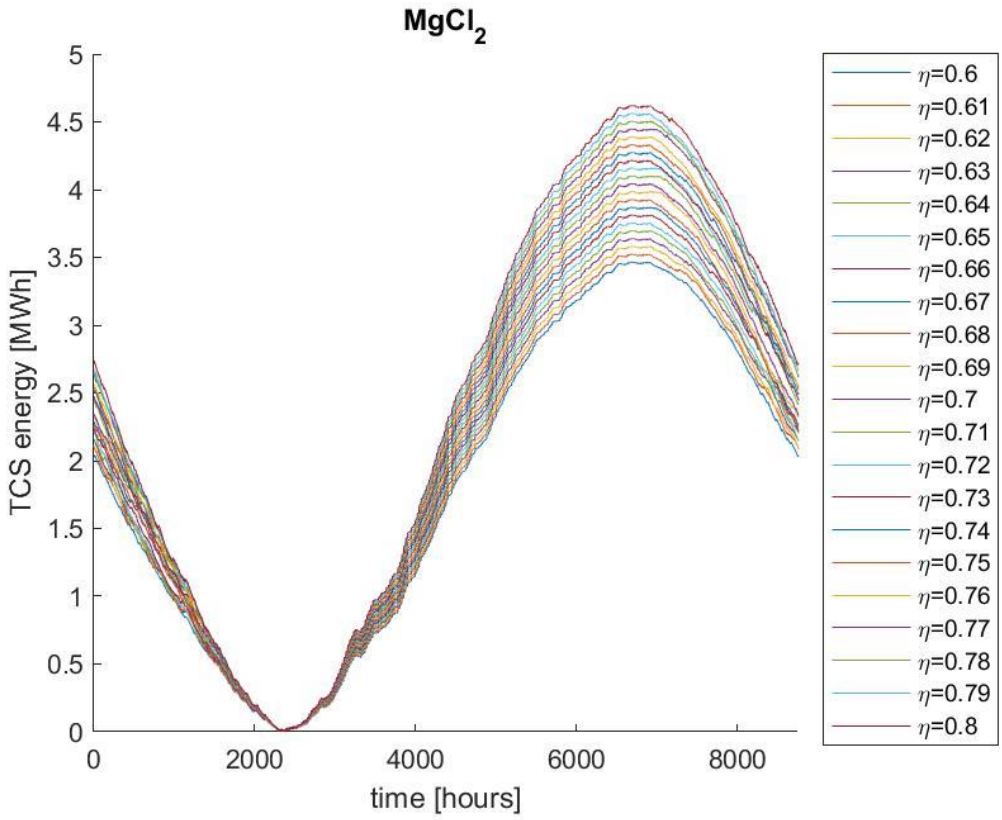

Figure B.3.Hourly yearly profile of the energy stored within the TCS system (Case 1, TCS material:$MgCl_2$, sensitivity parameter: η).

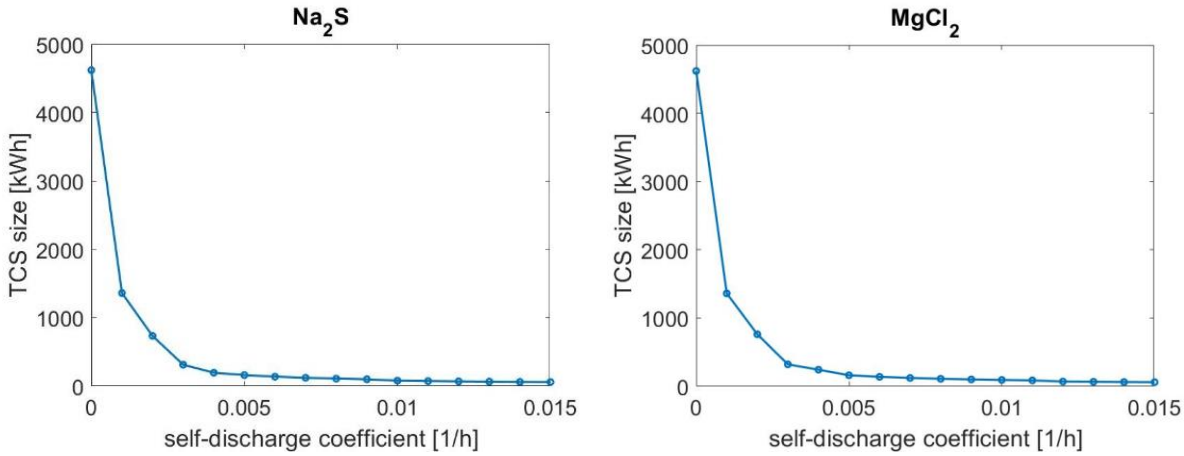

Figure B.4. Optimal energy capacity [kWh] as a function of self-discharge coefficient for Na_2S (left) and $MgCl_2$ (right) (Case 1).

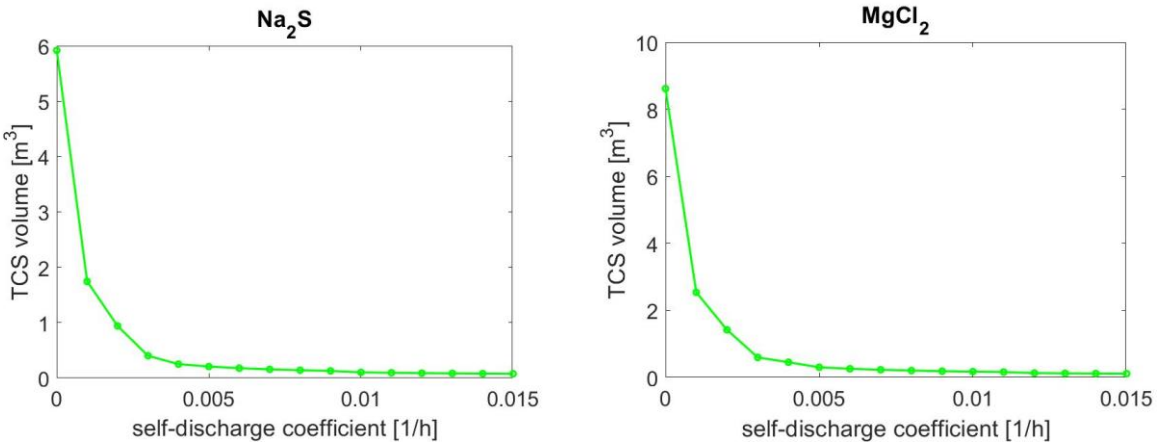

Figure B.5. TCS material volume as a function of self-discharge coefficient for Na_2S (left) and $MgCl_2$ (right) (Case 1).

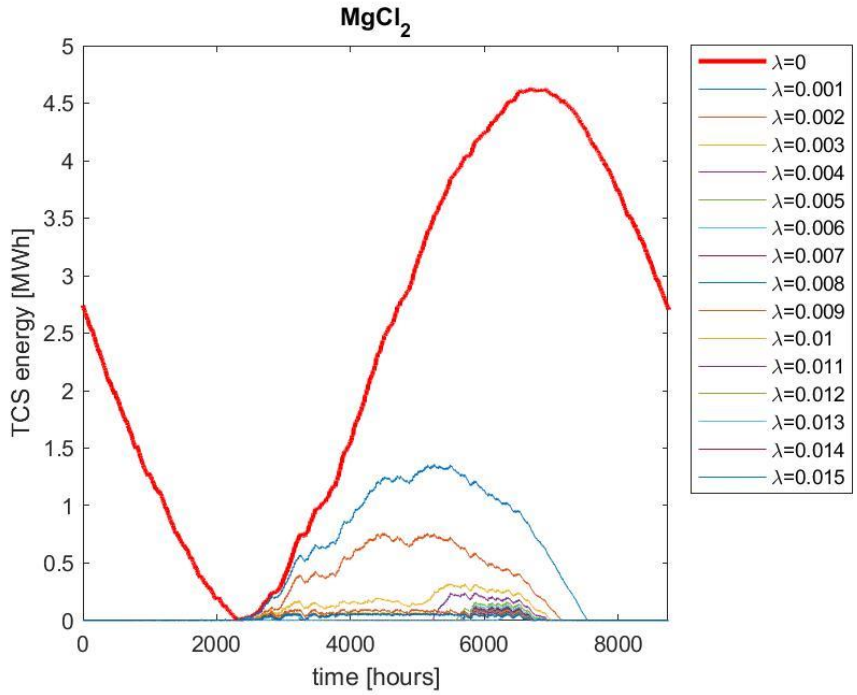

Figure B.6. Hourly yearly profile of the energy stored within the TCS system (Case 1, TCS material: $MgCl_2$, sensitivity parameter: Λ).

Case2

Role of charging/discharging efficiency

Magnesium Chloride ($MgCl_2$)

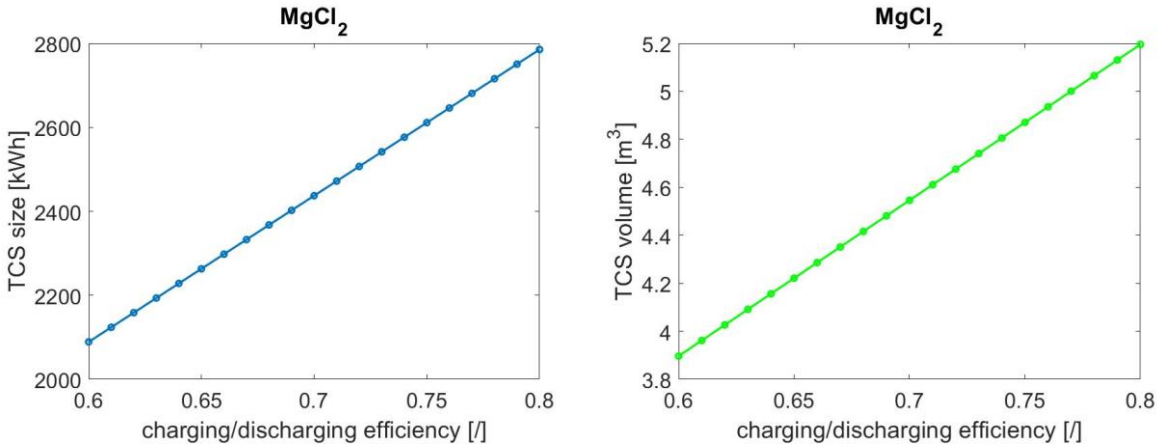

Figure B.7. Optimal energy capacity [kWh] (left) and correlated TCS volume [m^3] (right) as a function of charging/discharging efficiency (Case 2, $MgCl_2$).

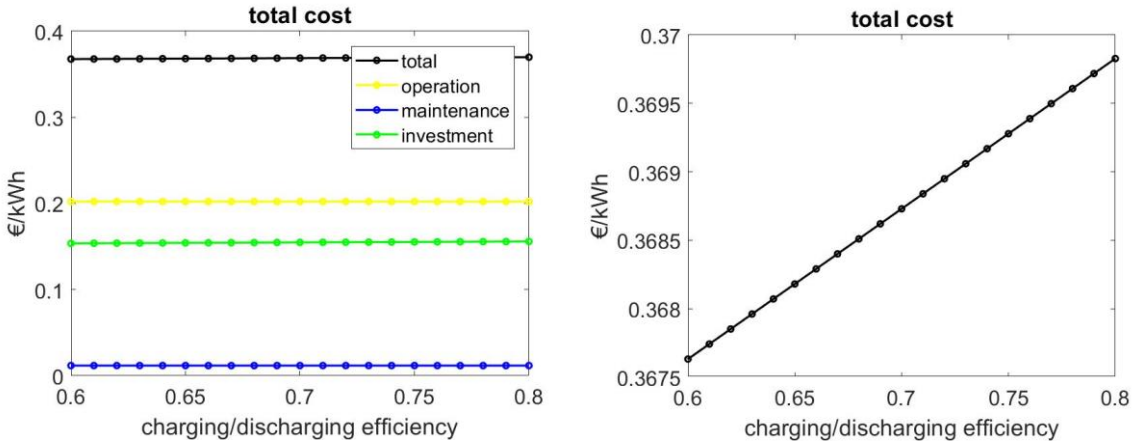

Figure B.8. System cost components (left) and total cost (right) as a function of charging/discharging efficiency (Case 2, TCS material: $MgCl_2$).

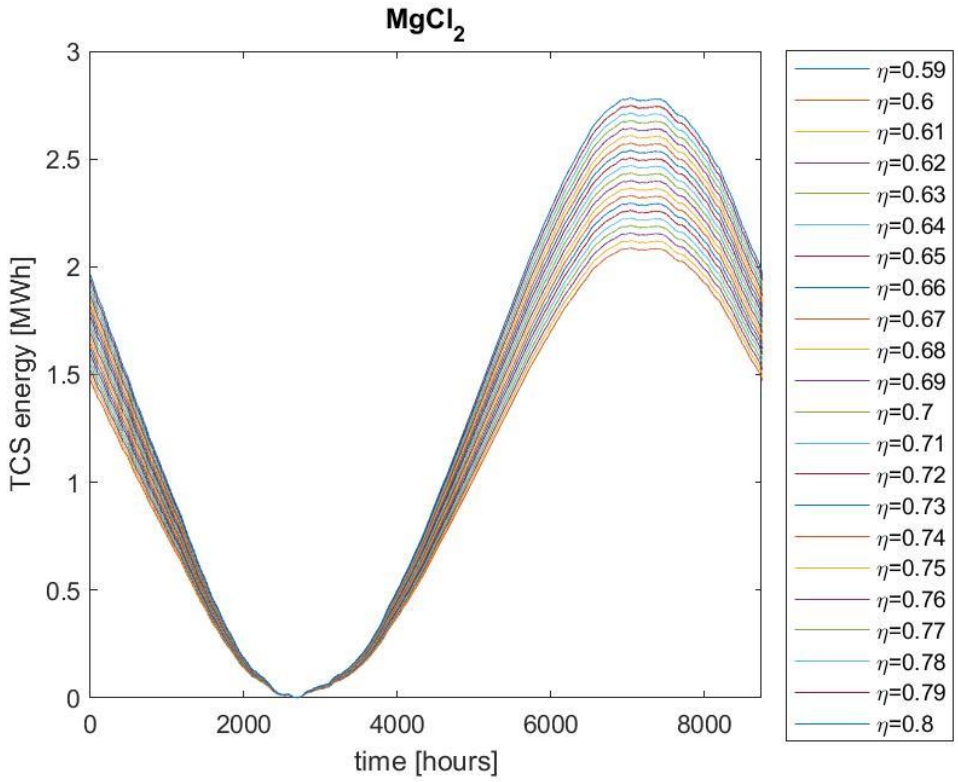

Figure B.9. Hourly yearly profile of the energy stored within the TCS system (Case 2, TCS material: K_2CO_3)

Role of self-discharge parameter

Potassium Carbonate (K_2CO_3)

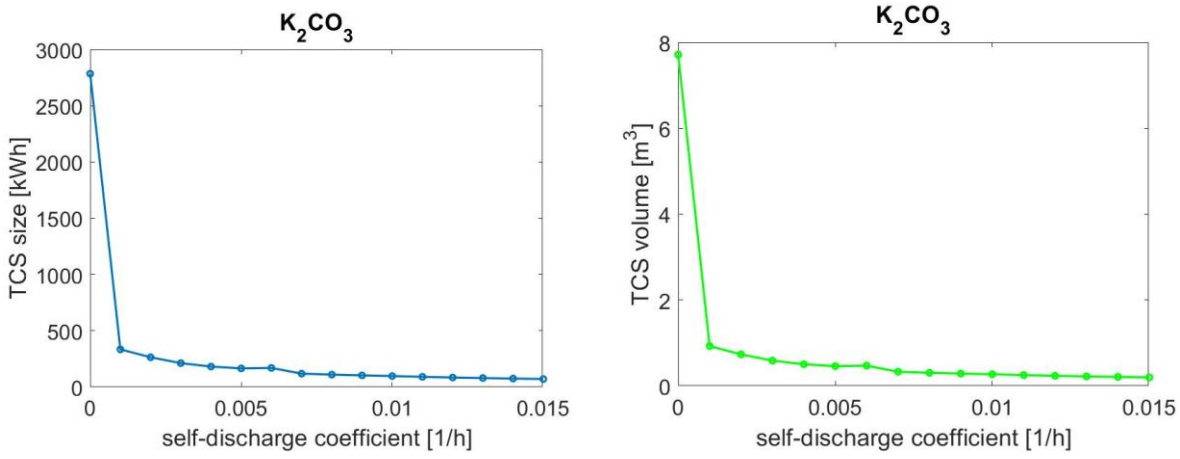

Figure B.10. Optimal energy capacity [kWh] (left) and correlated TCS volume [m^3] (right) as a function of self-discharge coefficient (Case 2, K_2CO_3).

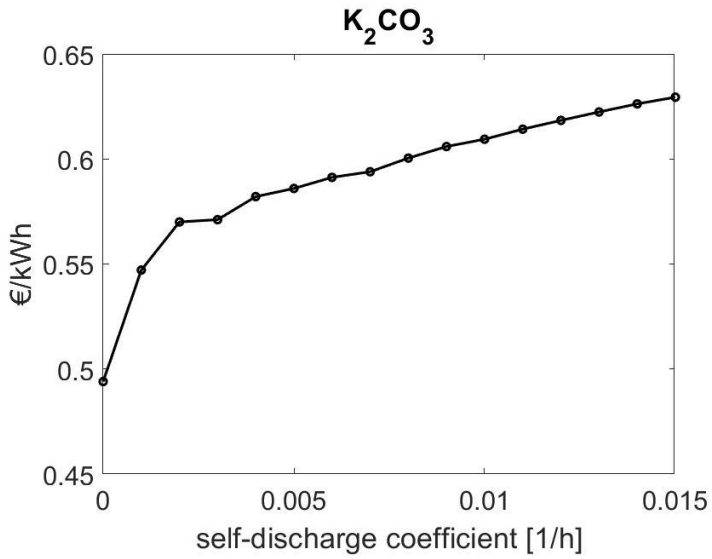

Figure B.11. System specific costs [€/kWh$_{th}$] as a function of self-discharge coefficient (Case 2, K_2CO_3).

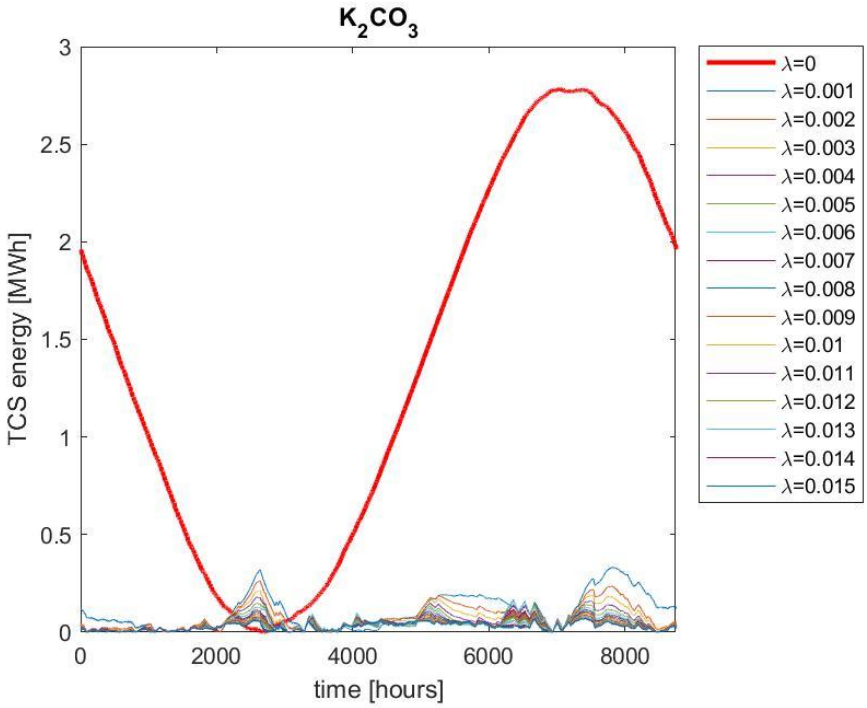

Figure B.12. Hourly yearly profile of the energy stored within the TCS system (Case 2, TCS material: K_2CO_3)

Magnesium Chloride ($MgCl_2$)

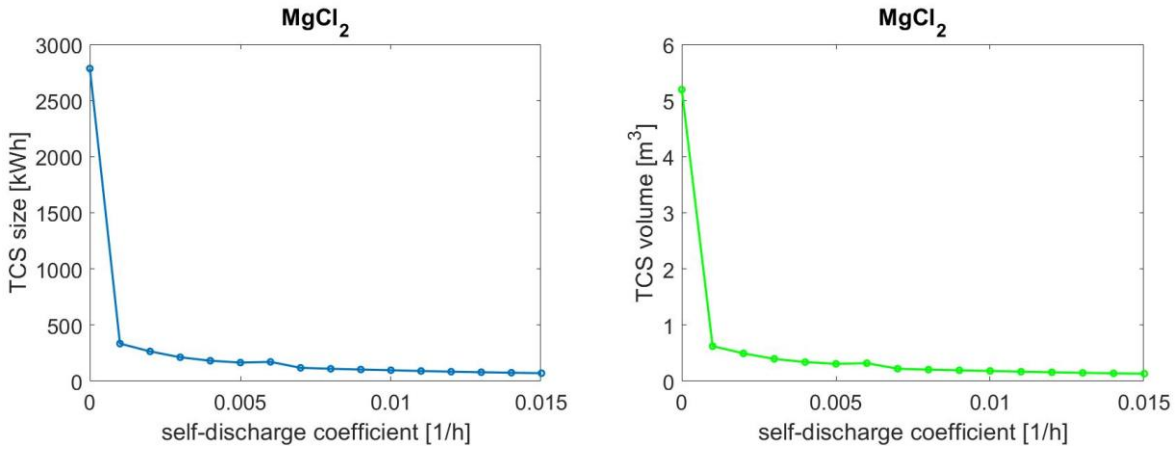

Figure B.13. Optimal energy capacity [kWh] (left) and correlated TCS volume [m^3] (right) as a function of self-discharge coefficient (Case 2, $MgCl_2$).

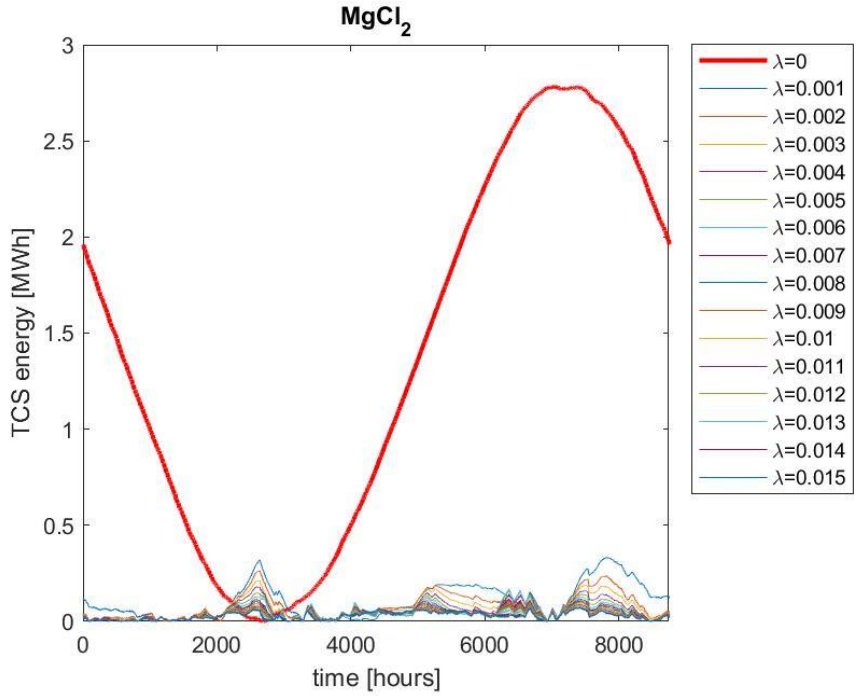

Figure B.14. Hourly yearly profile of the energy stored within the TCS system (Case 2, TCS material: $MgCl_2$)

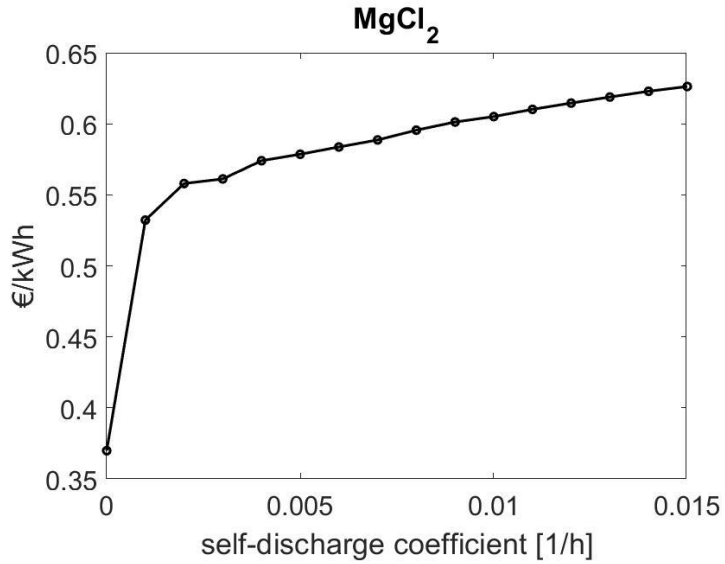

Figure B.15. System specific costs [€/kWh$_{th}$] as a function of self-discharge coefficient (Case 2, $MgCl_2$).

Role of cost of TCS system

Sodium sulphide (Na_2S)

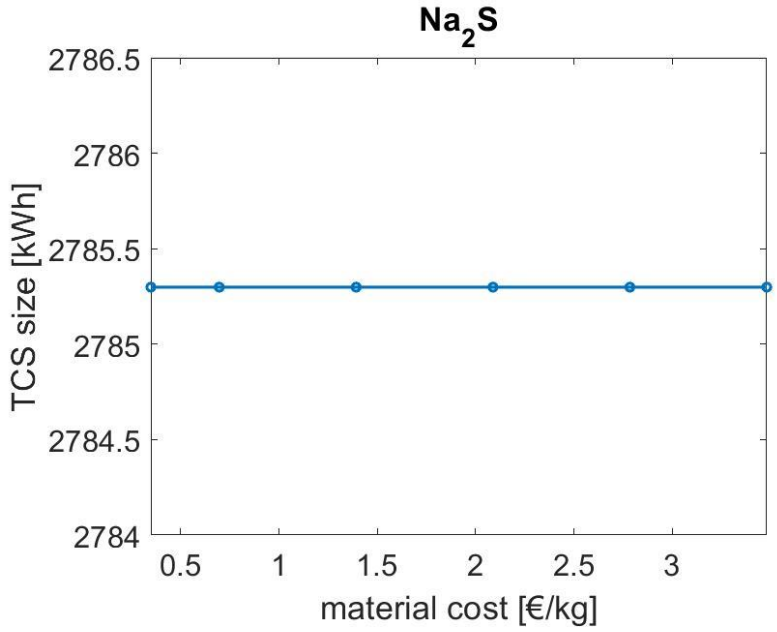

Figure B.16. Optimal energy capacity [kWh] as a function of cost of TCS system [€/kg] (Case 2, material=Na_2S).

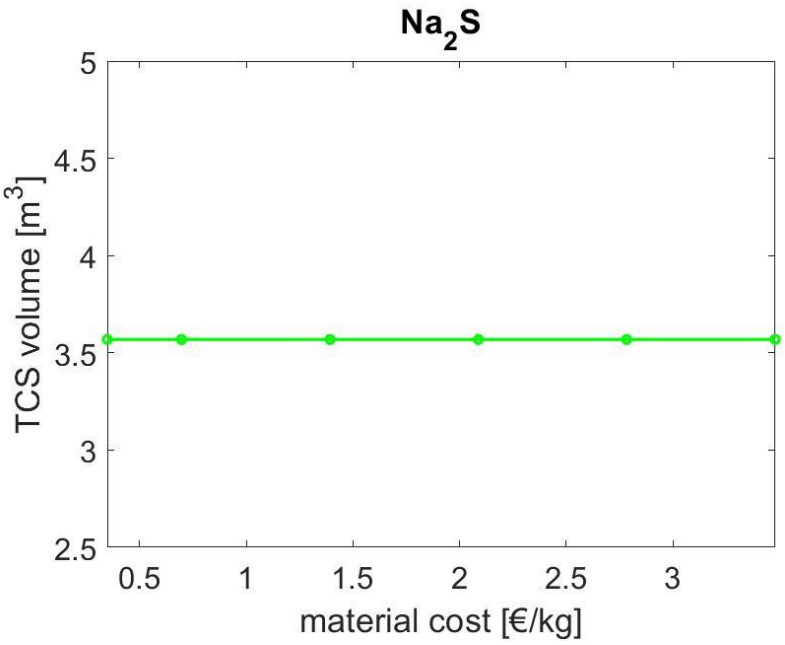

Figure B.17. TCS material volume [m^3] as a function of cost of TCS system [€/kg] (Case 2, material=Na_2S).

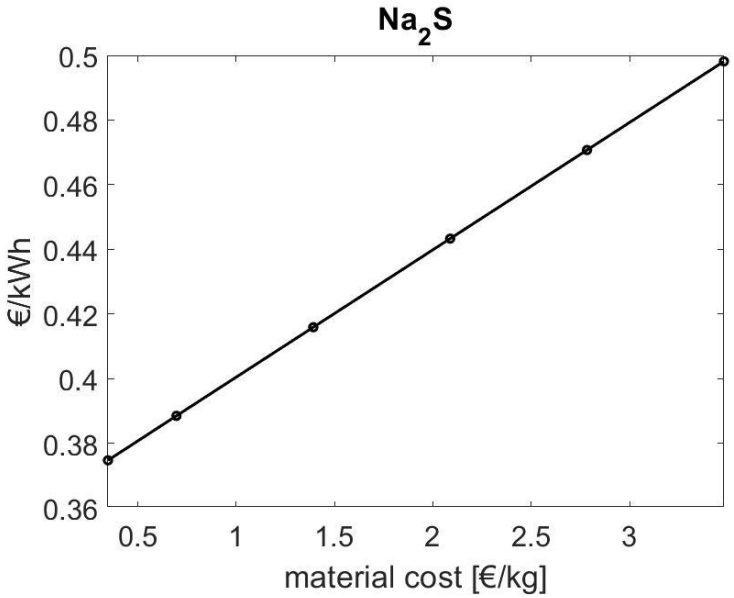

Figure B.18. MES total cost [€/kWh] as a function of cost of TCS system [€/kg] (Case 2, material=Na_2S).

In this case, as for Case 1, the size of the system is not affected by the TCS system cost, but it causes a significative increase of the system total cost.

Magnesium Chloride ($MgCl_2$)

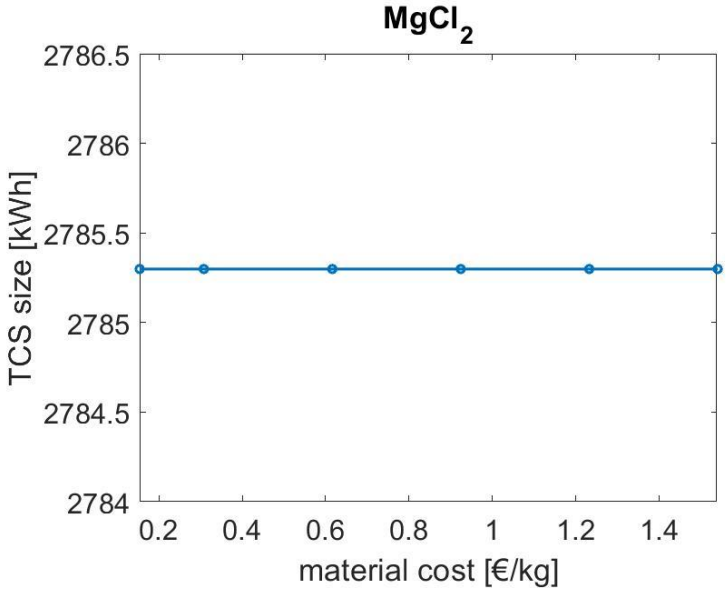

Figure B.19. Optimal energy capacity [kWh] as a function of cost of TCS system [€/kg] (Case 2, material=$MgCl_2$).

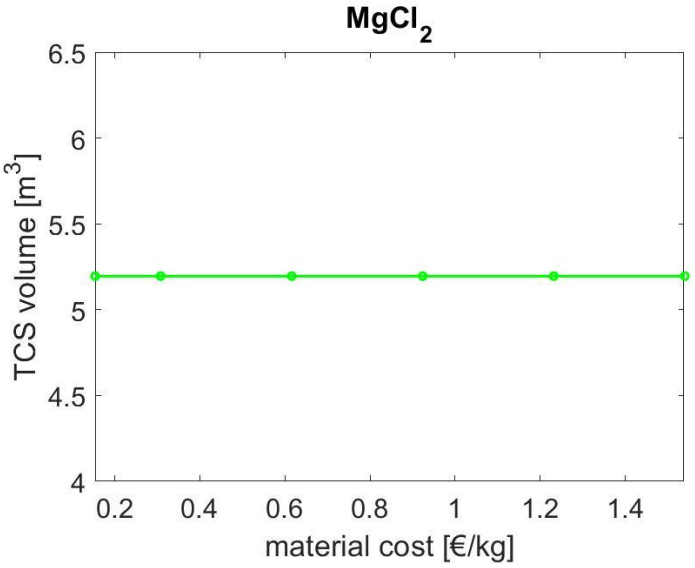

Figure B.20. TCS material volume [m^3] as a function of cost of TCS system [€/kg] (Case 2, material=$MgCl_2$).

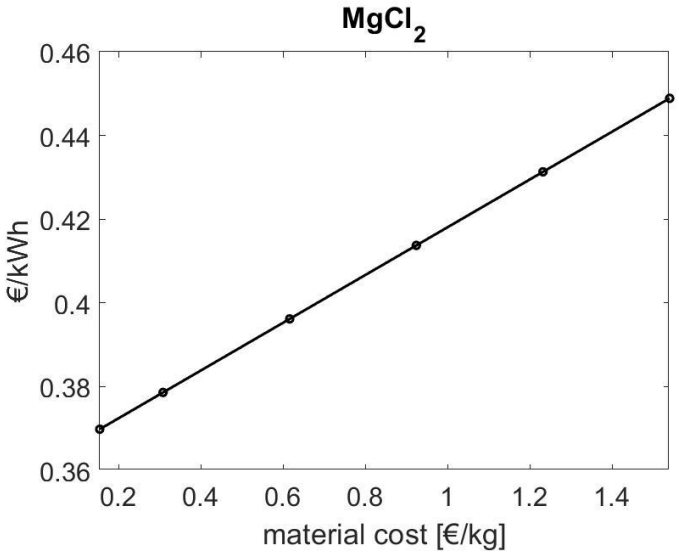

Figure B.21. MES total cost [€/kWh] as a function of cost of TCS system [€/kg] (Case 2, material=$MgCl_2$).

The same qualitatively observations done for Na_2S are valid.

References

[1] P.A.J. Donkers, L.C Soglutogu, H.P. Huinink, H.R Fischer, O.C.G Adan, 'A review of salt hydrates for seasonal heat storage in domestic applications', *Applied Energy*, vol. 199, pp.45-68, 2014.

[2] K. N'Tsoukpoe, T. Schmidt, H.U. Rammelberg, B.A. Watts, W.K.L. Ruck, 'A systematic multi-step screening of numerous salt hydrates for low temperature thermochemical energy storage', *Applied Energy*, vol. 124, pp. 1-16, 2014.

[3] B. Michel, N. Mazet, P. Neveu, 'Experimental investigation of an innovative thermochemical process operating with a hydrate salt and moist air for thermal storage of solar energy: Global performance', *Applied Energy*, vol. 129, pp. 177-186, 2014.

[4] L. Scapino, H. Zondag, J. Van Bael, J. Diriken, C. C. M. Rindt, 'Energy density and storage capacity cost comparison of conceptual solid and liquid sorption seasonal heat storage systems for low-temperature space heating', *Renewable and Sustainable Energy Reviews*, vol. 76, pp. 1314-1331, 2017.

[5] H. Zondag, B. Kikkert, S. Smeding, R. de Boer, M. Bakker, 'Prototype thermochemical heat storage with open reactor system', *Applied Energy*, vol. 109, pp. 360-365, 2013.

[6] L. Scapino, H. Zondag, J. Van Bael, J. Diriken, C. C. M. Rindt, 'Sorption heat storage for low-temperature applications: A review on the advancements at material and prototype scale', *Applied Energy*, vol. 190, pp. 920-948, 2017.

[7] A.J. de Jong, L. Van Vliet, C. Hoegaerts, M. Roelands, R. Cuypers, 'Thermochemical heat storage-from reaction storage density to system storage density', *SHC 2015: International Conference on Solar Heating and Cooling for Buildings and Industry*, *Energy Procedia*, vol. 91, pp. 128-137, 2016.

[8] "IRENA website" (2018). [online]. Available: https://www.irena.org/.

[9] G. Krese, R. Koželi, V. Butala, U. Stritih, 'Thermochemical seasonal solar energy storage for heating and cooling in buildings', *Energy and buildings*, vol. 164, pp. 239-253, 2018.

[10] N. Yu, R.Z. Wang, L.W. Wang, 'Sorption thermal storage for solar energy', *Progress in Energy and Combustion Science*, vol. 39, pp. 489-514, 2013.

[11] K.M Kim, H.T. Oh, S.J Lim, K. Ho, Y. Park, C.H. Lee, 'Adsorption Equilibria of Water Vapour on Zeolite 3A, Zeolite 13X, and Dealuminated Y Zeolite', *Journal of Chemical Engineering Data*, vol. 61, pp. 1547-1554, 2016.

[12] P. Tatsidjodoung, N. Le Pierrès, J. Heintz, D. Lagre, L. Luo, F. Durier, 'Experimental and numerical investigations of zeolite 13X/water reactor for solar heat storage in buildings', *Energy Conversion and Management*, vol. 108, pp. 488-500, 2016.

[13] M. Hefti, M. Mazzotti, 'Modeling water vapor adsorption/desorption cycles'', *Adsorption*, vol. 20, pp. 359-371, 2014.

[14] F.B. Cortés, F. Chejne, F. Carrasco-Marìn, C. Moreno-Castllia, A.F Pérez-Cadenas, 'Water adsorption on zeolite 13X: comparison of the two methods based on mass spectrometry and thermogravimetry', *Adsorption*, vol. 16, pp. 141-146, 2010.

[15] R. Weber, V. Dorer, 'Long-term heat storage with NaOH', *Vacuum*, vol. 82, pp. 708-716, 2008.

[16] Y. Sakamoto, H. Yamamoto, 'Performance of thermal energy storage unit using solid ammoniated salt ($CaCl_2 \cdot NH_3$system)', *Natural Resources*, vol. 5, pp. 337-342, 2014.

[17] N. Yu, R. Z. Wang, Z. S. Lu, L. W: Wang, 'Study on consolidated composite sorbents impregnated with LiCl for thermal energy storage', *International Journal of Heat and Mass Transfer*, vol. 84, pp. 660-670, 2015.

[18] G. Balasubramanian, M. Ghommem, M. R. Hajj, W. P. Wong, J. A. Tomlin, I. K. Puri, 'Modeling of thermochemical energy storage by salts hydrate', *International Journal of Heat and Mass Transfer*, vol. 53, pp. 5700-5706, 2010.

[19] L.C. Sogutoglu, P. A. J. Donkers, H. R. Fischer, H. P. Huinink, O. C. G. Adan ,'In-depth investigation of thermochemical performance in a heat battery: Cyclic analysis of K_2CO_3, $MgCl_2$ and Na_2S', *Applied Energy*, vol. 215, pp. 159-173, 2018.

[20] P. Gabrielli, M. Gazzani, E. Martelli, M. Mazzotti, 'Optimal design of multi-energy

systems with seasonal storage’*, Applied Energy*, vol. 219, pp. 408-424, 2018.

[21] P. Mancarella, ‘MES (multi-energy systems): An overview of concepts and evaluation models’, *Energy*, vol. 65, pp. 1-17, 2014.

[22] P. Gabrielli, M. Gazzani, M. Mazzotti, ‘Modeling fuel cells in integrated multi-energy systems’, *Energy Procedia*, vol. 142, pp. 1407-1413, 2017.